ISAS - INTERNATIONAL SCHOOL FOR ADVANCED STUDIES

Dark Matter Halos:

Properties

Thesis submitted for the degree of

"Magister Philosophiae"

Astrophysics Sector

Candidate:

Magda ARNABOLDI

Supervisor:

Prof. D.W. SCIAMA
Professor
M. CAPACCIOLI

Academic Year 1989/90

TRIESTE

SISSA - SCUOLA INTERNAZIONALE SUPERIORE DI STUDI AVANZATI
TRIESTE
Strada Costiera 11

Contents

Chapter 1

A General Review of Dark Matter

1.1 Introduction

The term "*dark matter*" (DM) is currently used to denote any form of matter whose existence is inferred solely from its gravitational effects. The very first evidence of DM was likely provided by the Swiss astronomer Fritz Zwicky in 1933. His estimate rested on a pioneering application of the Virial Theorem to the galaxies of the Coma Cluster. Zwicky interpreted the 700 km s^{-1} dispersion of the galaxies with respect to their mean velocity as a measure of their kinetic energy per unit mass and, by a crude estimate of the cluster radius, he was able to estimate the total mass of the cluster. Then he computed the cluster mass-to-light ratio $(M/L)_{cl}$ using the mass measured in this way and the luminosity integrated over the cluster galaxies, and compared the result with the $(M/L)_i$ ratio as measured from the rotation curves of nearby spirals. In this way he discovered that $(M/L)_{cl}$ exceeded $(M/L)_i$ by a factor of at least 400: this finding corresponds to the presently well established fact that M/L grows with the scale of the system. Zwicky concluded that virtually all the cluster mass was in the form of some invisible component that was undetectable except through its gravitational force: i.e. it was "missed" by conventional astronomical observations. This important mass component of the Universe was then called "missing mass", but the term has eventually been abandoned because of its misleading meaning.

Investigations of DM originate from a manifold of observational and theoretical motivations, and make use of a great variety of methodologies; and quite different results are obtained in relation to the scale of the systems under study. In this introduction we will shortly review the various approaches and summarize the main results.

1.2 DM in the Solar Neighborhood – [1 kpc scale]

In our galaxy the surface density in known components (main sequence and giant stars, stellar remnants, gas, and dust) at the distance of the Sun is 50 $M_\odot$ pc^{-2} (Bahcall and Soneira 1980), and the surface brightness in the visual band is 15 $L_\odot$ pc^{-2} (de Vaucouleurs and Pence 1978). Almost all of the light comes from objects at $z < 700$ pc from the midplane, thus M/L($R_0, |z| < 700$ pc) = 3.3, where M and L are in solar units $M_\odot$ and $L_\odot$, and R_0 is the distance from the galactic center of the Local Standard of Rest (see Allen 1973, Kerr and Lynden-Bell 1986). This is the best available estimate of the minimum mass-to-light ratio in a typical Population I system.

The measurement of the actual M/L in the solar neighborhood is based on the following model. The collisionless Boltzmann equation for a highly flattened system yields:

$$\frac{1}{\nu}\frac{\partial(\nu\bar{V_z^2})}{\partial z} = -\frac{\partial\Phi}{\partial z} \tag{1.1}$$

where f is the distribution function, $\nu = \int f d^3V$ the mass density, $\bar{V_i^2} = 1/\nu \int f V_i^2 d^3V$ the mean squared velocity. Since in this case the Poisson equation can be approximated by:

$$\frac{\partial^2\Phi}{\partial z^2} = 4\pi G\rho \tag{1.2}$$

then, from equations 1.1 and 1.2,

$$\frac{\partial}{\partial z}\left[\frac{1}{\nu}\frac{\partial(\bar{V_z^2}\nu)}{\partial z}\right] = -4\pi G\rho \tag{1.3}$$

If one can measure the number density ν as function of height z and the mean squared vertical velocity $\bar{V_z^2}$ of any population of stars in the solar neighborhood, equation 1.3 may be used to calculate the local mass density ρ. Oort (1932, 1965) concluded that $\rho_0 = \rho(R_0, z = 0) \cong 0.15\ M_\odot$ pc^{-3} and Σ(700pc) $\cong 90\ M_\odot$pc^{-2}, where Σ is the surface density. Bahcall (1984) arrived at the total local mass density of $\rho_0 \cong (0.18 \pm 0.03)\ M_\odot$pc^{-3}. The V–band luminosity near the Sun is $\sim 0.067\ L_\odot$pc^{-3}, thus the M/L ratio in the solar neighborhood is M/L$_v \cong 2.7$. Since different stellar populations have different thicknesses and since they evolve, a more fundamental quantity is M/L averaged over a column through the disk (the average can only be carried out to $z \cong 700$ pc since the density distribution cannot yet be determined beyond this level). The total surface brightness is $I \cong 15\ L_\odot$pc^{-2}, and it is almost all contained within 700 pc of the plane. Using Bahcall's surface density $\Sigma(700) \cong 75\ M_\odot$ pc^{-2}, it follows: $M/L(700\text{ pc}) \cong 5$. In a column through the plane the observed M/L ratio exceeds the M/L$_{min}$ by $\sim 50\%$.

Note that the nature of this kind of DM is not necessarily exotic because it can be accounted for by known galactic ingredients.

1.3 Rotation Curve and Escape Speed in the Solar Neighborhood – [10kpc]

The shape of the rotation curve outside the solar radius R_0 strongly suggests that the Galaxy contains a great deal of DM. Unfortunately, however, due to the absence of suitable tracers, it is difficult to determine the rotation curve at galactocentric distances exceeding $\sim 2R_0$. In other words, rotation curve observations cannot constrain the distribution of DM at much larger distances. A more powerful constraint to the extension of the Dark Halo (DH) is that the escape velocity from the solar neighborhood must exceed the maximum velocity observed among local stars. The presence of local stars with velocities exceeding 500 km s^{-1} (Carney and Latham 1987) implies that the Galaxy must extend to at least $R = 41$ kpc and have a total mass of at least $M = 4.6 \cdot 10^{11}\ M_\odot$ (Binney and Tremaine 1987). Based on a total luminosity $L_V = 1.4 \cdot 10^{10} L_\odot$ the derived M/L_V ratio is $M/L_V \geq 30$: almost 10 times the minimum value derived for the solar neighborhood.

Does the DM at large radii form a distinct population from the DM that was found in the solar neighborhood? The answer depends on the scale height of the DM in the solar neighborhood. If there is a single component of DM, with vertical distribution of the form $\rho(z) \propto \exp(-|z|/z_0)$, which accounts for the Oort discrepancy, for the shape of the rotation curve, and for the dynamics of high velocity stars, the scale height should be $z_0 \cong 1.1$ kpc. If the scale height of the local DM is smaller than this, then there must be at least two DM components: a disk, which contributes to the Oort limit, but not to the rotation curve, and a shallower spheroidal component which helps to produce a flat rotation curve while giving a negligible contribution to the Oort limit. In the following the component of DM that is needed to flatten the rotation curve and to bind the high velocity stars, will be referred to as Dark Halo.

1.4 Dynamics of Population II Tracers: Dynamics of Stars, Globular Clusters and Satellite Galaxies – [50 kpc]

These families of objects have large random velocities. We must use statistical methods to compare the predictions of a given model of galactic potential with the distribution of observed radial velocities. Because globular clusters and satellite galaxies are found out to distances $\gg R_0$, they can be used to constrain the force field at distances where the rotation curve cannot be directly measured. Using Lynden-Bell's et al. (1983) method, a total mass $M = 3.8 \cdot 10^{11}\ M_\odot$ is determined with an uncertainty of $\sim 40\%$. The corresponding M/L_V is 27. This value confirms

the large mass indicated by the high velocity stars and suggests that the dark halo extends to $R \simeq 34$ kpc.

In conclusion, Population II tracers appear to confirm that the galaxy contains substantial amounts of DM and show that the halo extends to about $R \cong 30$ kpc.

1.5 Magellanic Stream – [100 kpc]

The Magellanic Stream is a long tail of neutral hydrogen that stretches across the sky in a great circle, starting from the Magellanic Clouds. It is believed to consist of debris torn off the Clouds by tidal forces during a previous close passage near the Galaxy. Dynamical models of the stream (Murai and Fujimoto 1980, Lin and Lynden-Bell 1982) show that it is very difficult to fit the data if the galactic potential is that of a point mass (as seen from the stream): a much better fit is obtained with an extended mass distribution. The principal reason is that the material at the end of the stream, some 100° from the clouds is falling toward the Galaxy at high speed ($V_c \cong 220$ km s^{-1}). If there were no massive halo, this large infall velocity could arise only if the material at the end had fallen deep into the Galaxy potential well to a galactic distance ≤ 15 kpc. At this distance parallax effects due to the 8.5 kpc offset of the Sun from the galactic center would destroy the great circle shape of the stream. The stronger force field due to the halo permits the same large velocities to be reached at large galactocentric distances. The stream extends from a galactocentric distance of ~ 50 kpc out to ≥ 100 kpc; this suggests that the outer radius of the DH is at least $R = 100$ kpc and possibly much more. If so then more than 90% of the mass of the Galaxy consists of DM, and M/L exceeds 80.

1.6 Dark Matter in Galaxies – [50 kpc]

Rotation curves provide the most direct method of measuring the mass distribution inside a galaxy. In several spiral galaxies (but usually not in E and S0s) radial velocity curves can be measured optically using the emission lines from HII regions (stellar absorption lines are much more problematic), or at radio wavelengths using the 21 cm emission line of neutral hydrogen; the latter is generally detectable at greater galactocentric distances. The early optical measurements in the 1950's and 1960's, limited to the inner parts of galaxies, were well consistent with the current understanding of spiral galaxies as flat disks. In fact, the rotation curve of an exponential disk can be divided into three radial regimes according to its behaviour: *i)* an inner region where the velocity $V(R)$ increases linearly with the distance from the center R, *ii)* a region where V reaches a maximum and then begins to decline (at the so called turn over radius) , and *iii)* a Keplerian

regime corresponding to where the potential of the disk resembles a point mass potential so that the rotation speed falls as $R^{-1/2}$. The 21 cm observations of the 1970's showed that the flat portions of rotation curves extended further than an exponential disk model predicted, and there was no sign of a Keplerian fall off.

By now there are over 70 spiral galaxies with reliable rotation curves out to large radii (Faber and Gallagher 1979, Rubin et al. 1980, 1982, 1985; cf. the catalogue of Corradi 1989 Dissertation, Univ. of Padova). In almost all of these galaxies the rotation curve is flat or slowly rising out to the last measured point. Very few galaxies show falling rotation curves, and those that do either *i)* fall less rapidly than Keplerian, or *ii)* have nearby companions that may perturb the velocity field, or *iii)* have large spheroids that may increase the rotation curve near the center. So far there is no well-established example of a Keplerian region in any galaxy rotation curve, even when they extend to radii large enough to contain essentially all of the galaxy's light. Consequently there is no spiral galaxy with a well determined total mass. The simplest interpretation of these facts is that, as to our own galaxy, external spirals possess massive DHs extending to radii larger than the optical disk, a conclusion first stated by Freeman in 1970.

A deeper analysis of the mass distribution in spiral galaxies will be developed in the following chapters of this thesis.

1.6.1 Tidal Radii

The galactic mass distribution can be determined from the tidal radii of distant globular clusters and dwarf elliptical galaxies (Barnes and White 1984); but this is a rather uncertain method.

1.6.2 X-Ray Halos of Elliptical Galaxies

Many luminous elliptical galaxies contain up to $10^{10}\ M_\odot$ of hot X-ray emitting mass out to radii of order 50 kpc (Forman et al. 1985). The gas is probably produced by normal stellar mass loss. The X-rays are continuum photons emitted by the gas at temperature T$\cong 10^7$K as it cools through the Bremsstrahlung process. In a spherically symmetric galaxy hydrostatic equilibrium implies:

$$\frac{\mathrm{d}p}{\mathrm{d}R} = -G\frac{M(R)\rho}{R^2} \tag{1.4}$$

where p is the pressure and $M(R)$ is the mass internal to radius R. Using ideal gas laws, this rewrites as:

$$M(R) = \frac{K_B T(R)}{G\mu m_P}\left[-\frac{\mathrm{d}ln\rho}{\mathrm{d}lnR} - \frac{\mathrm{d}lnT}{\mathrm{d}lnR}\right] \tag{1.5}$$

where μ is the mean molecular weight and m_P is the proton mass. If we can measure the temperature profile $T(R)$ and the density profile $\rho(R)$ we can use equation 1.5 to find the mass distribution $M(R)$. Highly resolved maps of the X-ray surface brightness for about a dozen galaxies were provided by the Einstein satellite, but spectroscopically resolved temperature measurements are usually not available. The best data are for the giant elliptical galaxy M87. In this galaxy $M(R)$ rises roughly linearly with radius out to more than 300 kpc with $M(< 300$ kpc$) \cong 3 \cdot 10^{13}\ M_\odot$ (Fabricant and Gorestein 1983, Stewart et al. 1984). The M/L ratio is 750, far larger than the minimum M/L for Population II system (M/L=6). Apparently over 99% of the mass of M87 is composed of DM.

1.7 Dark Matter in Systems of Galaxies – [1 Mpc]

The nearest giant spiral galaxy is the Sb galaxy M31 at a distance of about 700 kpc. Our galaxy, M31, and their companions form a relatively isolated system known as the Local Group. The center of mass of M31 is approaching the center of mass of the Galaxy at $V_G = -119$ km s^{-1}. A natural explanation for this high relative velocity is that the relative Hubble expansion of M31 and the Milky Way has been stopped and reversed by their mutual gravitational attraction. Kahn and Woltjer (1959) pointed out that this hypothesis leads directly to an estimate of the total mass of the Local Group, which is between $5.5 \cdot 10^{12}\ M_\odot$ and $3.2 \cdot 10^{12}\ M_\odot$. Since the luminosity of the Galaxy in the V-band is $1.4 \cdot 10^{10}\ L_\odot$, and M31 is about twice as luminous, the corresponding M/L for the Local Group is between 76 and 130.

1.7.1 Binary Galaxies

The orbital periods of binary galaxies are so long that we cannot even hope to measure their relative proper motions. Consequently any investigation of binary galaxies must be based on statistical studies of the relative line-of-sight velocities in a large sample of galaxy pairs. Models of binaries with galaxies approximated by point masses predict a correlation between the line-of-sight velocity difference and the projected separation: the corresponding search has been carried out by White et al. (1983), but no such correlation has been found. The simplest interpretation of this result is that galaxies have DH that extend well beyond their optical boundaries.

1.7.2 Groups of Galaxies

Groups of galaxies are collections of three or more galaxies whose separations are much smaller than the typical intergalactic separations. The high density of galaxies in groups suggests that they are gravitationally bound, so that an analysis of the positions and velocities of the group members can yield an estimate of the mass and M/L of the group. Huchra and Geller (1982) determined M/L for their groups using the virial theorem. They found a median value in the V band of 260, but with a wide spread. The M/L in groups is much larger than the values seen in the luminous parts of galaxies.

1.8 Clusters of Galaxies – [1.5 h^{-1} Mpc]

Rich clusters of galaxies are considered to be among the best available sites for studying the nature and the distribution of DM. A cluster contains many more galaxies than a typical group. In some nearby clusters several hundred systemic velocities have been measured, thereby almost eliminating the statistical uncertainties that plague measurements of galaxy groups. As was the case at Zwicky's time, the best available data are for the Coma Cluster. The Kent and Gunn (1982) analysis yields a M/L$\cong$ 360 h where h is the relative Hubble constant, measured in units of 100 km s^{-1} Mpc^{-1}. A similar analysis of the Perseus cluster yields M/L$\cong$ 600h. These values are some 30 to 50 times larger than the minimum M/L ratios for the stellar population in elliptical cores.

A fundamental question is whether the DM in clusters is the same as the DM in the halos of galaxies. According to Binney (1987) it seems conceivable that the nature of the DM in groups and clusters is the same as in the DH's of individual galaxies. The DH that would normally form the halo of a galaxy has been stripped off by tidal interactions with the other galaxies into the cluster and now forms a diffuse background that comprises most of the mass of the cluster.

1.9 DM in Cosmology

Virgocentric flow: the nearest large cluster of galaxies is the Virgo cluster, which is receding from the Local Group at $\sim 10^3$ km s^{-1}. The gravitational accelerations of this mass concentration should perturb the velocity field of galaxies around Virgo, including the Local Group, away from a pure Hubble flow. Our recession velocity from Virgo should be smaller than $H_0 R_{V0}$, where R_{V0} is the distance to the Virgo cluster and H_0 is the asymptotic Hubble constant as determined from the velocity field well beyond Virgo. By measuring this difference it is possible to estimate the total mass and the M/L associated with the Virgo cluster. Different models

(Davis and Huchra 1982, Yahil et al. 1980, Aaronson et al. 1982, Davis and Peebles 1983) suggest $\Omega_0 = 0.25 \pm 0.15$, where $\Omega_0 = \rho_0/\rho_c$ is known as the density parameter, ρ_0 is the mean matter density of the universe at the present time and $\rho_c = 3H_0/8\pi G = 1.88 \cdot 10^{-29} h^2$ g cm^{-3} is the critical density: it corresponds to a M/L of 400 h. The Virgo distance represents the largest scale on which we have a direct dynamical measurement of Ω_0. The measurements confirm that large quantities of DM are present on this scale, but that there is not enough matter (either luminous or dark) on this scale to close the Universe (the upper limit to Ω_0 is substantially less than unity).

1.10 Gravitational Lenses

Galaxies act as gravitational lenses; occasionally, two or more images of a single distant object such as a quasar may become visible. By now there are a half dozen or so probable lenses, with up to 4 images produced by a single lens and image separations of up to 7 *arcsec* (Turner 1987). Typically two relatively bright quasar images will be seen on opposite sides of the lensing galaxy with a third faint one of the quasar lying near the center of the galaxy. The observed cases have separations of 2" to 7"; simple models predict surprisingly large masses for the lensing galaxies in order to obtain these separations. Moreover gravitational lenses seem to offer the exciting possibility of detecting mass concentrations that are completely dark. Moreover the complexities of the mass distributions of the lenses, cosmological effects, and poorly known quasar properties imply that simple models often yield misleading or ambiguous results. The only firm conclusion so far is that models in which the mass density in the lens is everywhere proportional to the luminosity density do not fit the data.

The evidence which we discuss below is of a completely different nature and involves the universe as a whole.

1.11 Primordial Nucleosynthesis

According to the standard Big Bang theory, the primordial deuteriun abundance provides a measure of the baryon density in the early universe. The present deuterium abundance can be measured from nuclear spectra in Jupiter's atmosphere, from ultraviolet line strengths in the interstellar medium, and from lunar samples, and yields $n_d/n_p \cong (1-2) \cdot 10^{-5}$, where n_d is the number density of deuterons and n_p that of protons. This should be regarded as a lower limit on the primordial density, since some deuterium may have already been burned in stellar interiors. Combining this result with data on He^3 and Li^7, one has that the present mass density in baryons is $\rho_B = (2-9) \cdot 10^{-31}$ g cm^{-3} with $\Omega_B = \rho_B/\rho_c = (0.011-0.048)$ h^{-2}

(Yang et al. 1984), where Ω_B is the fraction of the critical density supplied by baryons alone. Since $0.5 \leq h \leq 1$, than $0.011 \leq \Omega_B \leq 0.19$. This is roughly consistent with the measurements of Ω_0 from the Virgocentric flow and from the M/L of groups and clusters of galaxies. Essentially all the mass in structures up to the size of the Virgo supercluster may be in baryons.

1.12 Age of the Universe

A lower limit to the age of the Universe is given by the age of the oldest stars. Globular clusters yield ages of $(15 - 18) \cdot 10^9$ yr (Harris et al. 1983, VandenBerg 1983). Radioactive decay measurements yield similar values but with a larger spread $(7 - 20) \cdot 10^9$ yr (Hainebach and Schramm 1977). The age predicted by Friedman models for the Universe can be written as $t_0 = 9.78 \cdot 10^9\ h^{-1} f(\Omega_0)$ yr where $f(\Omega_0) = 1$ for $\Omega_0 = 0$ and $2/3$ for $\Omega_0 = 1$. Thus, if $\Omega_0 = 1$ and the stellar evolution chronometer gives an accurate estimate of the age of the Universe, we must have $h < 0.44$. If we accept that $0.5 \leq h \leq 1$, we can rule out models with $\Omega = 1$.

1.13 Is $\Omega_0 = 1$?

This thesis is supported by i) the Copernican argument and by ii) inflation. The Copernican or coincidence argument is based on the Copernican Principle: men do not occupy a special place or time in the Universe. If $\Omega(t)$ in any Friedman model is plotted on a logarithmic time scale, then it is almost always nearly 1, nearly 0 or very large. There is no obvious reason why the process of evolution of intelligent life should bring us to the point where we ask these questions during the relatively short time when Ω_0 is neither near zero, near unity, nor very large, and we know that Ω_0 is is neither near zero nor very large. Hence it must be near unity.

Then why do the dynamical measurements yield $\Omega_0 < 1$? One possible explanation is that galaxy formation is biased; galaxies preferentially form in high density spikes of otherwise normal density regions, then the excess of luminous matter around Virgo would not reflect an equivalent excess of mass.

How can the nucleosynthesis arguments giving $\Omega_0 \leq 0.2$ be consistent with $\Omega_0 = 1$? It may be that most of the mass in the Universe is some species of non baryonic particles that have not yet been detected.
As we have seen, the M/L ratio grows linearly with the dimension of the system under study, and we can guess that the quantity of DM is increasing with distance. The application of a plain Occam's razor argument leads us to conclude that there is only one type of DM, which accounts for the Oort mass discrepancy, for

the flat rotation curves of spirals, and for cosmological demands. But, since the methodologies used to determine these mass excesses are different, it is conceivable that there are different kinds of DM at different scales. The DM required by the Oort discrepancy can be easily accounted for by normal galactic ingredients, while DM in galactic halos and at larger scales can be constituted by the exotic particles predicted by GUT and Supersymmetry.

1.14 Dark Matter in Baryons

Even in the solar neighborhood roughly half of the mass is dark, and this DM component was almost certainly collisional at some time in the past since the present disklike configuration requires a dissipation mechanism to form . What are the candidates for baryonic DM?

a) Low luminosity stars and stellar remnants – Brown dwarf stars with masses too low to burn hydrogen ($\leq 0.08 M_{\odot}$), but they are difficult to detect. Stellar remnants such as white dwarfs, neutron stars or black holes: the principal observational constraint is that the density of such remnants cannot exceed $\Omega_0 \cong 0.03$ or else their integrated light output would contribute too much to the background radiation density (Carr et al. 1984). Stellar remnants could supply all the DM in the solar neighborhood but not all the DM in cluster of galaxies or in the Virgo supercluster. At the present time there is no known way to detect the required population of either brown dwarfs or massive remnants directly.

b) Small solid body objects – Comets, asteroids or dust grains are unlikely sources of the DM because they are mainly composed of elements such as Silicon, Carbon, and Oxygen, which are always much less abundant than Hydrogen and Helium. One might argue that the Hydrogen is hidden in the form of solid snowballs, but these would evaporate (Hegyi and Olive 1983).

c) Neutral and ionized gas – Most of the mass in any primordial gas must be in the form of hydrogen. Many elliptical galaxies contain hot gas that is detectable in the X-ray band, but the mass in this gas is too small to account for DM. An alternative hypothesis is that the gas is neutral and resides in an extended disk contribution. However radio observations at 21 cm show that the mass of neutral hydrogen gas in the outer parts of galaxies is far too small to provide the mass required for flat rotation curves. It is also possible to place stringent limits on the density of intergalactic hydrogen gas. Gunn and Peterson (1965) searched for neutral intergalactic gas by looking for attenuation of quasar radiation due to the absorption by the Lyman-α transition of Hydrogen at $\lambda = 1215A$. This test yields the remarkably strong limit $\Omega_{HI} < 4 \cdot 10^7\ \mathrm{h}^{-1}$, where Ω_{HI} is the fraction of the critical density of neutral hydrogen (Peebles 1971, Field 1972).

d) Massive black holes – One interesting possibility is that an early epoch of star

formation, that possibly occurred before galaxy formation, produced stars of very high mass that by now have collapsed into black holes (Carr et al. 1984). If the stars are sufficiently massive, greater than a few hundred solar masses, then they collapse directly to a black hole, without expelling mass in an explosion as less massive stars do. Strong limits can be set on the number density of exploding stars by requiring that they do not pollute the interstellar or intergalactic medium with too many heavy elements. The maximum allowed density in black hole remnants of stars with $M < M_c$ is only $\Omega_0 \leq 10^{-4}$ (Carr et al. 1984), while for $M > M_c$ the observational constraints are much less severe.

But if the inflationary scenario is correct and our understanding of primordial nucleosynthesis is correct too, then at least 80% of the matter in the universe cannot be composed of baryons. A large "zoo" of exotic particles has been proposed as candidates for this dark mass including massive neutrinos (Sciama 1982c, d), gravitinos, axions, monopoles, and photinos (Sciama 1982a, b, 1984, 1988). Although exotic particles are regarded by many cosmologists as the most attractive candidates for DM in galactic halos and at larger scales, they cannot provide the DM in the galactic disk since they are not dissipative.

1.15 Plan of This Work

This master thesis is not intended to provide a global view on the DM problem[1], but rather to focus on those aspects related to the phenomenological aspects and properties of the potential wells where galaxies were formed. Within this limited framework we will analyse the evidence for the existence of DM, its properties, and what is known about the shape of the galaxian DHs.

Chapter 2 presents the data from which one can infer the existence of DM in galaxies. In particular we will analyse the different methods to infer the mass distribution from optical rotation curves on one hand and HI rotation curve on the other hand. The procedures proposed by Rubin *et al.* (1980, 1982, 1985), Kent (1986, 1987, 1989) van Albada *et al.* (1985), Sancisi and van Albada (1987) and by Persic and Salucci (1988) are reviewed and compared.

In Chapter 3 we will explore if it is possible to explain observational data in the framework of the classical Newtonian theory of gravity, or whether modifications of the gravitational force are required. The theories of Sanders (1984, 1986b), and of Kuhn and Kruglyak (1987) are reviewed, particular emphasis is given to the theory formulated by Milgrom (1983). These alternatives are compared with

[1]Several contributions on different aspects of this problem are available in the literature. The reader is referred to the recent reviews by van Albada and Sancisi (1986) and Trimble (1987) as well as the articles in IAU Symp. 117 (Knapp and Kormendy 1986) for an overview of the subject, the review of Blumenthal (1987) on DM and galaxy formation, and the review of Sanders on non-Newtonian alternatives for the Gravitational law.

astronomical data and an original way of testing Milgrom's theory is proposed (Arnaboldi 1990).
In Chapter 4 we will review different estimates of the parameters for the DM distribution in galaxies; the constraints set by the theory of spiral structure to the M/L ratios proposed by Athanassoula, Bosma and Papaioannou (1987) and the mass decomposition method given by Persic and Salucci (1990a) are reviewed in detail.
In Chapter 5 a method for determining the shape of DM halos is presented. The study of polar ring[2] dynamics gives the opportunity of determining the spatial mass distribution. The different procedures and the predictions on the halo flattenings, proposed by Schweizer, Whitmore, and Rubin (1983), Whitmore, McElroy and Schweizer (1987), and by Sackett and Sparke (1989) are discussed and compared.

[2]For a general review on polar rings see Athanassoula and Bosma (1985)

Chapter 2

Dark Matter: Evidence from Galaxy Kinematics

2.1 Introduction

One of the strongest pieces of evidence for DM on galactic scales is the flatness of the rotation curves of field spirals. The implications of this flat trend on the density distribution are effectively illustrated by the following simple model. Let us assume that *(1)* the luminous matter in the equatorial plane of a disk galaxy is in circular orbits, and that *(2)* centrifugal equilibrium holds; the relation between the mass internal to radius R and the velocity $V(R)$ is

$$M(R) = f(R)\, G V^2(R) R$$

where $f(R)$ is a function of the spatial mass–distribution.
If the mass distribution is spherical, the function $f(R)$ is a constant, and

$$M(R) = 2.3265 \cdot 10^5 V^2(R) R\, M_\odot \tag{2.1}$$

if V is in km s^{-1}, R is in kpc. Therefore, in the outer parts of disk galaxies where the rotation curves are identically flat, the model integral mass increases linearly with radius; in fact

$$\begin{cases} G\dfrac{M(R)}{R^2} = \dfrac{V^2}{R} \\ V = const. \end{cases} \qquad \Longrightarrow \qquad M(R) \propto R.$$

Said in other words, the mass in every shell of thickness dR is constant

$$\frac{\mathrm{d}M(R)}{\mathrm{d}R} \cong V^2,$$

and the density decreases as R^{-2}

$$\rho(R) \propto \frac{\mathrm{d}M}{\mathrm{d}R^3} \propto \frac{V^2}{R^2}; \qquad \rho(R) \propto R^{-2}.$$

In a disk–dominated galaxy the luminosity falls off exponentially, i.e. more rapidly than R^{-2}. In regions where the curves are not flat but the velocity has value V at R, $V + \mathrm{d}V$ at $R + \mathrm{d}R$ one has

$$\mathrm{d}M = 2.3265 \cdot 10^5 \left[V^2 + 2VR \left(\frac{\mathrm{d}V}{\mathrm{d}R} \right) \right] dR\, M_\odot \tag{2.2}$$

$$\begin{aligned} \rho = & \quad 1.85 \cdot 10^{-5} \left[\frac{V^2}{R^2} + 2 \left(\frac{V}{R} \right) \frac{\mathrm{d}V}{\mathrm{d}R} \right] \; M_\odot pc^{-3} \\ = & \quad 1.25 \cdot 10^{-27} \left[\frac{V^2}{R^2} + 2 \left(\frac{V}{R} \right) \left(\frac{\mathrm{d}V}{\mathrm{d}R} \right) \right] \; gcm^{-3} \end{aligned}$$

HI rotation curves extend out to several optical radii, and their flatness requires another mass component in addition to the exponential (luminous) disk (see Fig. 2.1). Optical rotation curves are much less extended and, even when they are flat at the outer end, this trend does not necessarily require any dark component. But, if the kinematics in the inner (optical) regions is not dominated by a dark component, the rotation curve should correlate with the morphology and the optical properties of spiral galaxies. On the other hand, if DM dominates the potential wells of galaxies at all radii, this should result in a lack of correlation between optical rotation curves and morphology of spirals.

2.2 Evidence for Dark Matter from optical rotation curves of field spiral galaxies

In order to elucidate the relation between mass distribution and morphology of spirals, Rubin, Thonnard, Ford, and Burstein (1980, 1982, 1985; hereafter RTFB) analysed the systematic properties of the optical rotation curves of 60 field spiral galaxies against luminosity, optical size, and Hubble type. These authors tried to determine if the mass distribution is uniquely linked to galaxy type, and derived masses and densities as functions of radius and luminosity. The characteristics of the RTFB sample are summarized in Tab. 2.1. For each Hubble type, the galaxies contained in the RTFB sample cover a range of luminosity as large as possible.

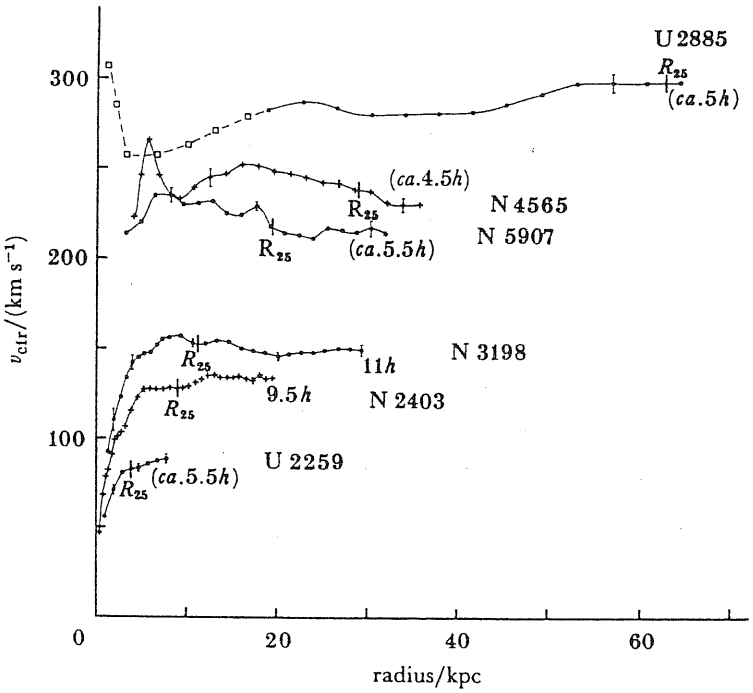

Figure 2.1: HI rotation curves for a number of spiral galaxies. Distances are based on $H_0 = 75$ km s^{-1} Mpc^{-1}. The optical radius, R_{25}, and the number of disk scale-lengths, h,at the last measured point are indicated.

TABLE 2.1
Sample ranges

	Sa	Sb	Sc
Ext.	66%	76%	83%
Lum. range	0.081 – 2.1	0.13 – 2.2	0.04 – 5
Radius	8 – 51	5 – 52	4 – 122
Mass	5 – 92	4 – 85	1 – 200

Table 2.1: the 1^{st} row refers to the extension of the optical rotation curves with respect to R_{25}, the luminosities are in units of $10^{11}L_{\odot}$, radii are in kpc, and masses are in units of $10^{10}M_{\odot}$.

2.2.1 Comparative Integrated Properties of the Spiral Family

RTFB found that the rotational velocities of objects with the same luminosity class are higher in Sa's than in Sb's or Sc's. They derived the following dependence of V_{max} on Hubble type:

- Sa $\rightarrow V_{max}$ from 367 km s^{-1} ($M_B = -22.8$) to 163 km s^{-1} ($M_B = -19.3$)
- Sb $\rightarrow V_{max}$ from 330 km s^{-1} ($M_B = -22.87$) to 144 km s^{-1} ($M_B = -19.55$)
- Sc $\rightarrow V_{max}$ from 304 km s^{-1} ($M_B = -23.70$) to 99 km s^{-1} ($M_B = -18.59$)

The mean value V_{mean} of the maximum velocity is different for each Hubble type (299 km s^{-1} for Sa, 222 for Sb, and 175 for Sc), but the intervals within which it varies overlap. For example, a V_{max} of $\cong$ 250 km s^{-1} can identify either a high–luminosity Sc, or an Sb of intermediate luminosity, or a low luminosity Sa.

From the analysis of the optical rotation curves of their 60 galaxies, Rubin *et al.* derived indications that galaxies of very different optical luminosities and morphologies might have rotation curves with very similar forms. All that suggests that the detailed optical morphology has little to do with the overall mass distribution.

In addition RFTB found that galaxies of very different bulge-to-disk ratios may have rotation curves with very similar central gradients, a fact implying that $(dV/dR)_{core}$ is not determined just by the degree of central concentration of light in these galaxies.

2.2.2 Properties of Optical Rotation Curves

The outer ends of optical rotation curves show no Keplerian decline. They are either flat or still rising untill the last observed point. They also show some degree of correlation with luminosity: galaxies of low luminosity generally have low central velocity gradients and low maximum rotational velocities, V_{max}, in contrast to galaxies of high luminosity which have high central velocity gradients and high values of V_{max}. RFTB do not find any high luminosity galaxy whose rotation curve rises very gradually with R; they also note that it is rare to observe a rotation curve of a low luminosity spiral which is flat over most of the radial range, (see Fig. 2.2).

RFTB described these correlations in a quantitative way introducing what they called the mass scale–length and using the following procedure. They derived the integral mass function $M(R)$ from the rotation curve through equation 2.1. Then, fixing a reference mass M_m (say 10^{10} $M_\odot$), for each sample galaxy they obtained the relative radius R_m, called *mass scale–length*, such that $M(R_m) = M_m$. In this

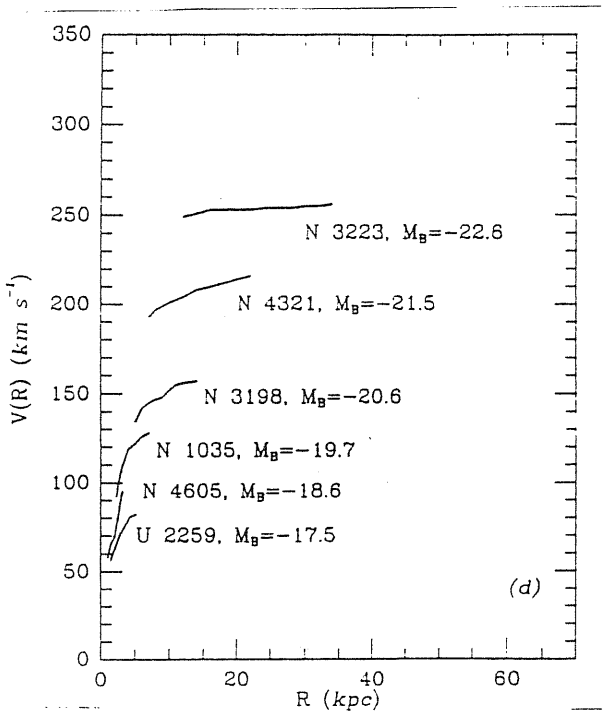

Figure 2.2: Plot of a representative sequence of observed curves (the data are respectively from Rubin *et al.*(1985) for NGC 3223, NGC 4321, NGC 1035, and NGC 4605; van Albada *et al.*(1985) for NGC 3198; Carignan, Sancisi, and van Albada (1988) for U 2259). Both the amplitude and slope of the circular velocity field show a marked progression with luminosity.

way they found that the same mass reached by a low luminosity galaxy near the edge of its small optical disk is reached in less than 1% of the size of the large optical disk of a high luminosity galaxy. In other words, the small disk of a low luminosity spiral galaxy contains a single mass scale-length R_m, while the large disk of a high luminosity galaxy contains many tens of mass scale lengths. When RTFB plotted V against $\xi = R/R_m$, the rotation curves for big galaxies turned out to be scaled–up versions of those for the smaller galaxies. This implies an inverse correlation of the characteristic mass scale-length with luminosity and mass.

For the Hubble type Sc, RTFB obtained $R_m(max) = 4.4$ kpc for the low luminosity galaxies and $R_m(min) = 1.5$ kpc for the high luminosity ones. Since $R_m \cong R_{25}$ (where R_{25} is the radius of the 25 B mag arcsec^{-2} isophote) for a low luminosity galaxy, and $R_m/R_{25} = 0.01$ for a high luminous one, the masses within an isophotal radius vary by a factor of 100, while the mass scale-lengths differ only by a factor of $\cong 3$. This implies the following relation between the velocity amplitudes

$$\frac{V_{high}^2}{V_{low}^2} = \frac{GM_m}{R_{min}} \frac{R_{max}}{GM_m} \cong 3$$

which is observed.

The rotation curves vary systematically with luminosity within a Hubble type, but their forms are generally similar for the Sa, Sb and Sc types, regardless of morphology, see Fig. 2.3. Taking into account that the bulge-to-disk ratios for the galaxies in the sample range from 4.0 to 0.1, the similar shape of the rotation curves does not reflect any of the marked structural differences which lead to the different morphological classifications. Moreover, the apparent similarity and relative simplicity in the forms of rotation curves of the Sa, Sb, and Sc galaxies are surprising, since the Sa have been chosen to be bulge-dominated.

This similarity among rotation curves of galaxies belonging to different Hubble types and with different bulge-to-disk ratios, provides evidence to the belief that the optical luminosity does not map the distribution of matter within the optical galaxy.

2.2.3 Local Density

In regions where the rotation curves are flat, one has

$$\rho \cong \frac{V^2}{R^2} \tag{2.3}$$

and this tells us that ρ is falling as R^{-2}. Using the rotation curve for two Sc galaxies, one of high and one of low luminosity, RTFB (1982) obtained the following radial behavior for the density $\rho \cong R^{-1.7\pm1}$. Thus if we assume a constant M/L ratio, in regions where ρ is falling as R^{-2} or even slower [i.e. velocity constant

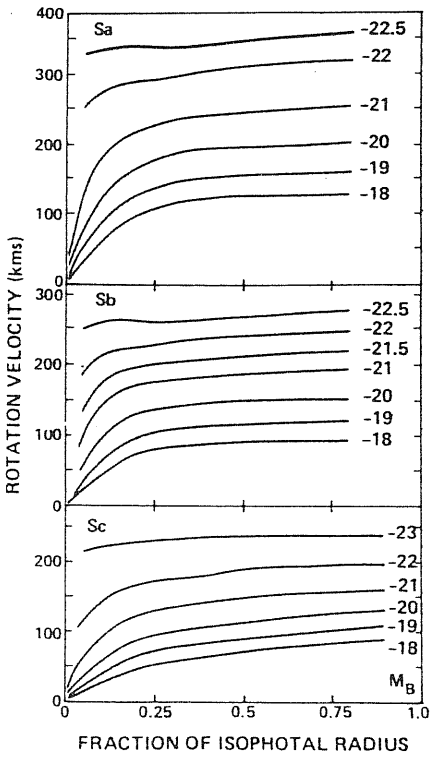

Figure 2.3: Rotation curves of Rubin *et al.* sample plotted as functions of isophotal radius, R_{25}, from (top) Sa galaxies of successive luminosities, (middle) Sb galaxies, and (bottom) Sc galaxies.

or rising] the ratio of dynamical-to-luminous mass increases with increasing radial distance. Locally the ratio of the dynamical mass to the blue luminosity increases by a factor of 10 over the outer 90% of the optical disk.
Rubin, Thonnard, Ford and Burstein (1982) analysed the implications that the progression of the shape of the rotation curves with luminosity would have on local density. Since

$$(R_m)_{high} = \frac{1}{3}(R_m)_{low}$$

and at the same value for $V^2 = V_m^2$, we get

$$\rho_{high} \cong \frac{V_m^2}{(R_m)_{high}^2} = \frac{V_m^2}{\frac{1}{9}(R_m)_{low}^2} = 9\frac{V_m^2}{(R_m)_{low}^2} \cong 9\rho_{low}.$$

Recalling that R_m is a radius which encompasses a fixed given mass, galaxies with small radial scale length (higher luminosity Sc) will have higher density at all radii.

Since an Sb galaxy will have a higher rotational velocity by 0.1 dex (26%) respect to an Sc galaxy (RFTB 1982) of the same size, i.e. with the same luminosity, the Sb will have a mass density higher by V^2, or 0.2dex (58%), as one can easily deduce from eq. 2.3. It follows from the rotation curve amplitude that an Sb has higher density at every nuclear distance than an Sc of equivalent luminosity; the same could be said for an Sa with respect to an Sb (RFTB 1985). So the Hubble sequence from Sa to Sc is a sequence of decreasing local density.

2.2.4 Integral Mass Distributions

Both the similarity in the form of rotation curves among galaxies of very different optical morphologies and the difference in the form of rotation curves among galaxies of similar optical morphologies, have prompted Rubin and Burstein (1985) to ask what could be learned about the overall mass distributions from the overall rotation curves.
Mass distributions for the 60 galaxies were derived using eq. 2.1 and the observed rotation velocity curves. The rotation curve for each galaxy was plotted in a $(\log V, \log R)$ graph and values were interpolated at intervals of 0.1 in $\log R$ and converted to integral mass distribution. The mass scale length was calculated by making use of the entire mass distribution: this means that mass curves in a $[\log M(R), \log R]$ plot are globally displaced in both coordinates in order to produce minimum scatter.
Rubin and Burstein identify three different types of integral mass distributions in the $\log M, \log R$ plane. Both the ordinate and the abscissa in this plane are scaled quantities:

- x axis is the radius in units of R_m, mass scale length,

- y axis is the mass in units of M_m, the fiducial mass.

The integral mass distribution of many Sb and even the Sa galaxies have the same form as the Sc's.

- Type I mass distribution contains 11 Sc, 5 Sb, 4 Sa;
- Type II mass distribution contains 2 Sc, 4 Sb, 5 Sa;
- Type III mass distribution contains 1 Sc, 5 Sb, 4 Sa.

All types show a significant curvature over the observed (scaled) range radii. Rubin and Burstein noticed that there was no correlation between the mass distribution types and the bulge to disk ratio or morphology (see Fig. 2.4). They reported the example of NGC 3198 belonging to the Type II mass distribution: although NGC 3198 is virtually a bulgeless Sc galaxy with a rotation curve known to a distance almost 3 times its optical diameter, its integral mass distribution matches that of other galaxies: NGC 6314, UGC 10205, two Sa's whose bulge-to-disc ratios are among the highest in the sample. They observe that:

- Mass types are basically a progression in the form of the rise of the rotation curve relative to the radius at which $V(R)$ becomes nearly flat. Faster rising rotation curves have less curvature in the $[\log M, \log R]$ plot. Galaxies of Type I mass distribution, which includes many Sc galaxies, have rotation curves rising faster than galaxies with Type III mass distributions (which include large bulged galaxies).
- Integral mass Type III is identical to the mass distribution which would be derived for a massless disc in coplanar rotation within an isothermal mass sphere.

2.2.5 Masses and Mass to Luminosity Ratios

Considering all the Sa, Sb and the Sc galaxies, RTFB find that the ratio of mass interior to R_{25} to the total blue luminosity is nearly constant within a Hubble type, i.e. it is independent of luminosity:

$$\frac{M(R_{25})}{L_B} = 6.2 \pm 0.6 \quad Sa$$

$$\frac{M(R_{25})}{L_B} = 4.5 \pm 0.4 \quad Sb$$

$$\frac{M(R_{25})}{L_B} = 2.6 \pm 0.2 \quad Sc$$

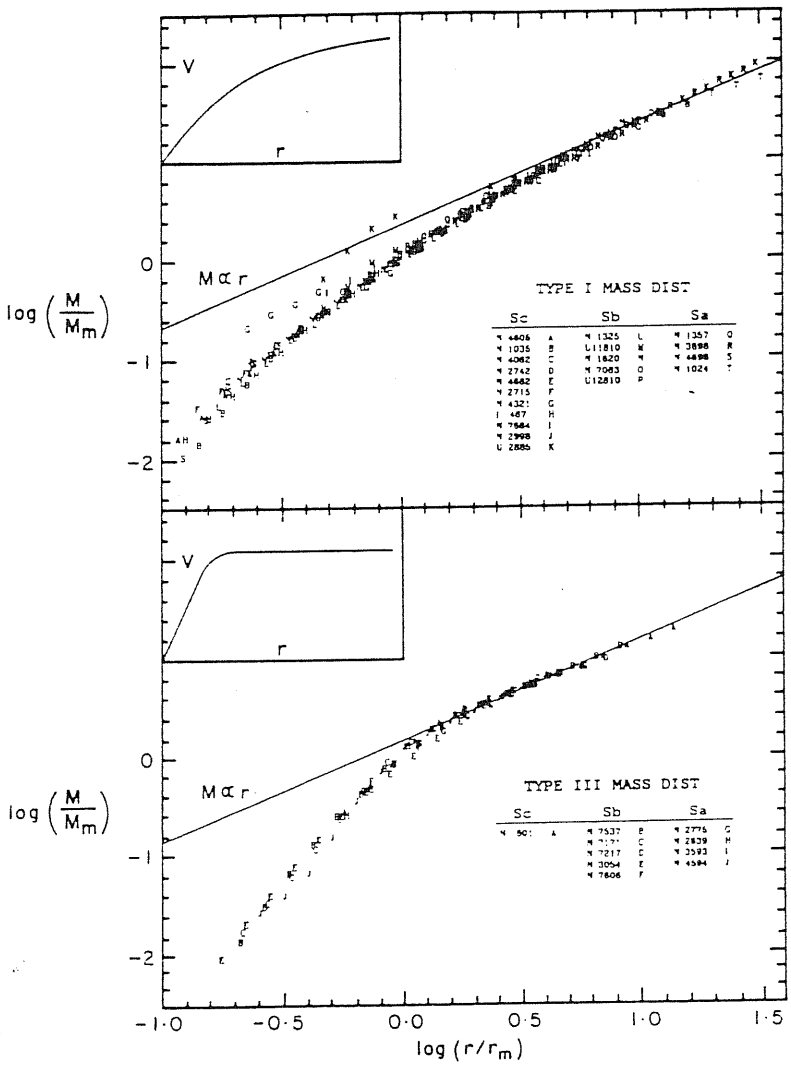

Figure 2.4: Integrated mass $M(R) = V^2R/G$ as a function of radius R for mass types I and III. Mass type II is intermediate. Each galaxy has separately been scaled by a mass scale M_m and a radius R_m (as explained in the text). The line $M \propto R$ is the mass distribution for a flat rotation curve. The inset shows schematic rotation curve types corresponding to the mass types.

These differences in the average mass-to-blue-luminosity-ratios among different Hubble types are significant and can be derived in a more fundamental way. It is well known (de Vaucouleurs 1959) that there exists a close relationship between isophotal radius and luminosity of spiral galaxies ($L_B \propto R_{25}$) which is essentially independent of the Hubble type. The reported results are the necessary consequences of the lack of dependence of the luminosity–radius relation on Hubble type and of the dependence of the mean value of V_{max} on Hubble type. If we write

$$V^2(R_{25}) = \frac{M(R_{25})}{R_{25}} = \frac{M(R_{25})}{L_B}\frac{L_B}{R_{25}}$$

one obtains at fixed luminosity for the Sb's and Sc's

$$\frac{V^2(R_{25})_{Sb}}{V^2(R_{25})_{Sc}} = \frac{\left(\frac{M(R_{25})}{L_B}\right)_{Sb}}{\left(\frac{M(R_{25})}{L_B}\right)_{Sc}} = \frac{4.4}{2.6} = 1.7$$

At fixed luminosity, the mass-to-blue-luminosity-ratio of Sb's should be a factor of 0.2 dex= 1.6 higher than that of the Sc's as observed. At equal luminosity, the rotational velocity for an Sb galaxy will be higher than that for an Sc by the square root of the ratio of their mass to blue luminosity ratios, $\sqrt{1.7} = 1.3$, as observed.

What Fraction of the Mass is not in the Disk?
The approximately constant dynamically determined M/L values [6 : 4 : 2] compared with those predicted from stellar models [3 : 2 : 1] suggested that M_{Dyn}/M_{Lum} is of order 2, independent of Hubble types and luminosities. RFTB suggested that the visible material in spiral galaxies contributes of order half of all mass within the optically defined isophotal radius.

2.2.6 Conclusion

Rubin and Burstein (1985) derived that:

- the mass distribution in spiral galaxies is a combination of luminous and non luminous material at all radii in the galaxy,
- the relative size of the bulge in spiral galaxies is not of importance in determining the integral mass distribution form,
- the form of mass distribution in spiral galaxies is determined by a process that is independent of absolute sizes and mass densities of the galaxies,

- a comparison of measured M/L values with those predicted from model stellar populations (Larson and Tinsley, 1978) gives evidence that the ratio of dark-to-luminous matter is not a function of either Hubble class or luminosity, and that $M_{tot}/M_{lum} \cong 2$ interior to R_{25}.

The very regular integral mass distribution of a spiral galaxy is determined by factors which are apparently independent of its well known global properties.

2.3 Evidence for Dark Matter from HI Rotation Curves

2.3.1 What are the characteristics of the rotation velocity curve predicted by the light distribution

A typical spiral galaxy consists of two distinct photometric components: a thin disk and a rather concentrated bulge. The bulge can be approximated by a de Vaucouleurs' (1959) $R^{1/4}$ law and the surface luminosity density of the disk decreases with radius following an exponential law

$$I = I_0 \exp\left(-\frac{R}{R_D}\right)$$

where R_D is the disk scale length. The surface brightness distributions of about half of the galaxies surveyed so far can indeed be accounted for by the sum of two such components (Freeman 1970, Boroson 1981, Simien and de Vaucouleurs 1986, van der Kruit 1987).

As a general property, colours show no substantial gradient across the disk (Griersmith, 1980); this strongly suggests a constant *stellar mass-to-light ratio* for each optical component of a spiral galaxy. If we assume constant M/L ratios for bulge and disk, it is possible to compute the total mass distribution under these geometrical assumptions and, using the Newtonian law of gravity, the circular velocity curve can be derived. The predicted rotation curve for a spheroid shows a steep rise for small R, peaks at 0.3 R_e and then declines (de Vaucouleurs 1959). The curve for the thin disk peaks at 2.2 disk scale lengths and then tends asymptotically to the Keplerian decline. In the interval between these two characteristic radii, the shape of the rotation curve depends on the ratio of the spheroid to the disk mass, and beyond them, at about 3 R_D, the rotation curve will start declining. Optical rotation curves extend up to a few disk scale lengths (typically $1.5 < R_D < 3.5$), and even in the most favorable case the rotation curve of an exponential disk has decreased by only 8% relative to its maximum value. In other words, with optical data alone it is not easy anyway to see the Keplerian decline of the rotation

curve. A combined model with bulge and disk can produce a circular velocity that is nearly flat out to $3R_D$.

A flat rotation curve in itself does not imply the presence of a hidden component: to establish the existence of dark halos it is necessary to measure the circular velocity well beyond the turnover radius of the disk. The HI rotation curves, after an initial rise, are all approximately flat out to the last measured point, (Bosma 1981; van Albada et al. 1985, van Albada and Sancisi 1986; Sancisi and van Albada 1987; Begeman 1986) at 5 or more scale lengths of the exponential distribution of light in the disk.

If the gravitational field results from the distribution of luminous matter, mapped by the light, the curves should begin their decline beyond about 2.5 disk scale lengths. If a discrepancy is found between the shape of the observed and the predicted rotation curves, this is attributed to the presence of dark matter (DM). The amount and the distribution of DM can be derived by calculating rotation curves from the distribution of light and by comparing them with the observed ones. Any excess in the observed rotation curve provides a measure of the contribution of a dark component.

2.3.2 HI Rotation Curves

Kent (1987) has analysed the luminosity profiles and the rotation curves of 16 galaxies. All objects have HI rotation curves, and a few have also optical rotation curves. These are especially valuable because HI observations seldom have adequate spatial resolution to map the inner parts of a galaxy.

Van Albada *et al.* (1985) have studied NGC 3198 and NGC 2403. These two galaxies were chosen because of their large and relatively unperturbed hydrogen disks seen at inclinations of about 50^o to 80^o. They are both Sc galaxies, NGC 3198 is at 9.2 Mpc, NGC 2403 at 3.2 Mpc. NGC 3198 has a regular velocity field which agrees with that for a disk in differential rotation; the HI distribution extends to at least 2.7 R_{25}=1.9 Holmberg radius, which corresponds to 11 scale lengths of the disk. The HI rotation curve for NGC 2403 extends to 2.3 R_{25} or 9.5 R_D.

One problem with interpreting HI rotation curves (and rotation curve data in general) is that it is not always clear whether they represent true circular motions in galaxies[1]. Another problem connected with the HI rotation curve is the presence of warps at the edges of the hydrogen distribution; in this case we have not coplanar motion and in principle centrifugal equilibrium does not hold.

[1]Centrifugal equilibrium is usually assumed (Rubin *et al.*1982), otherwise corrections for asymmetric drift should be computed (Binney and Tremaine 1987)

2.3.3 Rotation Curve Models

The mass distribution in a spiral galaxy is modeled as the sum of three discrete components: the bulge, the disk, and the halo. Then the circular velocity V_c in a galaxy at a radius R, is given by

$$V_c^2(R) = R\frac{\partial \Phi}{\partial R} \qquad \Phi = \Phi_{disk} + \Phi_{bulge} + \Phi_{halo} \tag{2.4}$$

where Φ_{disk}, Φ_{bulge}, and Φ_{halo} are the gravitational potentials generated by the disk, bulge, and halo matter distributions respectively.

The bulge and the disk mass distributions are given by their luminosity distributions apart from unknown mass-to-light ratios M/L which are assumed to be constant within each component. The modelling is done by parametrizing each component with some empirical density law having scale parameters, determined by fitting the laws to the observed light profile of the galaxy (Kent 1986, 1987, 1988, van Albada *et al.*1985, van Albada and Sancisi 1986, Sancisi and van Albada 1987).
The halo mass distribution can be either parametrized or it is derived from the observed rotation curves. For sake of simplicity, usually bulge and halo are supposed to be spherically symmetric and the disk to be infinitely thin. These density laws are listed in the following.

Disk
One can use Toomre models for disks (Toomre 1962) and their rotation curves. The Poisson equation in cylindrical coordinates takes the form

$$\frac{1}{R}\frac{\partial}{\partial R}R\frac{\partial \Phi}{\partial R} + \frac{\partial^2 \Phi}{\partial z^2} = 4\pi G\rho = 4\pi G\Sigma(R)\delta(z) \tag{2.5}$$

where $\Sigma(R)$ is the surface density profile, and $\delta(z)$ is Dirac's delta function. Applying the Fourier Bessel Transformation to the above equation, it becomes

$$\frac{\partial \Phi}{\partial R} = 2\pi \int_0^\infty a\Sigma(a)H(a,R)da \tag{2.6}$$

where

$$\begin{aligned} H(a,R) = \textstyle\int_0^\infty tJ_0(at)J_1(Rt)dt &= \frac{2}{\pi aR}[K(k) - \frac{E(k)}{1-k^2}] \quad k = \tfrac{R}{a} \quad (R < a) \\ &= \frac{2E(k)}{\pi R^2(1-k^2)} \qquad\qquad\qquad\qquad\quad (a < R) \end{aligned}$$

$H(a,R)$ is a Green's Function, and K(k) and E(k) are complete elliptic integrals of the 1^{st} and 2^{nd} kind respectively (Toomre 1963).

Bulge

For a spherically symmetric distribution, one has simply

$$\frac{\partial \Phi}{\partial R} = G\frac{M(R)}{R^2}$$

where M(R) is the mass interior to radius R. The profile decomposition yields the bulge profile as a projected density Σ, so two integrations are required to derive M(R)

$$\begin{aligned} \rho(s) = & \quad -\frac{1}{\pi}\int_s^\infty \frac{\mathrm{d}\Sigma}{(x^2-s^2)^{\frac{1}{2}}} \\ M(R) = & \int_0^R 4\pi s^2 \rho(s)\mathrm{d}s. \end{aligned} \tag{2.7}$$

With some manipulation (Kent 1986), these integrals can be combined to yield

$$M(R) = \int_0^r 2\pi x\Sigma(x)\mathrm{d}x + \int_r^\infty \left[4\sin^{-1}\left(\frac{r}{x}\right) - 4r(x^2-r^2)^{-\frac{1}{2}}\right] x\Sigma(x)\mathrm{d}x$$

Halo

The form of the halo density profile is not well constrained a priori other than by the fact that it produces an asymptotically flat rotation curve. It has been modelled with an isothermal sphere (Carignan and Freeman, 1985) or with a suitable family of density distributions that have this property. One of these density laws is

$$\rho = \frac{\rho_0}{1+\left(\frac{R}{a}\right)^\gamma} \tag{2.8}$$

where ρ_0 and a are adjustable parameters. This has been used by van Albada and Sancisi (1986) in their model of NGC 3198 and NGC 2403. The same density profile with $\gamma = 2$ has been used by Kent (1986, 1987). In this case eq. 2.8 can be rewritten as

$$\rho = \frac{\sigma^2}{2\pi G(R^2+a^2)} \tag{2.9}$$

This profile produces a rotation curve

$$V_c^2(R) = 2\sigma^2\left[1-\left(\frac{a}{R}\right)\tan^{-1}\left(\frac{R}{a}\right)\right] \tag{2.10}$$

with asymptotic velocity of $\sqrt{2}\sigma$ (see Fig. 2.5).

Model Fitting

A model rotation curve is computed from observed bulge and disk profiles and the assumed halo profile. The condition for centrifugal equilibrium gives

$$V_c^2 = V_B^2 + V_D^2 + V_H^2. \tag{2.11}$$

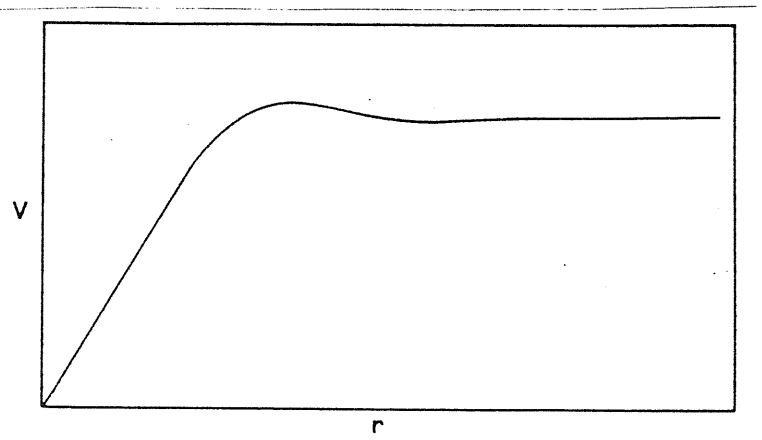

Figure 2.5: Schematic rotation curve of massless test particles in an isothermal sphere.

There are 4 free parameters: the bulge and the disk M/L ratios, and the scale parameters σ and a for the halo. These parameters can be determined by a least square fit to the observed rotation curve profile (the fit is actually made to V_c^2). The dependence of V_c on a is non linear so an iterative fit needs to be done (Kent 1986). It is necessary to constrain the disk or halo parameters in some way.

2.3.4 Maximum Disk Method

It is assumed that the stellar component dominates the mass distribution in the inner part of a galaxy (Kalnajs, 1983). The M/L ratio of the disk (and the bulge) are set to the maximum value consistent with the matching of the inner part of the rotation curve. The procedure consists in ignoring the halo component and in solving for bulge and disk M/L ratios in a region inside the radius at which the rotational velocity due to the disk component alone reaches a maximum. Any excess in the rotational velocity at large radii is then attributed to a dark halo component (see Fig. 2.6).
In this case, no a priori assumptions are made on the M/L ratios for the bulge and disk components.

Kent (1987) shows that in no case does the maximum-disk solution alone produce a good fit to an entire rotation curve: a halo component is always required. This need for dark matter contrasts with the case where optical rotation curves alone are used; this happens because the HI rotation curves extend much further out

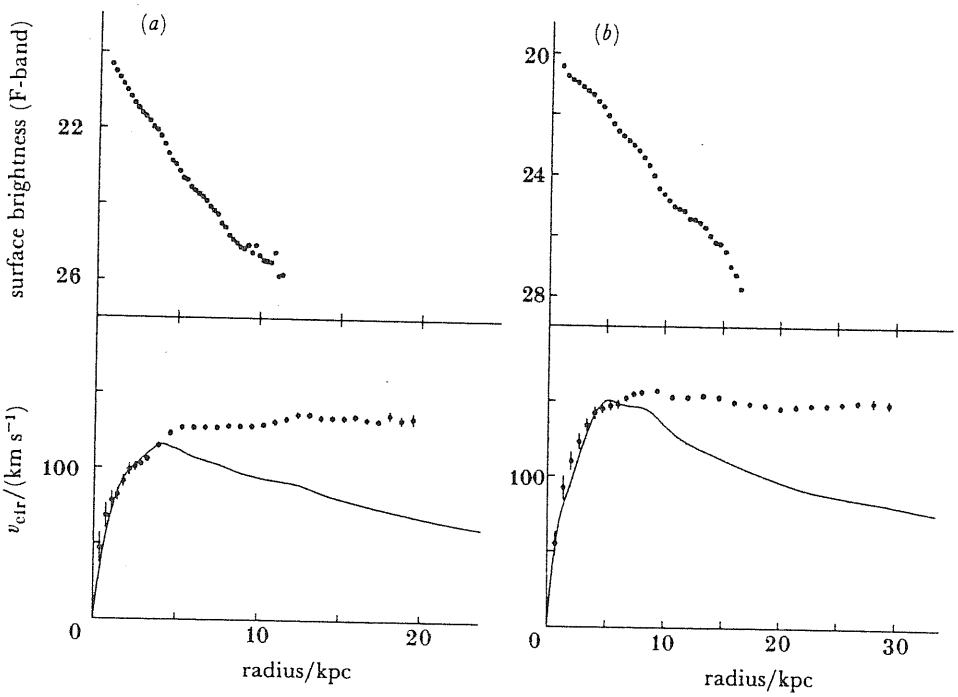

Figure 2.6: Light profiles and rotation curves for two galaxies ((a) NGC 2403 and (b) NGC 3198) with extended, symmetrical HI disks. Upper panels: luminosity profile from Wevers (1984). Lower panels: observed rotation curves and rotation curve calculated from the light profile and the distribution of HI, including a correction for helium (solid lines). The contribution of the stars to the calculated rotation curve contains the M/L ratio as an arbitrary scale factor. Maximization of the disk mass (stars only), while matching the observed rotation curve, gives $M/L_B = 1.9$ for NGC 2403 and 4.0 for NGC 3198.

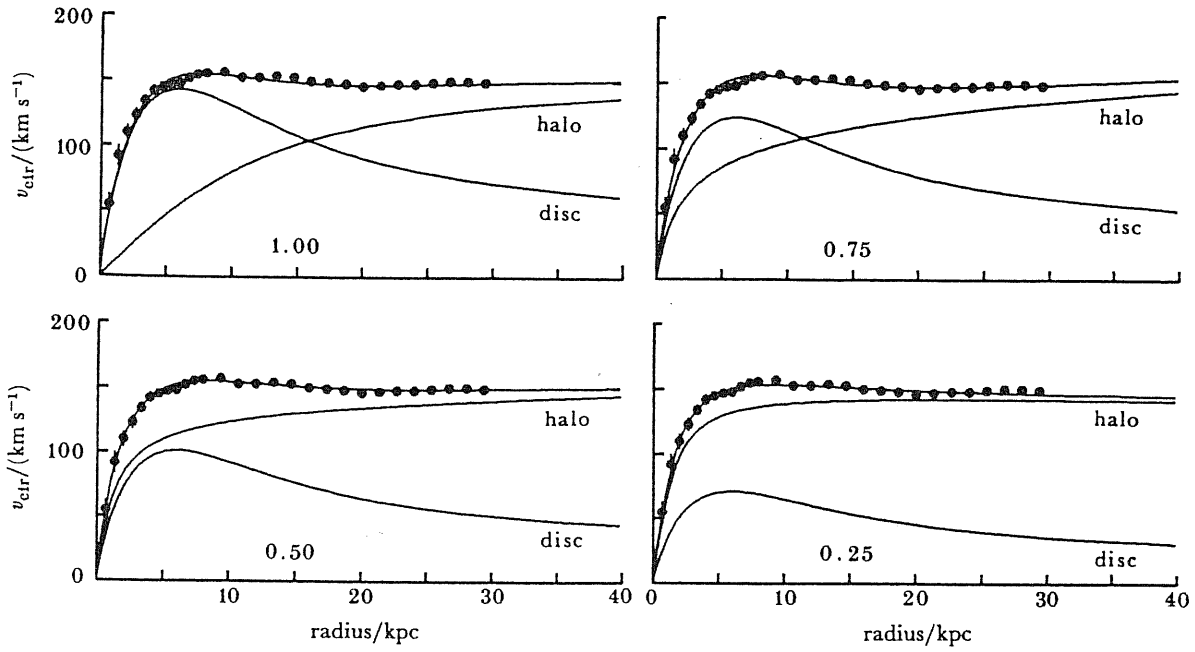

Figure 2.7: Fits of exponential disk and halo to the observed rotation curve (dots) for NGC 3198. Disk models with maximum mass (upper left) and also with masses 0.75, 0.50, and 0.25 times the maximum mass are shown.

than the optical curves, and they appear to be able to sample at galactocentric radii where the halo mass dominates.
Unfortunately even with the leverage provided by extended HI rotation curves, the various parameters are still highly coupled in the least squares solution. The reason is that the chosen parametric form for the halo density law produces a rotation curve that by itself makes a reasonable fit to the observed rotation curves.

Van Albada *et al.* (1985) and van Albada and Sancisi (1986) made models for NGC 3198 and NGC 2403 galaxies. These models showed that a good fit to the rotation curve is obtained by choosing the maximum disk and a halo, but it was not possible to calculate a lower limit for the M/L ratio of the disk. Equally good fits could be obtained for any assumed disk mass less than the maximum value (see Fig. 2.7). Their first model for NGC 3198 consists of a disk with the largest possible mass and of a halo. The upper limit for V_{max}(disk) was 150 km s^{-1} but this choice would require a halo with hollow core which is implausible.

A reduction of V_{max}(disk) to 140 km s^{-1} is sufficient to allow a halo with a density that decreases monotonically with galactocentric distance . The parameters that van Albada *et al.* deduced for the halo are not unique–the halo exponent γ and

the scale length a are derived in a correlated fashion

$$1.9 < \gamma < 2.9 \qquad 7 < a < 12$$

while $\rho(R = 0)$ is determined with less uncertainty. Defining the core radius of the halo mass distribution by $\rho(R_c) = 2^{-\frac{3}{2}}\rho(R = 0)$ we have

$$R_c = (2^{\frac{3}{2}} - 1)^{\gamma} a$$

The fitting made by Van Albada *et al.* gave a subjective 95% confidence interval for R_c

$$9.6 < R_c < 15.4$$

(R_c in kpc). This is an upper limit for R_c: for smaller disk masses R_c decreases. The main difference between the resulting halos is the core radius: it decreases from $R_c = 12$ kpc for the maximum disk mass to 1.7 kpc when the dark halo dominates, whereas for the exponent they obtained $\gamma \cong 2$ for all models.

2.3.5 Value of M/L for the Disk

Is the amount of visible matter negligible with respect to the amount of DM? Or is the maximum-disk model more reasonable?
The available data cannot discriminate between disk models with either low or high M/L but there are arguments which suggest that the true M/L ratio of the disk is close to the maximum value:

- measurements of mass and luminosity density in the solar neighborhood yield $M/L_V \cong 3.1 \pm 0.6\ M_\odot/L_\odot$ (Bahcall 1984). This value is of the same order as the M/L values of the maximum disk case for NGC 2403 (M/L=2.61) and NGC 3198 (M/L=5.73),

- shapes of the rising parts of rotation curves agree with those expected for a disk (or bulge+disk) with scale length as given by the light distribution (measured photometrically),

- the close relationship between the luminosity of spiral galaxies and the maximum circular velocity implied by the Tully-Fisher relation indicates that after all it is the amount of visible matter that determines the maximum rotational velocity in a galaxy. If this were not the case, the amount of DM inside say 2.5 disk scale lengths should be related in a unique way to the amount of visible matter,

- the presence of two armed spiral structure. Well developed two armed spiral structure appears possible only if the disk mass is at least 70% of the

maximum disk mass (van Albada et al. 1985). If this is lowered to 50% of the maximum disk mass, the growth of the two-armed spiral structure is definitely inhibited and only multiple armed features develop.

2.3.6 Conclusions: Disk–Halo Conspiracy

We have seen above that the rotation curves of spirals are remarkably flat and featureless. It is clear that, if the disk mass exceeds 70% of the maximum disk mass, the flat behaviour of the observed rotation curve between 3 R_D and the last measured point is due to a falling rotation curve for the disc and a rising one for the halo. It seems implausible that two supposedly independent components of a galaxy, a flat disk and a more or less spherical halo, could produce such a result as a rule. If stellar matter dominates in the inner part of a galaxy and DM outside, then the peak rotation velocity due to the luminous component must be about the same as that due to the halo in order that they combine to produce the observed flat curve. This implies that the luminous matter also controls the approximately constant value of the circular velocity in the outer regions.
This apparent coincidence is referred to as the disk halo conspiracy. A way around the disc-halo conspiracy while keeping the luminous matter dominant in the inner regions, would be to relax the initial assumption of constant M/L for the disk. The mass-to-light could be approximately constant in the inner regions and increase gradually in the outer parts with a functional form M/L(r) similar for all galaxies. An inspection of the various rotation curve fits given by Kent shows that the individual components display a considerable variety of shapes and that there is no single relation between the disk and halo contributions. We can characterize the conspiracy by comparing the peak velocity from the maximum disk solution with the asymptotic (or last measured) rotation velocity. In less luminous objects the peak disk velocity is smaller than the asymptotic velocity: by 30% in extreme cases. Since the true M/L ratio of the disk is likely to be lower than its maximum disk value, this short fall is likely to be even larger. Other galaxies show the opposite behaviour: in NGC 4736 the peak of the bulge+disk velocity is larger than the asymptotic halo velocity by 30% or more. Kent finds that whereas the ratio between the peak disk velocity and the halo velocity is not universal, there is a reasonably good correlation of this ratio with the galaxy luminosity.

2.4 Evidence for Dark Matter from Optical Rotation Curves

2.4.1 Observed Profiles of Optical Rotation Curves of Field Spiral Galaxies

As we have already said the luminosity profiles of most spiral galaxies are decomposed into two main components (Freeman 1970, van der Kruit 1987): a very concentrated bulge and a thin disc, whose surface luminosity density decreases with radius as

$$I(R) = I_0 \exp\left(-\frac{R}{R_D}\right), \tag{2.12}$$

I_0 being the central surface luminosity density and R_D the exponential disk scale-length. The bulge is usually less luminous and smaller than the disk and its contribution to the equilibrium is usually negligible at $R \geq 2R_B$. From eq. 2.12 the surface brightness at radius R is

$$\mu(R) = \mu_0 + 1.086\frac{R}{R_D} \tag{2.13}$$

the peak brightness μ_0 having a small scatter among spirals (Freeman 1970, van der Kruit 1987): $\mu_0 = 21.7 \pm 0.4$mag arcsec^{-2} which implies $R_{25}/R_D = 3.0 \pm 0.4$, where R_{25} is the radius at which $\mu_B = 25$.
As colours show no substantial gradient across disks, this strongly suggests a constant stellar mass-to-light ratio in each galaxy. This implies

$$R\left(\frac{\mathrm{d}\Phi}{\mathrm{d}R}\right)_{lum} \cong R\left(\frac{\mathrm{d}\Phi}{\mathrm{d}R}\right)_{disk} = V^2_{disk}(R) \tag{2.14}$$

where Φ_{lum} is the gravitational potential due to all luminous matter, and $V_{disk}(R)$ is the circular velocity of the exponential thin disk model (Freeman 1970),

$$V^2_{disk} = G\frac{M_D}{R_D}F(R). \tag{2.15}$$

Here M_D is the disc mass, $x = R/R_D$, and $F(x) = (1/2)x^2(I_0K_0 - I_1K_1)$; I_n and K_n are modified Bessel functions of order n evaluated at $x/2$.
As a very general property, virtually all extended optical rotation curves show a constant gradient in the region $R_1 \cong (0.1 - 0.2)R_{25} \leq R \leq R_{25}$. The observed rotation velocities V_{obs}, collected from the literature by Persic and Salucci (1990) and whose main characteristics are summarized in Tab. 2.2,

TABLE 2.2
Observational Data

Ident.	M_B	R_{opt}	V_{25}	∇_{obs}
NGC 488	−22.52	33.3	385	0.20
NGC 753	−22.60	20.8	222	0.05
NGC 1035	−19.69	7.4	140	0.41
NGC 1085	−22.55	32.0	310	0.01
NGC 1300	−21.47	20.8	200	0.00
NGC 1325	−20.87	18.2	212	0.46
NGC 1417	−22.28	25.6	329	0.21
NGC 1421	−20.80	26.6	200	0.42
NGC 1620	−21.90	28.5	260	0.36
NGC 2336	−22.50	50.6	251	0.03
NGC 2708	−20.60	13.8	293	0.52
NGC 2715	−21.29	28.5	158	0.39
NGC 2742	−20.54	12.2	192	0.39
NGC 2815	−22.00	29.4	284	0.07
NGC 2997	−21.19	21.1	160	0.00
NGC 2998	−22.00	26.6	229	0.14
NGC 3054	−21.63	17.3	264	0.22
NGC 3198	−20.60	13.8	162	0.16
NGC 3200	−22.87	47.4	287	0.13
NGC 3145	−22.58	35.8	275	0.08
NGC 3223	−22.64	37.1	255	0.02
NGC 3672	−21.75	19.8	189	0.06
NGC 3963	−22.37	23.7	178	0.02
NGC 3992	−21.70	28.2	273	0.10
NGC 4062	−19.50	13.1	168	0.52
NGC 4254	−21.51	14.1	210	0.27
NGC 4321	−21.53	22.1	223	0.22
NGC 4565	−23.20	42.2	254	0.00
NGC 4605	−18.59	3.2	119	0.66

are interpolated in this region with the simple linear function

$$V(R) = V_0 + V_1 \left(\frac{R}{R_{25}}\right) \tag{2.16}$$

which reproduces the observed circular velocity at a high level of confidence. Therefore, in the range $R_1 \leq R \leq R_{25}$ we can assume a simple straight line to represent the circular velocity.

2.4.2 Is There DM?

In order to understand at which radius in each galaxy the discrepancy between visible and dynamical mass begins we need a local mass indicator which avoids the problem of translating disk luminosity into disk mass. Let us introduce the logarithmic gradient of the rotation velocity curve defined as

$$\nabla = \frac{R}{V(R)} \frac{\mathrm{d}V(R)}{\mathrm{d}R}$$

For the rotational velocity generated by an exponential disk distribution of mass, it takes the form (Persic and Salucci 1988)

$$\nabla_{disk} = \frac{I_0K_0 + 0.5x(I_1K_0 - I_0K_1)}{I_0K_0 - I_1K_1} \tag{2.17}$$

and the value of the logarithmic derivative for the observed velocity curves is given by

$$\nabla_{obs} = \frac{V_1 \dfrac{R}{R_{25}}}{V_0 + V_1 \dfrac{R}{R_{25}}} \tag{2.18}$$

The aim is to compare the logarithmic gradients of the circular velocities predicted by the exponential thin disc model with the observed ones.
Obviously if the disk matter were the only component contributing to the dynamics, we would find

$$\nabla_{obs} \cong \nabla_{disk} \tag{2.19}$$

over the whole range of the disk. In each and every galaxy of the sample of Persic and Salucci a dramatic discrepancy is found between these two quantities (see Fig. 2.8). In regions where $\nabla_{disk} > \nabla_{obs}$ this discrepancy can neither be eliminated nor even reduced by introducing possible contributions from a bulge and/or stellar halo.
Bulge: it appears as a point mass to the outer regions. Its contribution to the velocity field is

$$V_B^2 = G\frac{M_B}{R}, \tag{2.20}$$

Observational Data: Continued

Ident.	M_B	R_{opt}	V_{25}	∇_{obs}
NGC 4682	−20.85	15.4	184	0.22
NGC 4800	−20.00	4.2	175	0.15
NGC 5033	−21.30	38.4	212	0.13
NGC 5055	−21.55	18.9	200	0.00
NGC 5290	−21.51	17.6	230	0.09
NGC 5371	−22.60	32.6	240	0.04
NGC 5383	−22.50	19.2	207	−0.06
NGC 5426	−21.24	20.2	157	0.00
NGC 5673	−20.50	11.2	138	0.22
NGC 5905	−21.84	52.8	242	0.14
NGC 5908	−22.00	29.8	352	0.04
NGC 7083	−22.40	38.4	223	0.04
NGC 7171	−21.25	23.7	227	0.13
NGC 7331	−22.40	33.9	226	0.06
NGC 7531	−22.14	12.2	180	0.00
NGC 7537	−21.23	37.1	137	0.00
NGC 7591	−21.21	37.1	195	0.00
NGC 7606	−22.54	37.1	242	−0.12
NGC 7631	−21.17	37.1	205	0.24
NGC 7664	−21.60	37.1	183	0.00
NGC 7723	−21.57	37.1	209	0.00
UGC 467	−20.55	37.1	155	0.20
UGC 807	−21.80	37.1	211	0.00
UGC 2259	−17.50	37.1	93	0.50
UGC 4375	−20.02	37.1	200	0.15
UGC 11810	−21.10	37.1	187	0.14
UGC 12470	−20.05	37.1	160	0.61
UGC 12810	−22.40	37.1	234	0.09
WR 66	−20.77	37.1	170	0.09

Table 2.2: *Column (1)*: name of the galaxy. *Column (2)*: absolute blue magnitude. *Column (3)*: optical radius in kpc, defined as $R_{opt} = 3.2R_D$. *Column (4)*: rotational velocity (in km s^{-1}) at the R_{25} isophotal radius. *Column (5)*: logarithmic derivative of the rotation curve at R_{opt}. This quantity is computed from the parameters of a linear fit $V(R) = V_0 + V_1(R/R_{25})$, to the observed rotation curve such that $\nabla_{obs} = V_1(R/R_{25})/(V_0 + V_1(R/R_{25}))$.

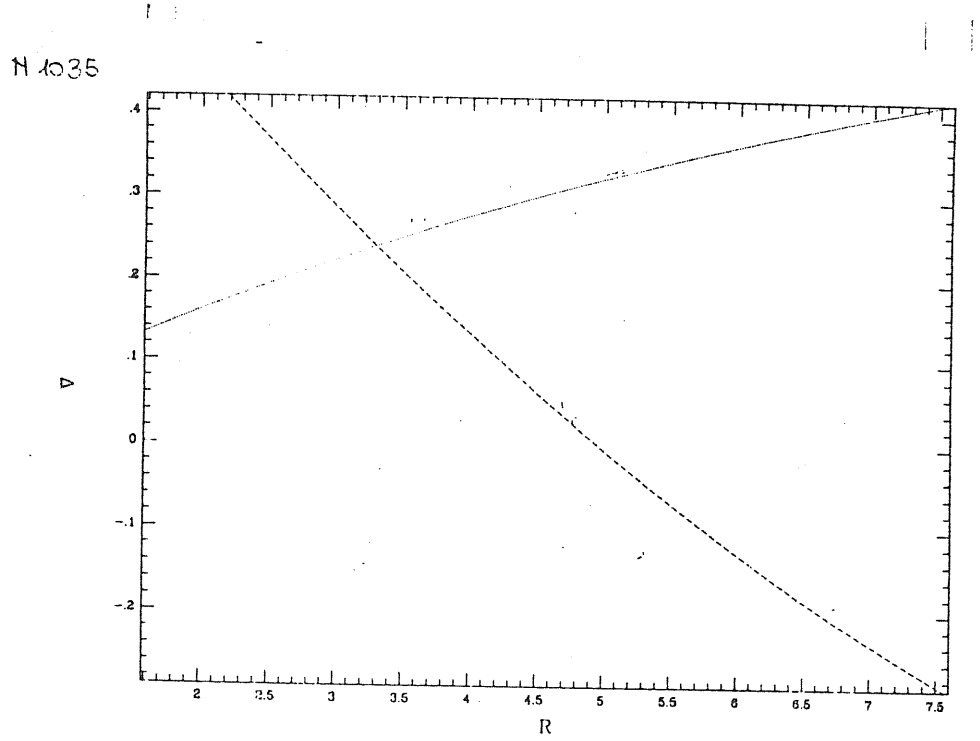

Figure 2.8: $\bigtriangledown_{disk}$(dashed line) and $\bigtriangledown_{obs}$ (solid line) plotted as functions of galactocentric radii (in kpc) for NGC 1035, for the other galaxies in the sample we have the same behaviour.

and the contribution to the logarithmic gradient amounts to

$$\nabla_{bulge} = -\frac{1}{2}. \tag{2.21}$$

If the total velocity field were given by the sum of the bulge and disk components, the total velocity gradient would be even steeper

$$\nabla_{tot} < \nabla_{disk}$$

Therefore, the bulge contribution enhances the observed discrepancy, instead of reducing it.
Stellar halo: the stellar halo or "corona"[2] has a radial density dependence $\rho \propto R^{-3}$. The derived rotation curve has the following radius dependence

$$V_{corona} \propto \left(\frac{\log R}{R}\right)^{\frac{1}{2}} \tag{2.22}$$

and its logarithmic gradient, evaluated at $R_{25} \cong 3.2R_D$ is negative

$$\nabla_{corona} \propto \frac{1}{2}\frac{(\log R)^{-1} - 1}{R} \tag{2.23}$$

Also in this case, the rotation curve derived using the stellar halo in addition to the disk mass component will be in disagreement with the observed one. Its logarithmic gradient, evaluated at $3.2R_D$, will show even larger discrepancies than those derived in the case of a pure disk matter distribution.

In the outer regions of the optical disk, the only way to solve the discrepancy between the luminous and dynamical velocity curves is by allowing the presence of a dark matter component having $dV^2_{halo}/dR > 0$ (Persic and Salucci 1988). This implies that its density radial dependence should be $\rho \propto R^{-|\gamma|}$ with $|\gamma| < 2$. In regions where $\nabla_{disk} > \nabla_{obs}$ the situation is more open and a bulge and or a stellar halo could be introduced to eliminate it.

2.5 Dark Matter and Disk Stability

2.5.1 Global Behaviour of Cold Disk Galaxies

From the investigation carried out by Kalnajs (1972) on disk stability there are theoretical arguments to believe that highly flattened disks supported mainly by rotation are subject to large-scale bar-like instabilities. Yet many galaxies exist

[2]We use this term not to generate confusion between stellar and dark halos

where most of the light originates from an apparently flat rotating disk, and where the random stellar motions appear to be small compared to the systematic circular motions: i.e. they are apparently cold. Our own galaxy is such a system: in a column through the solar neighborhood the RMS random velocity of the late type dwarfs that dominate the stellar mass contribution is about 60 km s^{-1}compared to a rotation speed of about 220 km s^{-1}; it does not seem to suffer from any large-scale, large-amplitude, short-time-scale instability. So is a "cold" rotating disk of stars truly unstable? If so, how can we account for the apparent stability of our galaxy? Futhermore, what (if any) critical value of the random component of the total kinetic energy is needed to prevent these instabilities and what could be done to add stability to a flat system whose disk would be, by itself, unstable?

2.5.2 Numerical Work on Disk Stability

A variety of N-body simulations of galactic disks have been carried out since 1970. One of the earliest was carried out by Hohl (1971). In his simulations the initial surface density and potential of the 100,000 stars were those of a Kalnajs disk

$$\Sigma(R) = \Sigma_0\sqrt{1-\frac{R^2}{a^2}} \quad ; \qquad \Phi_0(R) = \frac{1}{2}\Omega_0^2 R^2, \tag{2.24}$$

where $\Omega_0 = \sqrt{\frac{1}{2}\pi^2 G\Sigma_0/a}$. Hohl chose the initial distribution function of the stars to be the Schwarzschild one; and the radial velocity dispersion $\sigma_R(R)$ was chosen so that $Q(R) = 1$ at all radii, where Q is the parameter that satisfies the Toomre stability criterion (Toomre 1964, 1974). This distribution function is not the exact solution of the collisionless Boltzmann equation [the Kalnajs solution is exact, but it is a singular solution] but it closely resembles the velocity distribution in the solar neighborhood. To obtain the equilibrium, Hohl ran the program for several orbital times while constraining the gravitational field to remain radial. After 8 orbital times, with the disk now in equilibrium, Hohl removed the constraint that the gravitational field should remain radial. The resulting evolution is dramatically different: in less than two orbital times, the disk evolves into a bar-like structure. At later times the model settles into a nearly axisymmetric disk with large random velocities. Hohl's results are consistent with the analytic studies of the normal modes of the Kalnajs disk. The crucial difference between the stable disk and the earlier unstable one is the velocity dispersion: disks with large velocity dispersion (hot disks) are not subject to bar instabilities, while cold disks are unstable.

Ostriker and Peebles (1973, hereafter OP) investigated the importance of the bar instability in differentially rotating disks. They studied a direct 300-body simulation of a truncated Mestel disk with $Q = 1$. An N-body system in equilibrium

satisfies the virial theorem in the form

$$T + \frac{1}{2}\Pi = \frac{1}{2}W \tag{2.25}$$

where T is the kinetic energy of rotation, 1/2 Π is the kinetic energy in random motions and W is the potential energy. If we divide everything by $|W|$, we get

$$t + \frac{1}{2}u = \frac{1}{2} \qquad 0 \leq t \leq \frac{1}{2} \tag{2.26}$$

and the relative magnitudes of t and u represent the relative importance of "rotation" and "pressure" for maintaining equilibrium. Using this normalization it is straightforward to see that $\Pi/T = t^{-1} - 2$. OP noticed that their N-body models were stable if $t < t_{crit} = 0.14 \pm 0.02$ and that this limit was similar to the stability criterion for bar-like modes in Kalnajs disks, $t < \frac{1}{2}\Omega^2/\Omega_0^2 = 0.1286$. $t \cong 0.14$ implies that $\Pi/T > 7.14 - 2 = 5.14$.
The behaviour of their simulations of a cold disk ($u/t \ll 1 \rightarrow t \cong 0.50$) was the following: during the first rotation time period the system of particles goes from a symmetric disk to a highly non axisymmetric bar-like structure, which tends to dissolve and approach rough axial symmetry again. After one orbital period, t is roughly comparable to what was indicated as the critical value in analytic studies of fluid models. When t has fallen to the range 0.1-0.2 further changes are slower, and the system appears to be approaching a stationary state.
OP were the first to point out the grave consequences of the bar instability for the Galaxy and other disk galaxies. For our Galaxy, if the values of the random and rotational velocity listed above are roughly constant across the disk, then $\Pi/T \cong 0.15$, which is much less than the value of 5.1 needed for stability according to their criterion.
N-body simulations of a wide range of disk models have subsequently been carried out (Sellwood 1981, Zang and Hohl 1978, Efstathiou *et al.* 1982), and these have been supplemented by linear normal mode calculations (Zang 1976, Kalnajs 1978). They confirm that if most of the kinetic energy of a disk is in rotational rather than random motion, then the disk is usually strongly unstable to large scale bar-like modes.

2.5.3 Ways to Construct Stable Systems

The first way is the one followed in the course of the evolution of many of the N-body models: the disk heats up until t is approximately 0.14. This state, *a hot flat disk* appears to be a quite satisfactory stable equilibrium, but it does not correspond to the observed stellar motions in the apparently flat spiral galaxy.
The second way could be the following: the system might evolve into an equilibrium rotating bar which is cold (streaming motions dominate over random motions

but the bar is stable against further deformation). This is not a satisfactory model for an ordinary non–barred spiral galaxy.
The third way may be to add another hot component, which stabilizes the total system. Adding a hot disk component reduces to the first alternative and would require an unseen disk component with large mass and largely radial orbits. OP introduced in their N-body simulation a halo, a spherically symmetrical component which did not rotate. They simulated the evolution of the disk by adding halos with increasing masses. The sequence of bar-instabilities and heating of the disk was reproduced in a less pronounced way. A halo mass of 1 to 2.5 times the disk mass appears to be required to reduce the initial value of t to the stable range $t \cong 0.14$. If we write the virial theorem for this system (cold disk with a hot, non–rotating halo) we get

$$T_{disk} + \frac{1}{2}\Pi_{halo} = \frac{1}{2}W_{tot} \tag{2.27}$$

where we have neglected Π_{disk} (cold disk), and $1/2W_{tot} = 1/2(W_{disk} + W_{halo})$. In this system the OP criterion for stability, $t \cong 0.14$, can be satisfied without heating up the disk.
The requirement of the dark halo coming from the stability criterion seems rather compelling. The dark halo introduced in the mass modeling, using photometry and rotation curves (van Albada *et al.* 1985, Kent 1986), seems to sustain only the outer parts of galaxies as pointed out by Kalnajs (IAU Symp. 1987). He outlined that in order to prevent bar like instabilities bulges are better than the dark halos derived according to the maximum disk hypothesis (i.e. halos with a hollow core).

Chapter 3

No Dark Matter: Alternatives

3.1 Classical Framework: Optical and HI Rotation Curves of Field Spiral Galaxies

The flat feature of optical rotation curves was considered in the early 1980's as strong proof of the existence of a DM component, but as early as 1983 Kalnajs showed that the rotation curves of 4 galaxies which are flat or rising can be explained entirely in terms of a constant M/L ratio for the disk.
Moreover, the evidence for DM obtained by Rubin and her collaborators, based on the absence of correlation between optical rotation curves and morphology or Hubble type, has been weakened by Kent (1986, 1988). He has computed the mass models for spiral galaxies in Rubin's *et al.*. sample (1985) deriving the matter distribution from his photometric data. The free parameters in the mass densities are constrained using the rotation curves given by Rubin *et al.*. (1980, 1982, 1985), and the maximum disk hypothesis. Kent obtains different results for the Sb and Sc types on one hand and for the Sa type on the other. For the Sb and Sc subsample he derives that:

- the maximum disc solution provides good fits over the entire velocity profiles for many objects. In other objects the maximum disk solutions fall short only for the last few observed velocity points. The M/L ratios for the maximum disk solution range from 0.79 to 7.78 for the disk, and from 1.47 to 19.5 for the bulge.

- Few measured rotation curves extended much beyond the peak in the predicted disk portion of the rotation curve. Hence the curves are never in the region of a true Keplerian drop off in velocity.

- Ten objects are best fit with no halo at all.

- The flat nature of the measured curves is due to the form of the bulge + disk profile.

- In most galaxies the observed shape of the inner rotation curve is well matched by the maximum disk solution and for at least half of all galaxies the match extends over the entire observed rotation curve.

On the basis of the rotation curve fits, the Sa galaxies in the sample break up into two classes: for half of them the contribution of the bulge and disk stellar components are sufficient to reproduce the entire observed rotation curve with reasonable M/L ratios. For the remaining ones the rotation curves rise too slowly for any reasonable M/L ratios: the fits to the rotation curves demand that the bulge is essentially massless. These galaxies have significant and often dominant bulge component and a slowly rising rotation curve requires that the total M/L ratio increases rapidly with radius.

For most of the Sb and Sc galaxies and for several Sa's the optical rotation curves do not always place strong constraints on the amount of DM in galaxies. The rotation curve that one computes from the luminosity profile assuming a constant M/L ratio provides a good match to the observed curve out to a radius where the predicted curve turns over (most of the optical rotation curves do not extend much past this peak). Kent finds that the light distribution correlates well with mass distribution in so far as the shape of the inferred rotation curve agrees well with the observed rotation curve. Several have rotation curves that can be reproduced by assuming a constant M/L ratio for the luminosity distribution and no halo.
About half of the Sa galaxies have slowly rising rotation curves that are inconsistent with both the light distribution and the bulge dynamics. The most likely explanation for this fact is that the rotation curves in the bulge-dominated regions are not measuring the true circular velocity. In those parts the dynamics is more similar to that in elliptical galaxies and the radius at which the rotation curve becomes reliable is not easily determined. Kent concludes that the similarity between the integral distribution of matter in different Hubble types found by RTBF (1985) and Burstein and Rubin (1985) loses its significance, and should not be considered as proof of the dominance of DM inside the optical radius.

3.1.1 HI Rotation Curve: NGC 3198

Since Kent (1986, 1988) has weakened the evidence provided by the optical rotation curves of Rubin *et al.* (1980, 1982, 1985) for the existence of DM halos, much more confidence has been given to the radio observations of Bosma (1978) and Begeman (1986): particularly those of NGC 3198.

Let us pose the following question: are the measurements of HI around the Sc galaxy NGC 3198 incompatible with all its mass being contained in a standard stellar population?
The hypothesis to be tested can be examined either (1) by using photometry to predict kinematics, or (2) by using kinematics to predict photometry. The latter is to be preferred because at large radii the photometry of galaxies like NGC 3198 is a good deal less certain than the kinematical measurements. For NGC 3198 all the light distribution is contained in a flat disk. The surface density $\Sigma(R)$ at radius R in the disk that generates a given run of circular speed $V_c(R)$ is given by:

$$\Sigma(R) = \frac{1}{\pi^2 G} \int_0^\infty H(R, R') dV_c^2(R') \tag{3.1}$$

where

$$H(R, R') = \begin{cases} R^{-1} K(R'/R) & \text{if } R' < R; \\ R'^{-1} K(R/R') & \text{if } R' > R, \end{cases}$$

and K is the complete elliptic integral of the 1^{st} kind (Binney 1986). Unfortunately this formula does not lead readily to the interpretation of the observational data because the logarithmic singularity of $K(k)$ at $k = 1$ causes $\Sigma(R)$ to depend very strongly on the ill determined gradient of V_c^2 near R. Binney (1986) has developed an iterative procedure to overcome this problem, obtaining a surface mass density that reproduces the observed velocity field. Then he compared this surface mass density with the surface brightness obtained by Wevers's (1984). These two curves plotted as functions of radius are nearly parallel to each other: this seems to imply that a surface density proportional to the surface brightness can account for the flat HI curve of NGC 3198.
Binney scales the surface density in order to superimpose the two curves and finds a discrepancy between the theoretical surface brightness that has been taken proportional to the computed surface density and Wevers' profile that rises to 8% of the sky surface brightness at 8 kpc, falling to about 4%at the last photometric point, at about $R = 23$ kpc far from the center (see Fig. 3.1). Begeman's 21 cm observations (1986) indicate that NGC 3198 possesses much more mass beyond 2.5 R_D than Wevers' observations would indicate. But Binney has shown that this conclusion would be nullified by an 8% uncertainty in Wevers' light background. One must examine carefully the possibility that Wevers' sky level suffers from systematic errors: all discussion of DM rests on these and similar photometric data. The conventional techniques for determining the light background assumes that galaxies emit no light at radii comparable to those at which they are currently suspected of possessing mass, this assumption may seriously compromise the background level derived for smaller radii. Current photometric techniques may be simply incapable of detecting the extended light distributions that are predicted by the hypothesis $M/L \cong const.$

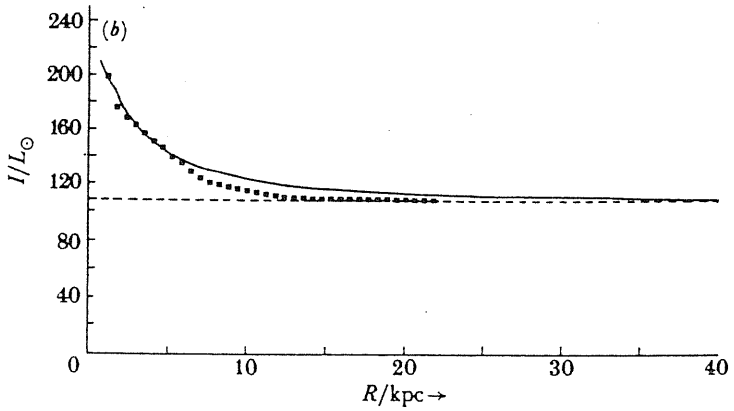

Figure 3.1: Comparison of Wevers' (1984) surface brightness measurements (squares) with the surface brightness predicted by the rotation curve of NGC 3198. The dashed line shows Wevers' estimate of sky brightness.

3.2 Non Newtonian Alternatives

3.2.1 Modification of Newtonian Gravity

The introduction of Dark Matter (DM) as the dynamical component governing the outer regions of rotation curves is needed if we assume that (1) the Newtonian formulation of dynamics and (2) gravity hold. The validity of both assumptions has been tested for distances of the order of the separations of the stellar components in binary systems. A similar test of validity of Newtonian Gravity (NG) over galactic distances is impossible, so in principle we must consider it as an assumption which could turn out to be incorrect. In other words, the flatness of the rotation curves of spirals might be a consequence of deviations from Newtonian laws, and DM would then not be needed.
A straightforward modification of NG is achieved by acting on the distance dependence in the gravitational force:

$$\mathbf{F}(m, M, R) = -G\frac{mM}{R^2} f(R)\frac{\mathbf{R}}{R}, \tag{3.2}$$

where $f(R)$ is a dimensionless function satisfying $f(0) = 1$ and $\mathrm{d}f/\mathrm{d}R > 0$. The basic prediction of such a formula is an increase in the mass discrepancy with distance from the center of the system.

In order to account for the flatness of rotation curves in the outer regions of spirals without introducing any DM component or any rapid increase of the mass-to-light ratio M/L (so that $\mathrm{d}M/\mathrm{d}R = 0$ for $R > R_0$), $f(R)$ must already deviate from unity on the scale of galaxies. Since reliably measured extended rotation

curves of spirals become flat at large radii, from centrifugal equilibrium:

$$\frac{V^2}{R} = f(R)\frac{GM(R)}{R^2}, \tag{3.3}$$

and we have

$$\begin{cases} v^2 = f(R)\dfrac{GM}{R} \\ v^2 = const \end{cases} \qquad \Longrightarrow \qquad M(R)\frac{f(R)}{R} = const$$

If we suppose that the relation between the mass interior to a distance R from the center and the corresponding luminosity $M(R) = (M/L)L(R)$ with $M/L = const$, and that the total luminosity tends to a finite limit, also $M(R)$ will tend to a limit for large R. This behaviour of $M(R)$ leads to the following asymptotic dependence of $f(R)$ on R:

$$f(R) \propto R.$$

This implies that the force law must be more like $1/R$ than $1/R^2$ on galactic scales. Sanders (1984, 1986b) and Kuhn and Kruglyak (1987) have suggested a modification to Newtonian gravity for distances greater than a characteristic radius, which is equal for all galaxies.
Sanders has investigated a gravitation law containing a repulsive Yukawa component characterized by a coupling constant α and a scale length R_0. For a point mass M the potential is:

$$\Phi(R) = \frac{G_\infty M}{R}\left[1 + \alpha \exp\left(-\frac{R}{R_0}\right)\right] \tag{3.4}$$

where G_∞ is the gravitational constant measured at infinity and is related to the local value G_0 by $G_0 = G_\infty(1+\alpha)$. Using the galaxy NGC 3198 for calibration, the parameters α and R_0 are fixed at: $\alpha = -0.92 \pm 0.01$, $R_0 = (36 \pm 4)(H_0/50)$kpc to give a good fit to the rotation curve, using only the visible matter distribution. The extra component added by Sanders is indeed repulsive: such a modified gravity law is referred to as finite–length–scale anti–gravity (FLAG). Sanders applied this FLAG potential to five other spiral galaxies ranging in size from 5 kpc to 40 kpc and produced *flat* rotation curves from an exponential thin disk surface density distribution with reasonable mass-to-light values.

A different non-Newtonian effective potential has been proposed by Kuhn and Kruglyak (1987). According to their phenomenological suggestion a correction term $\propto 1/R$ is claimed to be present in the Newtonian force law in order to reproduce the observed rotation curves. Such a correction is thought to be due to spatial variation of the gravitational constant. This correction is then explained as the first term of a power law expansion which approximates this spatial variation

on galactic length scales. The modified force between two point masses m_1 and m_2 takes the form:

$$F(R) = G\frac{m_1 m_2}{R^2}\left(1+\frac{R}{\lambda}\right)^{-1} \tag{3.5}$$

where 5 kpc $\leq \lambda \leq$ 10 kpc in order to produce a flat rotation curve for the calibration galaxy NGC 3198 (Kuhn and Kruglyak 1987).

The $1/R$ behaviour of the effective force (which implies $f(R) \propto R$) leads to a relation between the total mass of the galaxy and the velocity which is $M \cong V^2$, but this relation disagrees with the observed Tully-Fisher relation between luminosity and velocity (in the hypothesis of fixed M/L ratio). So, the modification of the distance dependence in the Newtonian law of gravity is inadequate to explain the mass discrepancy.
In principle, there is another class of candidate theories involving velocity dependent terms in the form

$$\mathbf{F}(R) = -\frac{GM}{R^2} f(V,R)\frac{\mathbf{R}}{R}. \tag{3.6}$$

If $f(V,R)$ increases for increasing values of V, and R as is natural to require, the disagreement with the Tully-Fisher relation worsens.

3.2.2 Modified Newtonian Dynamics (MOND) at Small Accelerations: Microdynamic Regime

Milgrom, in a remarkable series of papers (1983 a, b, c), first pointed out that any deviation from Newton's laws in large astronomical systems has to appear below a critical acceleration in order to be consistent with observational facts: notably the flat trend of the rotation curves of spiral galaxies and the $L \propto V^4$ Tully-Fisher law. His proposal may be framed as a modification of either Newtonian dynamics or Newtonian gravity. As a modification of dynamics, the law of inertia which describes the relationship between the acceleration a of a test particle and an arbitrary force field f is written

$$\mu\,(a/a_0)\,\mathbf{a} = \mathbf{f} \tag{3.7}$$

where a_0 is a new fundamental constant of acceleration with a value comparable to the acceleration in outer parts of galaxies ($\cong 10^{-8}$cm sec $^{-2}$), and μ is some function of a/a_0 which is not specified but must have an asymptotic behaviour of the form:

$$\begin{aligned} \mu(x) &= 1, \qquad x \gg 1 \\ \mu(x) &= x, \qquad x \ll 1 \end{aligned} \tag{3.8}$$

This modified law of inertia implies that the linear momentum of an isolated system is not conserved (Felten 1984) which seems unphysical.

Considered as a modification of Newtonian gravity, the true gravitational field g, is related to the Newtonian one g_N as

$$\mu(g/a_0)\,\mathrm{g} = \mathrm{g}_N \tag{3.9}$$

and the law of inertia is retained. With respect to galaxy rotation curves the two formulations are equivalent. The latter formulation implies

$$\frac{a^2}{a_0} \cong \frac{GM}{R^2}$$

in the limit

$$\frac{GM}{R^2} \ll a_0 \quad or \quad a \ll a_0.$$

In the latter case the asymptotic velocity of a test particle is:

$$\begin{cases} \dfrac{a^2}{a_0} \propto G\dfrac{M}{R^2} \\ a^2 = \dfrac{V^2}{R} \end{cases} \qquad \Longrightarrow \qquad V \propto (GMa_0)^{\frac{1}{4}}. \tag{3.10}$$

The constant acceleration a_0 represents the transition from the Newtonian to non-Newtonian regime, and the coincidence:

$$a_0 \cong H_0 c \tag{3.11}$$

where H_0 is the Hubble constant and c is the velocity of light, seems significant and perhaps Machian. Its value is determined to be about

$$a_0 \cong 2\ 10^{-8} \frac{H_0}{50km\ s^{-1}\ Mpc^{-1}} cm\ s^{-2}.$$

with H_0 is in km s^{-1} Mpc^{-1}.

3.2.3 MOND Predictions

Predictions which are incompatible with DM

Can all the predictions of MOND be mimicked with hidden matter, maintaining Newtonian Dynamics?

Negative Dark Matter: If a density $\rho(r)$ gives rise to an acceleration field $\mathrm{g}(r)$ according to MOND, the only way we could make the measured acceleration in this field consistent with ND is by assuming that the actual density distribution is:

$$\rho^* = -(4\pi G)^{-1}\nabla \mathrm{g} \tag{3.12}$$

If ND is not applicable, the determined density ρ^*, through eq. 3.12 is not the true density $\rho(r)$ which gives rise to the measured $\mathrm{g}(r)$. We will define $\rho_P = \rho^*(r) - \rho(r)$. In MOND, the true density $\rho(r)$ is related to the measured test particle acceleration field $\mathrm{g}(r)$ by:

$$\rho = -(4\pi G)^{-1}\nabla[\mu(\frac{g}{a_0})\mathrm{g}] \qquad \text{and} \qquad \mathrm{g} = -\nabla\Phi$$

If we take $\mu(\frac{g}{a_0})\mathrm{g} = \mathrm{g}_N$, then g_N is the Newtonian acceleration produced by ρ, so:

$$\begin{aligned} \rho = \quad & -(4\pi G)^{-1}[\nabla\mathrm{g}\cdot\mu(\tfrac{g}{a_0}) + \mathrm{g}\cdot\nabla[\mu(\tfrac{g}{a_0})]] \\ = \quad & \rho^*\mu(\tfrac{g}{a_0}) + (4\pi G)^{-1}\mu(\tfrac{g}{a_0})' a_0^{-1}\mathrm{g}\cdot\nabla\mathrm{g} \qquad (3.13) \\ \rho_P(r) = \quad & \rho(r)[\tfrac{1}{\mu} - 1] + (4\pi G)^{-1} L \mathrm{e}_g \cdot \nabla\mathrm{g} \end{aligned}$$

where $L = \mathrm{d}\lg\mu(x)/\mathrm{d}\lg x$, $x = g/a_0$, and e_g is the unit vector in the direction of g.
L varies between 0 (very high acceleration) and 1 in the opposite limit as we assume that $\mu(\frac{g}{a_0})$ is increasing and convex. The first term is never negative ($\mu \leq 1$), the second is negative if $|\mathrm{g}|$ decreases in the direction of g. The total ρ_P of a finite system as measured in a large sphere surrounding the system is positive, and diverges with increasing radius of a sphere. For such a system, at large distances $g \propto R^{-1}$ (and $\rho = 0$ at large R); thus from eq. 3.13, $\rho_P \propto R^{-2}$ as expected (since ρ_P is to produce a flat asymptotic curve).

We must note that a point mass cannot produce such an effect in any reasonable alternative to the dark matter hypothesis because the acceleration must decrease with distance more slowly than R^{-2}, giving a contribution to the "DM density" $\cong \mathrm{d}(R^2 g_R)/\mathrm{d}R$; thus in a "linear" theory negative DM cannot appear for any mass distribution.
Breakdown of the Strong Equivalence Principle (SEP): MOND does not satisfy the SEP even in the non relativistic regime. For instance, a self gravitating many-particle-system (gas cloud) with isotropic pressure (or velocity dispersion) in an external field g_{ext} such that $\mathrm{g}_{in} < \mathrm{g}_{ext} < a_0$, will not be spherical (as in the Newtonian case) even if $\mathrm{g}_{ext} = const.$
It will be an ellipsoid of revolution with its long axis along g_{ext}.

Predictions concerning galaxies

The rotation curve of a galaxy deduced from the observed mass=light distribution using MOND should match with the observed rotation curve, thus

1. the velocity of a test body in a circular orbit around an isolated galaxy should become independent of the radius of the orbit at large radii,

2. the asymptotic circular velocity V_∞ should depend only on the total mass M of the galaxy via $V_\infty^4 = a_0 GM$,
3. for high rotational velocity galaxies (such that $V_\infty^2/h > a_0$, h being the galaxy scale length) the local M/L value (as deduced from Newton's laws) should be constant at small radii, and then start to increase around the radius where $V^2/r = a_0$.

MOND models have been made for the following galaxies : NGC 3198, NGC 247, and NGC 300 using eq. 3.9 and pure exponential disks. In this case eq. 3.9 becomes

$$\mu\left(a/a_0\right) a = G\left(\frac{M_D}{R^2}\right)\frac{1}{2}(I_0K_0 - I_1K_1) \tag{3.14}$$

where R_D is the exponential disk scale-length as usual, I_n,K_n are the modified Bessel functions evaluated at $\frac{1}{2}(R/R_D)$, and M_D is the total disk-mass.
If we define the following variables $s \equiv R/R_D$, $v(s) \equiv V(s)/V_\infty$, $\xi \equiv V_\infty^2/a_0R_D = \sqrt{G}M_D/a_0R_D$, eq. 3.9 can be rewritten in dimensionless form, so that the reduced rotation velocity reads:

$$v^2 = \frac{s^{-1}\xi F(s)}{\mu(s^{-1}v^2\xi)} \tag{3.15}$$

where $F(s) = \frac{1}{2}(R/R_D)(I_0K_0 - I_1K_1)$. MOND predicts a family of velocity curves which depend on the parameter ξ and are nearly independent of the particular form of μ. Milgrom (1983b) used

$$\mu(x) = \frac{x}{\sqrt{1+x^2}} \tag{3.16}$$

because this satisfies the limits in eq. 3.8. The predicted rotation curves are shown in Fig. 3.2. In these models we have only one parameter for each galaxy: the value of M/L.

Surface densities

The constant acceleration a_0 defines a quantity with the dimension of a mass surface density $\Sigma_0 = a_0G^{-1}$. When a galaxy has an average surface density $\langle\Sigma\rangle \gg \Sigma_0$, its dynamics will be Newtonian out to large radii, compared to the half mass radius. There will be a range of radii with a Keplerian decline of the rotational velocity before the latter reaches the asymptotic value v_∞. When $\langle\Sigma\rangle \gg \Sigma_0$the rotaton curve should exhibit an appreciable hump.
When $\langle\Sigma\rangle \ll \Sigma_0$ velocities rise slowly, peak at a few scale lengths, and then decrease by a few percent to their asymptotic values. If galaxies are not observed to have considerably humped rotation curves they should all have $\langle\Sigma\rangle \leq \Sigma_0$.

Very low surface density (LSD) galaxies are particularly good test cases because: a) if the average surface density is very small $\langle\Sigma\rangle \ll \Sigma_0 = a_0G^{-1}$, the

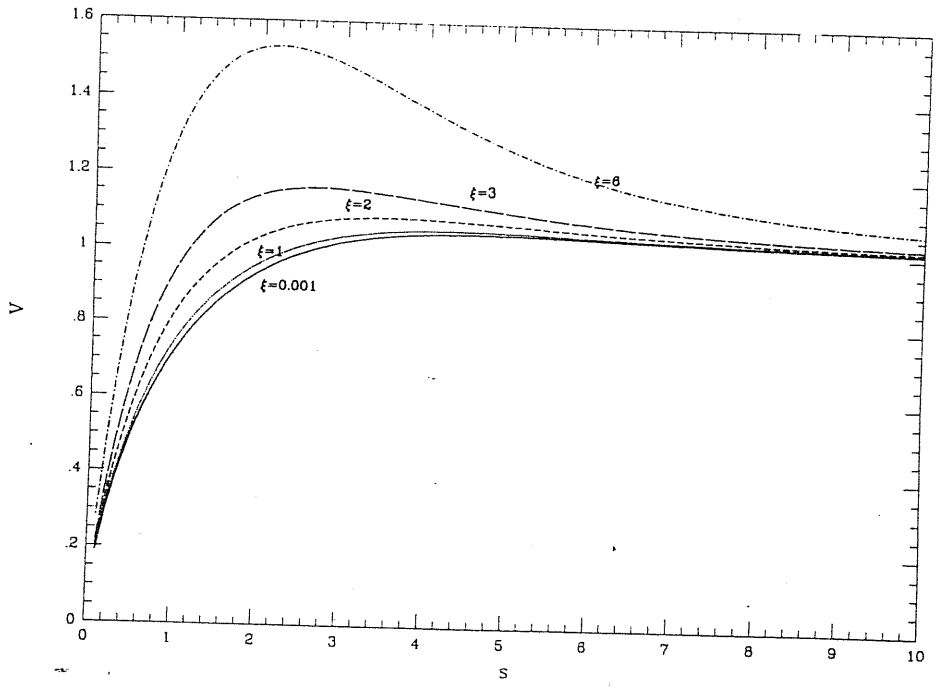

Figure 3.2: Velocity curves predicted by MOND for different values of the parameter ξ.

accelerations are much smaller than a_0, and hence we predict large departures from Newtonian behaviour, b) they are bulgeless (fewer parameters involved) so there is only the thin exponential disk component, c) $g \ll a_0$ for these systems everywhere, so we do not require the exact form of $\mu(\frac{g}{a_0})$ and it is a good approximation to use $\mu(x) = x$, and d) all the uncertainties involved in comparing calculated and measured rotation curves (galaxy distances, inclination, extinction, M/L, a_0, etc) lump into a single multiplicative factor.

Oort discrepancy

Predictions can be made concerning the dynamics of the motions perpendicular to the plane of a thin planar galactic disk. Bahcall (1984) has claimed that near the Sun, the dynamically determined mass is larger than that accounted for by the known components. For the MOND model of our Galaxy further approximations are used:

- the acceleration perpendicular to the plane is small compared with the radial acceleration,
- the density in the disk is large compared with the galactic density averaged within the galactic radius R, $\rho \gg M/4\pi R^3$.

Under these assumptions we find that the dynamics is Newtonian but with an effective gravitational constant: $G_{eff} = \mu(V_0^2/R_0 a_0)$, when the above approximation are valid:

1. the distribution of DM is the same as that of the visible mass,
2. the Oort discrepancy factor (which for MOND is $[\mu(V_0^2/R_0 a_0)]^{-1}$) is the same as that for the total galactic mass discrepancy within the orbit of the Sun,
3. the same factor appears in the dynamics of very wide binaries in the solar neighborhood.

Elliptical Galaxies

For ellipticals, one needs to make an assumption about the stellar distribution function, leaving free the parameters which specify it. Then it should be asked how such models look if they obey MOND instead of Poisson's equation, and to what extent they resemble the astronomical systems they purport to represent . Assuming MOND, the main traits of self-gravitating many-particle-spherical-systems with radius-independent radial and tangential velocity dispersion are [1]:

[1]Independent of the values of the parameters which determine their exact structure: velocity dispersion, ratio of radial to tangential dispersion

- all such spheres have a finite mass; their density distributions tend to a power law asymptotically: $\rho(R) \rightarrow R^{-\alpha}, \quad \alpha < 3$,
- Σ_0 is an upper limit on the average surface density that such isothermal spheres can have,
- M_{tot} of a sphere is approximately proportional to the 4^{th} power of the phase space dispersion σ_s:

$$(a_0 G)^{-1} \leq \frac{M}{\sigma_s^4} \leq 2(a_0 G)^{-1}.$$

Or simply one tries to map the test particle acceleration field in elliptical galaxies and see if it agrees with that calculated from the observed light distribution.

- In ellipticals with test-particle gas-discs, the rotation curve of the disc will be the one MOND dictates for the observed light distribution.
- Dwarf ellipticals or spheroidals with $\langle\Sigma\rangle \ll \Sigma_0$ will contain large quantities of DM when treated with ND.
- The observed temperature and density distributions in X-ray emitting envelopes of ellipticals will be those given by MOND.

3.2.4 Observational Evidence

HI rotation curves

Several HI rotation curves have been fitted by Kent (1987) using Milgrom's modified Newtonian dynamics. He found that the use of MOND has a few interesting properties, in particular:

- for a galaxy with high mass density, the computed rotation curve will be the normal newtonian curve out to some transition radius R_t, where $V^2/R \cong a_0$;
- the shape of the curve is determined by the shape of the mass distribution and the amplitude by the M/L ratio;
- for a galaxy with a low mass density the rotation curve has a different shape, but again is determined only by the mass distribution.

If $V_N(R)$ is the former (high density galaxy) and $V_M(R)$ is the latter curve (for a low density galaxy), then to within a constant they are related by:

$$V_M \propto (V_N^2 R)^{\frac{1}{4}}$$

Kent has found a curious feature of MOND for disc galaxies. Although the dynamical laws were invented to produce flat rotation curves at large radii, the computed curves still decline slightly. The quantity $V_N^2 R/G$ which equals the disc mass M as $R \rightarrow \infty$, actually exceeds M for radii greater than about 2.8 scale lengths, reaching a maximum of 1.21M at about 4 scale lengths. So in the low density limit, the MOND rotation curve will have a peak value of 1.05 V_∞ at this radius. This feature is independent of the shape of the function $\mu(x)$, and is simply a consequence of rotation curves produced by disc mass distributions. Kent has used MOND to compute rotation curves for 16 galaxies (with optical and HI rotation curves) with stellar M/L ratios and a_0 taken as free parameters. Since a_0 is inversely proportional to the distance assigned to a galaxy, some scatter is expected in the deduced values of a_0 (the relative distance scale used in Kent's sample is not uniform).
Milgrom suggested a rough value of $2 \cdot 10^{-8}$cm s^{-2} for a_0. Out of the 16 galaxies of Kent's sample, only 7 gave a useful estimate of a_0. For galaxies in the low density limit a value of $a_0 = 1 \cdot 10^{-8}$ was used. One galaxy from this sample, NGC 2403, is also best fitted by a model in the low density limit, but it requires a value of $a_0 > 3 \cdot 10^{-8}$cm s^{-2}.
Kent's fits with MOND were good, although not as good as with dark halo models: this is not surprising because MOND models have less free parameters which should be identical for all galaxies. A potential problem for MOND could be in reproducing the slope of the outer rotation curve, because it predicts a very slightly falling trend in the low density limits, and in higher density galaxies the drop should be even larger. But:

1. the observed rotation curves in those regions are slightly in error because the HI distribution is always warped there,
2. there is additional light, hence mass at large radii, which is just too faint for current photometry to pick up,
3. there might be a variation of the mass-to-light ratio with radius.

So, MOND seems to work nearly as well as DM models in fitting the observed rotation curves with one degree of freedom less. However, a_0 shows an uncomfortably large variation among galaxies.

Optical rotation curves

One observable quantity describing the profile of rotation curves in the outer disk regions of spiral galaxies is the logarithmic velocity gradient, d log V/d log R, evaluated at $R_{opt} \equiv 3.2 R_D$ [2].

[2]We adopt here $R_{opt} \equiv 3.2 R_D$. Such a definition makes R_{opt} statistically equivalent to R_{25}, the 25 mag arcsec^{-2} isophotal radius (van der Kruit 1987).

For the sample of galaxies collected from the literature by Persic and Salucci (1990 a, b) which spans a range in blue absolute magnitude $-17.5 \geq \mathrm{M}_B \geq -23.2$, in circular velocity $120 \leq V \leq 385$ (in km s^{-1}), and in disk radius $3 \leq R_{opt} \leq 55$ (in kpc), they find that

$$-0.12 \leq \left(\frac{\mathrm{d}\log V}{\mathrm{d}\log R}\right)_{R_{opt}} \leq 0.70.$$

By contrast, a value d log V/d log $R = -0.15$ is expected from the distribution of light in the hypothesis that light traces mass and that Newtonian gravity holds. The velocity gradient is strongly correlated with luminosity, according to

$$\frac{\mathrm{d}\log V}{\mathrm{d}\log R} = (-0.30 \pm 0.04)\log L_B + (0.35 \pm 0.03) \tag{3.17}$$

with a correlation coefficient $r = -0.70$, or

$$\frac{\mathrm{d}\log V}{\mathrm{d}\log R} = (-0.60 \pm 0.12)\log R_{25} + (1.04 \pm 0.15) \tag{3.18}$$

with a correlation coefficient $r = -0.69$ see Fig. 3.3 . The correlation between logarithmic velocity gradient and luminosity (or galaxy radius) is a central property of spiral galaxies (Rubin *et al.* 1985; Persic and Salucci 1990c), and implies that galaxies with steeper rotation curves tend to have lower values of circular velocity and also tend to be smaller and fainter too. In the framework of non-Newtonian theories, the above correlation should be natural consequence of the modified dynamics and/or gravitation.

3.2.5 A Non-Conventional Test for Non-Newtonian Theories

A test of FLAG

According to Sanders (1984) we have:

$$V^2_{25,FLAG} = G\frac{M_D}{R_{25}}[1 + \alpha(1+x)\exp(-x)] \tag{3.19}$$

where M_D is the disk mass and $x = R_{25}/R_0$ and the logarithmic gradient is then:

$$\left(\frac{\mathrm{d}\log V}{\mathrm{d}\log R}\right)_{25,FLAG} = \frac{-0.5 - 0.5\alpha(1+x+x^2)\exp(-x)}{1+\alpha(1+x)\exp(-x)} \tag{3.20}$$

In eq. 3.19 the mass has been supposed to be spherically distributed: in particular the sign of the logarithmic gradient of circular velocity and its qualitative behaviour along the luminosity sequence, remains unaffected by this approximation.

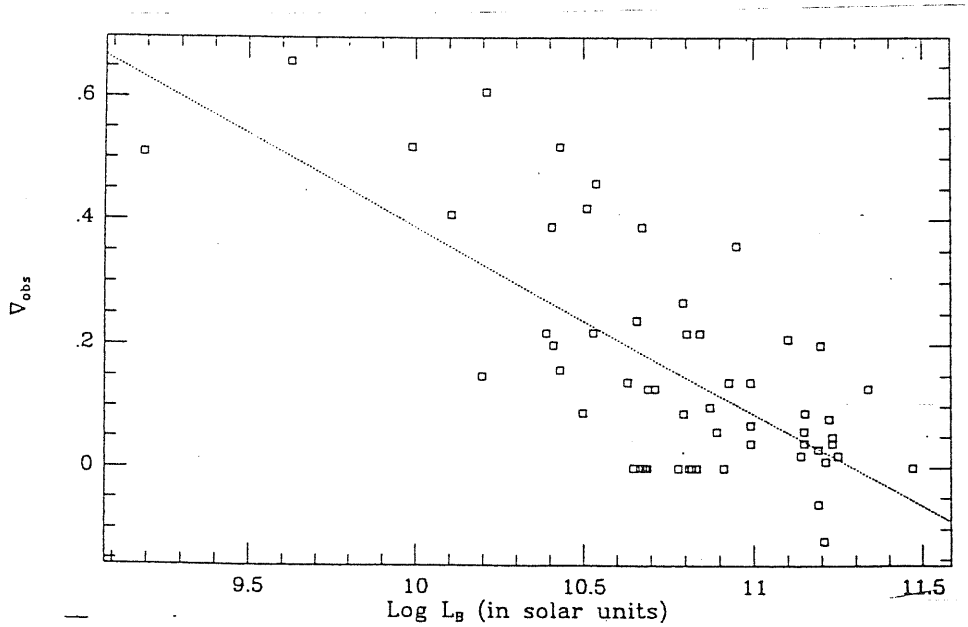

Figure 3.3: The observed velocity gradients as function of of absolute blue luminosity for the rotation curves of the galaxies in Tab. 2.2. A strong correlation is clearly visible.

Dubal, Persic and Salucci (1990) have tested the FLAG scenario by investigating whether eq. 3.20 agrees with the observational properties, eq. 3.17 and eq. 3.18. They calculated the value of the logarithmic derivative predicted by FLAG for the sample of galaxies given by Persic and Salucci (1990 *a*), obtaining the following correlation

$$\left(\frac{\mathrm{d}\log V}{\mathrm{d}\log R}\right)_{25} = (0.35 \pm 0.03)\log R_{25} - (0.55 \pm 0.02) \tag{3.21}$$

with a correlation coefficient $r = 0.85$. This is the relation that the sample of galaxies would have if we modified the gravity law, by means of the FLAG theory, in order to account for the rotation curve of NGC 3198. This relation clearly disagrees with the observed one: galaxies show a dependence on R_{25} which is converse to that predicted by eq. 3.18 (see Fig. 3.4).

A test for Kuhn and Kruglyak's (KK) theory

Using the KK force law, eq. 3.5, the circular velocity at R_{25} and its logarithmic gradient are given by:

$$V_{25,KK} = \left(G\frac{M_D}{\lambda}\right)^{\frac{1}{2}}\left(1+\frac{\lambda}{R_{25}}\right)^{\frac{1}{2}} \tag{3.22}$$

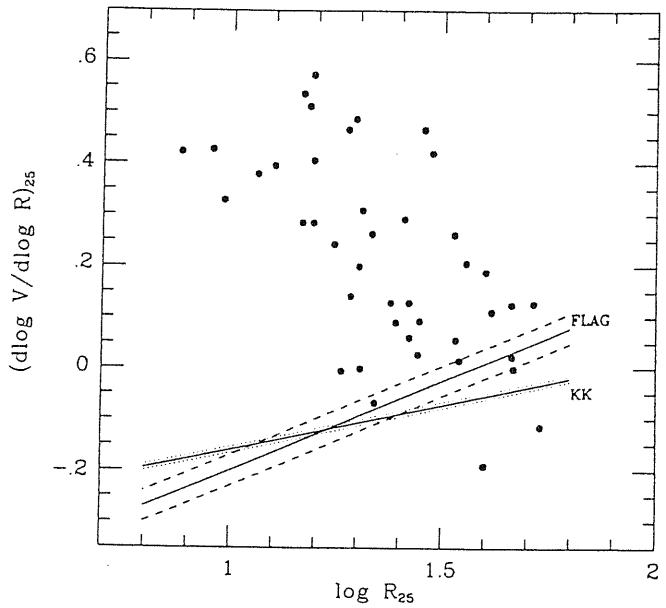

Figure 3.4: $(\mathrm{d}\log V/\mathrm{d}\log R)_{25}$ as a function of R_{25} for the sample of Persic and Salucci (1988). The theoretical relationships predicted by the KK and FLAG theories are shown. The broken lines indicate the 3σ limit.

$$\left(\frac{\mathrm{d}\log V}{\mathrm{d}\log R}\right) = -\frac{1}{2}\frac{\lambda}{R_{25}}\left(1+\frac{\lambda}{R_{25}}\right)^{-1}. \tag{3.23}$$

We see that eq. 3.23 predicts that small galaxies ($\cong \lambda$, $V \cong 100$ km s^{-1}) have negative logarithmic gradients, which is in sharp contrast with observations (see Tab.1). For Persic and Salucci's sample KK's theory predicts the following correlation:

$$\left(\frac{\mathrm{d}\log V_{KK}}{\mathrm{d}\log R}\right)_{25} = (0.175 \pm 0.003)\log R_{25} - (0.335 \pm 0.006) \tag{3.24}$$

with a correlation coefficient $r = 0.97$. Again the slope predicted by this theory is irreconciliable with the observations (see Fig. 3.4).

A Test for MOND.

From eq. 3.15, and using $\mu = x/\sqrt{1+x^2}$ (Milgrom 1983b), the MOND rotation curve is:

$$V = \left[\frac{2s^2}{\xi^2\left(\sqrt{1+\left(\frac{2s^2}{\xi^2 F}\right)^2}-1\right)}\right]^{\frac{1}{4}} \tag{3.25}$$

and the ensuing logarithmic velocity gradient is (Arnaboldi 1990):

$$\left(\frac{\mathrm{d}\log V}{\mathrm{d}\log R}\right)_{s=3.2} = \frac{1}{2}\left[1+\frac{1}{2}\left(1+\frac{1}{\sqrt{1+\left(\frac{2s^2}{\xi^2 F}\right)}}\right)\left(2-\frac{\mathrm{d}\log F}{\mathrm{d}\log s}\right)\right]_{s=3.2} . \quad (3.26)$$

By inserting the numerical values $s = 3.2$, $F = 1.11$, and $\mathrm{d}\log F/\mathrm{d}\log s = 0.45$, eq. 3.26 transforms into

$$\left(\frac{\mathrm{d}\log V}{\mathrm{d}\log R}\right)_{s=3.2} = \frac{1}{2}\left[1+\frac{1.55}{2}\left(1+\frac{1}{\sqrt{1+\left(\frac{20.48}{1.11\xi^2}\right)}}\right)\right] . \quad (3.27)$$

For each galaxy in our sample we calculate the value of ξ according to its definition [with the assumption $V_\infty \equiv V(R_{25})$ [3], consistent with Milgrom 1983*b*], and from eq. 3.27 we derive the value of $\mathrm{d}\log V/\mathrm{d}\log R$ predicted by MOND. The results are reported in Tab. 3.1. As shown in Fig. 3.5 there is no correlation between the predicted MOND values of $\mathrm{d}\log V/\mathrm{d}\log R$ and luminosity, *i.e.*,

$$\frac{\mathrm{d}\log V}{\mathrm{d}\log R} = (0.006 \pm 0.009)\log L_B + (0.08 \pm 0.007), \quad (3.28)$$

with a correlation coefficient $r = 0.09$. In Fig. 3.6 we plot the differences between observed and predicted velocity gradients *vs* luminosity: the disagreement between the predictions of MOND and the data increase for decreasing luminosities, where steeper rotation curves are observed. Indeed, the steepest predicted velocity gradient (for $\xi \ll 1$) is

$$\left(\frac{\mathrm{d}\log V}{\mathrm{d}\log s}\right)^{max}_{MOND} = \frac{1}{4}\frac{\mathrm{d}\log F}{\mathrm{d}\log s} = 0.11 . \quad (3.29)$$

So, MOND appears to be unable to reproduce the data (at least in the limit $\mu(x) = x$ and $\mu = x/\sqrt{1+x^2}$) for 29 out of 58 galaxies of Persic and Salucci's sample.

So far we have computed ξ according to its definition, $\xi \equiv V_\infty^2/(a_0 R_D)$, where a_0 is supposed to be independent of luminosity or radius. Can this latter hypothesis

[3] Most galaxies in our sample have $\mathrm{d}\log V/\mathrm{d}\log R > 0$, so the assumption $V_\infty = V(R_{25})$ leads to an underestimate of ξ for those galaxies. This however will only act to strengthen our conclusions.

TABLE 3.1
Theoretical Predictions

Ident.	ξ_{obs}	∇_{theor}	Ident.	ξ_{obs}	∇_{theor}
NGC 488	2.313	0.485	NGC 4682	1.145	8.536
NGC 753	1.23	8.115	NGC 4800	3.795	−12.564
NGC 1035	1.377	7.320	NGC 5033	0.608	10.508
NGC 1085	1.56	6.213	NGC 5055	1.100	8.747
NGC 1300	0.999	9.190	NGC 5290	1.561	6.206
NGC 1325	1.284	7.833	NGC 5371	0.918	9.515
NGC 1417	2.196	1.478	NGC 5383	1.159	8.468
NGC 1421	0.781	10.003	NGC 5426	0.635	10.438
NGC 1620	1.233	8.100	NGC 5673	0.883	9.647
NGC 2336	0.647	10.405	NGC 5905	0.576	10.588
NGC 2708	3.233	−7.824	NGC 5908	2.160	1.777
NGC 2715	0.455	10.850	NGC 7083	0.672	10.336
NGC 2742	1.570	6.149	NGC 7171	1.130	8.607
NGC 2815	1.438	6.965	NGC 7331	0.782	10.000
NGC 2997	0.630	10.451	NGC 7531	1.380	7.302
NGC 2998	1.024	9.084	NGC 7537	0.827	9.848
NGC 3054	2.095	2.309	NGC 7591	0.964	9.334
NGC 3198	0.988	9.236	NGC 7606	1.114	8.541
NGC 3200	0.902	9.576	NGC 7631	1.220	8.166
NGC 3145	1.098	8.756	NGC 7664	1.553	6.258
NGC 3223	0.910	9.546	NGC 7723	1.474	6.749
NGC 3672	0.938	9.437	UGC 467	0.833	9.827
NGC 3963	0.695	10.270	UGC 807	0.623	10.469
NGC 3992	1.373	7.342	UGC 2259	0.883	9.648
NGC 4062	1.120	8.654	UGC 4375	1.961	3.372
NGC 4254	1.627	5.776	UGC 11810	0.644	10.413
NGC 4321	1.169	8.420	UGC 12470	1.187	8.331
NGC 4565	0.794	9.961	UGC 12810	0.795	9.957
NGC 4605	2.298	0.613	WR 66	0.586	10.563

Table 3.1: *Column (1)*: name of the galaxy. *Column (2)*: observed value of ξ given by $\xi = V_{25}^2/(R_D a_0)$ with $a_0 = 2 \cdot 10^{-8}$ cm s^{-2}. *Column (3)*: predicted values of ∇ (in units of 10^{-2}).

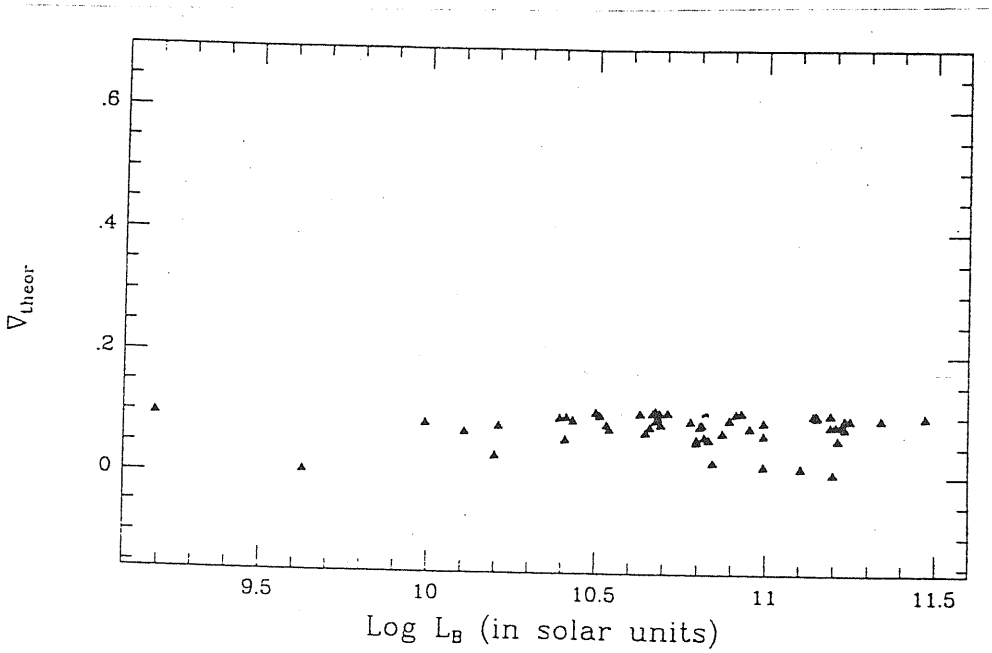

Figure 3.5: The MOND-predicted velocity gradients as a function of luminosity. No correlation is visible. (Luminosities are in solar units.)

be relaxed? In order to check possible variations of ξ (or equivalently a_0) with luminosity, we now compute ξ from purely observational quantities, *i.e.* from the shapes of rotation curves. By inverting eq. 3.27 we get

$$\xi = \frac{s\sqrt{0.45 - 4\left(\frac{\mathrm{d}\log V}{\mathrm{d}\log s}\right)}}{\sqrt{1.1}\left[1 - 2\left(\frac{\mathrm{d}\log V}{\mathrm{d}\log s}\right)\right]^{\frac{1}{4}}\left[1 - 0.45 + 2\left(\frac{\mathrm{d}\log V}{\mathrm{d}\log s}\right)\right]^{\frac{1}{4}}}. \tag{3.30}$$

The results are listed in Tab. 3.2. From eq. 3.30 we notice that there are no real solutions for ξ when $\mathrm{d}\log V/\mathrm{d}\log s > 1/4\,(\mathrm{d}\log F/\mathrm{d}\log s) = 0.11$. For the remaining 29 real solutions there is no correlation between ξ (or equivalently a_0) and luminosity or radius (see Fig. 3.7). This strengthens our previous conclusion that under no circumstances can MOND reproduce the steep rotation curves of low-luminosity galaxies.

3.2.6 Conclusions

The approximate constancy of rotation curves is only one of many observational properties of the dynamics of spiral galaxies. As Rubin *et al.* (1985) pointed out, one key observational fact is the correlation between the shapes of (optical)

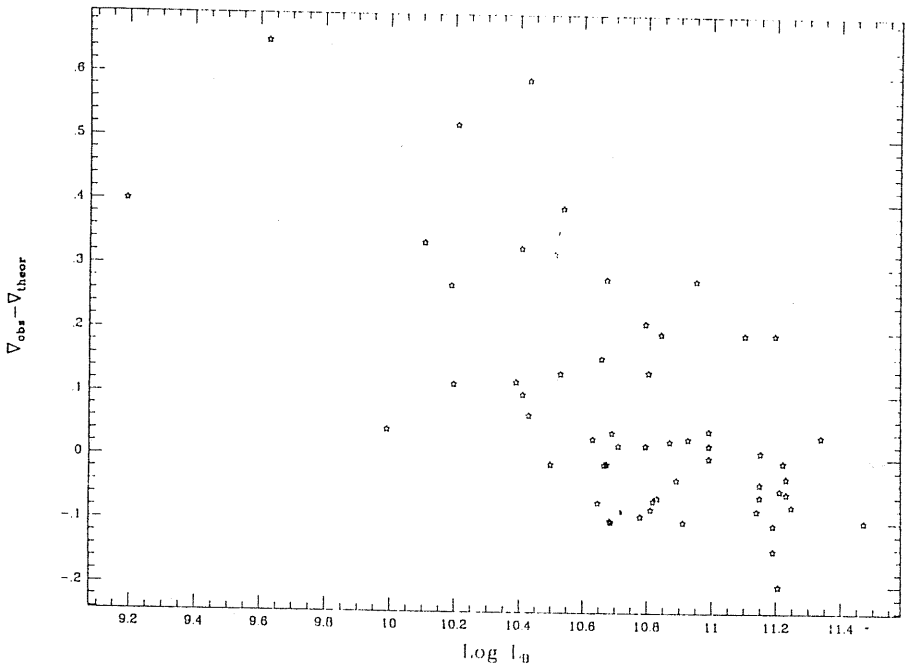

Figure 3.6: Differences between observed and MOND-predicted velocity gradients as a function of luminosity (in solar units). A strong correlation is apparent: discrepancies are bigger for lower-luminosity galaxies.

TABLE 3.2
Theoretical Predictions

Ident.	ξ_{theor}	∇_{obs}	Ident.	ξ_{theor}	∇_{obs}
NGC 488	–	0.20	NGC 4682	–	0.22
NGC 753	1.741	0.05	NGC 4800	–	0.15
NGC 1035	–	0.41	NGC 5033	–	0.13
NGC 1085	2.252	0.01	NGC 5055	2.369	0.00
NGC 1300	2.369	0.00	NGC 5290	1.043	0.09
NGC 1325	–	0.46	NGC 5371	1.878	0.04
NGC 1417	–	0.21	NGC 5383	3.031	−0.06
NGC 1421	–	0.42	NGC 5426	2.369	0.00
NGC 1620	–	0.36	NGC 5673	–	0.22
NGC 2336	2.009	0.03	NGC 5905	–	0.14
NGC 2708	–	0.52	NGC 5908	1.878	0.04
NGC 2715	–	0.39	NGC 7083	1.878	0.04
NGC 2742	–	0.39	NGC 7171	–	0.13
NGC 2815	1.432	0.07	NGC 7331	1.593	0.06
NGC 2997	2.369	0.00	NGC 7531	2.369	0.00
NGC 2998	–	0.14	NGC 7537	2.369	0.00
NGC 3054	–	0.22	NGC 7591	2.369	0.00
NGC 3198	–	0.16	NGC 7606	3.723	−0.12
NGC 3200	–	0.13	NGC 7631	–	0.24
NGC 3145	1.252	0.08	NGC 7664	2.369	0.00
NGC 3223	2.132	0.02	NGC 7723	2.369	0.00
NGC 3672	1.593	0.06	UGC 467	–	0.20
NGC 3953	2.132	0.02	UGC 807	2.369	0.00
NGC 3992	0.782	0.10	UGC 2259	–	0.51
NGC 4062	–	0.52	UGC 4375	–	0.15
NGC 4254	–	0.27	UGC 11810	–	0.14
NGC 4321	–	0.22	UGC 12470	–	0.61
NGC 4565	2.369	0.00	UGC 12810	1.043	0.09
NGC 4605	–	0.66	WR 66	1.043	0.09

Table 3.2: *Column (1)*: name of the galaxy. *Column (2)*: predicted value of ξ using ∇_{obs}. *Column (3)*: observed value of ∇.

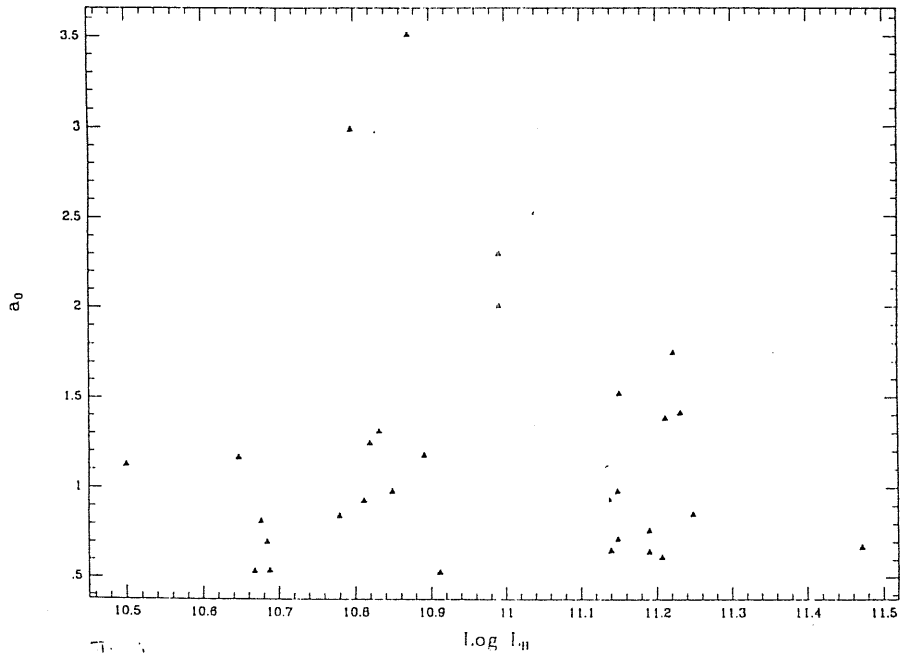

Figure 3.7: The values of a_0 derived from the observed velocity gradients as a function of luminosity. No correlation is visible.

rotation curves and luminosity. In a non-orthodox scenario involving modifications of Newtonian gravity, this property must arise naturally. We have reviewed (1) the introduction of a Yukawa-type potential (Sanders, 1986b), (2) the introduction of a logarithmic term in the potential (Kuhn and Kruglyak, 1987), and (3) Milgrom's (1983a, b, c) Modified Newtonian Dynamics (MOND). We have found that the derived force law is insufficient to account for the observational evidence that low-luminosity, optically small galaxies have steep rotation curves. Our analysis leads us to conclude that all these proposed modifications of Newtonian gravity, at least in their present formulation, fail to reproduce the data.

The present result suggests that a deeper understanding of the observed dynamical properties of galaxies is needed before alternatives to Newtonian gravity are attempted.

Chapter 4

Dark Matter in Spiral Galaxies: Properties

4.1 Introduction

In the previous Chapters we have discussed the possibility that some peculiar features of the rotation curves of galaxies may be considered as proof of the existence of unseen matter. The dark matter turns out to be arranged differently from the disk shaped luminous matter, being possibly in spherical halos.
However there are still quite discrepant views on the amount of dark matter in the disk regions of spirals, and whether this component shows any systematics with the other properties of galaxies such as luminosity, colour, and morphology. Different assumptions and mass decomposition techniques have led to different conclusions, whereby the abundance of DM deduced from optical rotation curves is claimed to be any of:

1. minimal, the disk dynamics in the inner regions being supported only by luminous matter (Kalnajs 1983, van Albada *et al.* 1985, Kent 1986),
2. virtually constant in all spiral galaxies (Bahcall and Casertano, 1985),
3. independent of luminosity (Carignan and Freeman 1985, Rubin *et al.* 1985, van Albada and Sancisi 1986, Sancisi and Van Albada 1987, Begeman 1988),
4. a specific function of luminosity (Salucci 1986, Persic and Salucci 1988, 1990a and 1990b, Salucci and Frenk 1989),
5. a function of colour (Tinsley 1981, Athanassoula *et al.* 1987).

The analysis of the relative abundances of dark and luminous matter is related to galaxy formation theories. In Faber's "dissipation picture" (Faber 1982) the

fraction of non luminous matter within the radius of ordinary matter is expected to be greater in late-type spirals that in early-types. This should arise from lower condensation of late-type galaxies within their surrounding halos. Faber argued that this could be seen in the data. While the situation is unclear for very early-type galaxies, she found a mean ratio of non-luminous to luminous matter of 1.7 (1.2 – 2.1) for Sc and 2.2 (1.8 – 2.6) for Irr I (for models with an assumed H_2 mass of $0.3M_{HI}$).

4.1.1 Minimal Dark-to-Luminous Mass Ratio

We have already introduced the mass models and the debate relative to the point i). The Maximum-disk hypothesis has been adopted: this implies that luminous matter dominates the gravitational field and DM is eventually introduced to sustain the rotation curves in the outer regions. A DM halo is always needed in order to account for the HI kinematical data.
It should be pointed out that two different solutions can be found in the literature under the name "maximum-disk":

1. solutions with the disk really at maximum such as shown in Kalnajs (1983) and Kent (1986) so that any halo present beyond the last well fitted point of the rotation curve would have a hollow core;
2. solutions where, if a halo is present (because we have HI data together with optical rotation curves), the disk M/L is slightly diminished in order to assume a non hollow core for the halo. van Albada *et al.* (1985) made such a choice for NGC 3198 which resulted in a M/L_D 15% lower than the maximum possible value.

We should also mention that the analysis of Kent's sample done by Athanassoula, Bosma and Papaioannau (1987) has shown that all the models with really maximum disks are unstable against m=1 perturbations, (bar-instability). They have obtained models for Kent's galaxies which are stable against m=1 perturbations by introducing a halo without a hollow core. The "no m=1" constraint requires reduction of the M/L of the disk compared to the really maximum disk case and a non-hollow core for the halo leads in general to models which are stable against m=1 perturbations.

4.1.2 Constant Dark-to-Luminous Mass Ratio

Bahcall and Casertano (1985) have collected from the literature detailed mass models for eight spirals. The parameters of the mass distributions are summarized in Tab. 4.1.2. The sample covers a fairly wide range in galaxy types (from Sb to

TABLE 4.1.2
Parameters of the mass distribution of some spiral galaxies

Ident.	M_D $10^{10}M_\odot$	M_H $10^{10}M_\odot$	M_H/M_D	ρ_D $M_\odot pc^{-3}$	ρ_H $M_\odot pc^{-3}$	ρ_H/ρ_D
MW	6.6	9.5	1.4	0.0103	0.0047	0.46
N 891	9.1	9.0	0.99	0.0042	0.0004	0.10
N 3198	3.1	3.1	1.0	0.0055	0.0014	0.26
N 4565	13.0	14.6	1.1	0.0034	0.0009	0.28
N 5907	8.8	13.6	1.5	0.0102	0.0015	0.15
N 247	1.20	1.08	0.90	0.0067	0.0025	0.38
N 300	0.63	0.54	0.84	0.0080	0.0026	0.33
N 3109	0.16	0.15	0.93	0.0041	0.0016	0.38

SBm) and external scale properties (mass, velocity, scalelengths). Despite these differences the ratio M_{halo}/M_D of the halo to disk mass inside the outer optical radius seems to be always close to unity (the outer radius R_{out} has been defined as the radius at which the surface brightness drops to 26.6 B-mag arcsec^{-2}). They derived the halo mass inside R_{out} directly from the mass models and the disk masses from the published rotation curves.
They claimed that it was possible to summarize the relatively well determined parameters that characterize the internal properties of the mass in their sample with the following three equations:

$$\frac{M_{halo}}{M_D} \cong 1 \tag{4.1}$$

$$\frac{\rho_{halo}}{\rho_D} \cong 0.3 \tag{4.2}$$

$$\rho_{halo} \cong 0.0015 M_\odot pc^{-3} \tag{4.3}$$

The mass models in the Bahcall and Casertano sample have been derived by different authors using a variety of methods. For NGC 3198 (van Albada *et al.*1985), and NGC 247, 300, 3109 (Carignan and Freeman 1985) the maximum-disk hypothesis has been used. For the Milky Way, the disk mass has been normalized

TABLE 4.1
Parameters and Results of the Mass Models

Object	M_B	M_D $10^{10}M_\odot$	M_H/M_D	R_c kpc	σ kms^{-1}	ρ_0 $M_\odot pc^{-3}$
N 7793	−18.31	0.60				
N 247	−18.01	1.20	0.85	22.5	100	0.0033
N 300	−18.01	0.52	0.70	12.0	60	0.0042
N 3109	−16.84	0.16	1.52	10.5	40	0.0024

Table 4.1: R_c, *sigma*, and ρ_0 are respectively the core radius, the one-dimensional velocity dispersion and the central density of the isothermal DH model. The central density can be derived from the previous parameters: $\rho_0 = 9\sigma^2/4\pi G R_c^2$.

(Bahcall, Schmidt, and Soneira, 1982) to the value in the solar neighborhood. For NGC 891 and NGC 4565, Bahcall (1983) and Casertano (1983b) have used a standard mass to light ratio for the disk mass.
They noticed that, given the variety of methods it is surprising to obtain eq. 4.1 valid to 30%.

4.1.3 Dark-to-Luminous Mass Ratio Independent of Luminosity and Morphological Types.

We have already discussed the Rubin *et al.* (1985) analysis of optical rotation curves. To sum up, they have obtained that the shapes of rotation curves are not correlated either with morphological types nor with luminosity. They concluded that DM should dominate the potential wells of galaxies at all radii.
Carignan and Freeman (1985) have calculated the mass models for NGC 7793, 247, 300, and 3109. A one component disk model succeeds in fitting the observed rotation curve of NGC 7793, which extends only out to 0.75 R_{25} while an additional dark component is needed to explain the observed rotation curves of the other three galaxies which extend to $(1.5 - 3.0)$ R_{25}. The parameters and the results of the mass models are given in Tab. 4.1.
With respect to their mass models Carignan and Freeman have obtained that galaxies around $-M_B = (17-18)$ have a mean halo-to-disk mass ratio of 1.0 $(0.7-1.5)$ (at R_{25}) which is comparable to the ratio of 1.2 $(0.8 - 1.6)$ found for the Sc's

with $-23 \leq M_B \leq -19$. Based on these data, the ratio of non-luminous to luminous matter does not seem to vary with galaxy luminosity or morphological types.

4.1.4 Dark-to-Luminous Mass Ratio a Function of Luminosity

In a series of papers Persic and Salucci (1988, 1990 a, 1991) have analysed the integral properties of spirals using a non standard mass decomposition technique starting from the rotation curves. They model a spiral galaxy as a stellar disk embedded in a spherical halo, assuming

1. an infinitely thin stellar disk of surface density

$$\sigma(R) = \sigma_0 \exp(-R/R_D);$$

2. in each galaxy the disk mass-to-light ratio is constant with radius, and
3. in the region of interest between 2.3 and 3.2 scale lengths, the bulge and the HI disk give negligible contributions to the circular velocity V(R).

Moreover they assume a spherical halo and no *a priori* profile for it.
Writing the condition of centrifugal equilibrium, they have:

$$V^2(R) = V_D^2(R) + V_H^2(R) \tag{4.4}$$

where $V_D(R)$ and $V_H(R)$ are the disk and halo contributions to the circular velocity. Taking the first derivative

$$V(R)\frac{\mathrm{d}V(R)}{\mathrm{d}R} = V_D(R)\frac{\mathrm{d}V_D(R)}{\mathrm{d}R} + V_H(R)\frac{\mathrm{d}V_H(R)}{\mathrm{d}R} \tag{4.5}$$

from which

$$V_D^2(R) = V_H^2(R)\left(\frac{\frac{\mathrm{d}\log V_H(R)}{\mathrm{d}\log R} - \frac{\mathrm{d}\log V(R)}{\mathrm{d}\log R}}{\frac{\mathrm{d}\log V(R)}{\mathrm{d}\log R} - \frac{\mathrm{d}\log V_D(R)}{\mathrm{d}\log R}}\right) \tag{4.6}$$

The halo and disk masses integrated up to a radius R are given respectively by:

$$M_H(R) = G^{-1}V_H^2(R)R \tag{4.7}$$

$$M_D(R) = G^{-1}f^{-1}V_D^2(R)R \tag{4.8}$$

where $f = \frac{1}{2}(R/R_D)^3(I_0K_0+I_1K_1)$ accounts for the disk's departure from spherical symmetry. For an exponential thin disk we have:

$$\frac{\mathrm{d}\log V_D(R)}{\mathrm{d}\log R} = \frac{I_0K_0 + 0.5\left(\frac{R}{R_D}\right)(I_1K_0 - I_0K_1)}{(I_0K_0 - I_1K_1)}.$$

The disk-to-total mass ratio is given by:

$$\frac{M_D(R)}{M_{tot}(R)} = \frac{M_D(R)}{M_H + M_D} = \frac{\frac{\mathrm{d}\log V_H}{\mathrm{d}\log R} - \frac{\mathrm{d}\log V}{\mathrm{d}\log R}}{f\left(\frac{R}{R_D}\right)\left(\frac{\mathrm{d}\log V}{\mathrm{d}\log R} - \frac{\mathrm{d}\log V_D}{\mathrm{d}\log R}\right) + \frac{\mathrm{d}\log V_H}{\mathrm{d}\log R} - \frac{\mathrm{d}\log V}{\mathrm{d}\log R}} \tag{4.9}$$

If we compute the mass ratio at $R = 3.2R_D = R_{opt}$, the disk-to-total mass ratio at the optical radius can be written as:

$$\frac{M_D}{M_{tot}} = \frac{\nabla_H - \nabla}{\nabla_H + 0.11\,\nabla + 0.30} \tag{4.10}$$

where $\nabla = \mathrm{d}\log V(R)/\mathrm{d}\log R|_{R_{opt}}$, and $\nabla_H = \mathrm{d}\log V_H(R)/\mathrm{d}\log R|_{R_{opt}}$. Eq. 4.10 is a function of the observed slope of the rotation curve and of the unknown slope of the halo velocity field, which is related to the DM mass distribution as:

$$\frac{\mathrm{d}\log M_H}{\mathrm{d}\log R} = 2\,\nabla_H + 1$$

∇_H is not directly observable in individual objects but in the case of a sample of galaxies we can estimate its sample-averaged value arguing that for such a value the correlation between luminosity and disk mass has the smallest scatter. Salucci and Persic postulate the existence of the relationship:

$$\log L_B = b + a\log M_D \tag{4.11}$$

where L_B is observed and M_D is given by:

$$M_D(\nabla_H) = G^{-1}V^2(R_{opt})\frac{\nabla_H - \nabla}{1.11\,\nabla_H + 0.30}R_{opt} \tag{4.12}$$

where ∇, R_{opt} and $V(R_{opt})$ are all observable quantities.
The parameters a, b, and ∇_H have been obtained by searching in the sample (Tab. 2.2) for a relationship of the form 4.11 and minimizing the corresponding

$$\chi^2 = \sum_i (\log L_B^i - b - a\log M_D^i(\nabla_H))^2$$

with respect to a, b, and ∇_H. Persic and Salucci find $\nabla_H = 0.76 \pm 0.10$, $a = 0.74 \pm 0.04$, and $b = 2.7 \pm 0.2$. This method carries a statistical uncertainty which

is estimated to be a few percent for $M_D/M_{tot} \cong 0.7$ and $< 30\%$ for $M_D/M_{tot} \cong 0.2$. To within these uncertainties, the disk-to-total mass ratio at R_{opt} is then given by:

$$\frac{M_D}{M_{tot}} = \frac{0.76 - \bigtriangledown}{0.11 \bigtriangledown + 1.06} \tag{4.13}$$

The first important result is that spirals show a large range of values in disk to total mass ratio: this reflects the intrinsic variety in the shapes of galactic rotation curves.

By means of the above mass decomposition technique there should be a simple linear correspondence, virtually independent of details of the disk structure, between the fractional amount of DM at the disk edge and the slope of the rotation curve: the steeper the curve, the larger is the DM mass fraction. Quantitatively, galaxies with $\bigtriangledown = -0.1$ have $M_D/M_{tot} \cong 0.8$ while galaxies with $\bigtriangledown = 0.6$ have $M_D/M_{tot} \cong 0.1$. Persic and Salucci have derived also the abundance of DM to luminosity relation. The high luminosity spirals have considerably more mass in luminous form than resides in the dark component. In the low luminosity regime the situation is reversed and the amount of DM exceeds the mass in stars by a factor of up to ten.

They have found the following scaling laws:

$$\frac{M_D}{M_{tot}} \cong 0.5 \left(\frac{L_B}{L_{B*}}\right)^{0.4} \tag{4.14}$$

and

$$\frac{M_D}{M_H} \cong 1.0 \left(\frac{L_B}{L_{B*}}\right)^{0.7} \tag{4.15}$$

where L_{B*} corresponds to $M_{B*} = -21.5$, the knee of the luminosity function of galaxies (Felten 1985).

4.1.5 Dark-to-Luminous Mass Ratio Proportional to the Colour

Studies of the M/L ratio as a function of morphological type (Tinsley 1981, Vader 1983) support the hypothesis that bluer spiral galaxies have relatively more massive halos. In particular, Tinsley (1981) analyzed integrated M/L ratios within the Holmberg radius and suggested that the increasing discrepancy between observed and predicted M/L ratios for the bluer galaxies is due to an increase in the ratio of halo to luminous mass.

Athanassoula, Bosma and Papaioannau (1987) have made an analysis of the rotation curve of a sample of spiral galaxies for which both photometric and kinematical data were available in the literature. They have combined photometric

and kinematical data to construct models using a disk with constant M/L and spherical halo, and have applied spiral structure theory to restrict the range of the allowable disk masses.
In principle these masses range from the "maximum disk" solution chosen with M/L as high as possible without exceeding the observed velocities, and the "minimum disk" solution, for which M/L is zero and all the mass is attributed to the halo. The evidence of the spiral structure constrains the maximum value to that which prevents the development of m=1 instabilities, and the minimum value as that at which m=2 structures are inhibited. Decreasing the disk contribution to the rotation curve reduces the scale length of the allowed instabilities: thus the amount of halo will establish which spirals are permissible. A direct upper limit to the halo mass and a lower limit to the disk mass can be set for galaxies with global spiral structures.
For the disk, they first choose the largest M/L ratio that gives a disk rotation curve compatible with the observed rotational data. In the case that a halo is present, they require it to have a non-hollow core, and than calculate the maximum possible amplification according to the local theory for one, two, and sometimes more arms. If the allowed m=1 amplification is large, they lower the M/L_D if necessary. The amplification drops sharply as the M/L is decreased, so the range of M/L_D over which the transition from significant to no amplification occurs is relatively small. Once the M/L is adopted they calculate the corresponding halo component, first deriving the halo velocities and then using three different approaches to parametrize the halo:

1. they use the numerical value of the halo velocities to calculate the halo mass within R_{25} and two concentration indices $MH(0.5R_{25})/MH(R_{25})$ and $MH(0.33R_{25})/MH(R_{25})$;
2. an isothermal sphere model is fitted to the halo velocities, and core radius R_c, central density ρ_0, dispersion σ and halo mass within R_{25} are calculated;
3. a power law is fitted to the halo densities.

The means and dispersions of some parameters concerning the relative mass and the shapes of the halos are give in Tab. 4.1.5. For the maximum-disk solution most of their galaxies have a halo-to-disk mass ratio less than 1.5. Athanassoula *et al.* found that the max-disk solution, modified by the requirement that no m=1 amplification is allowed, is compatible with models of galactic evolution. They have also checked Tinsley's idea of an increase in the ratio of halo-to-luminous mass going from redder to bluer spirals: they plot the ratio M_{halo}/M_{lum} and the trend as suggested by Tinsley is present at a significant level, see Fig.4.1. It seems that Dark Halos are more important in the inner parts of bluer galaxies than in

TABLE 4.1.5
Means of halo parameters

Solutions	Number	M_H/M_D	R_c	σ	$\log \rho_0$
max	25	0.82	20	98	0.68
no m=1	28	0.89	19	97	0.71
no m=2	28	2.5	9.7	96	1.3
min	28		3.8	114	2.2

the inner parts of redder galaxies. They have also found that there is a relation between halo velocity dispersion and absolute magnitude, a trend indicating that disk and halo densities are related and an indication that in earlier type spirals the halo is more centrally concentrated than in late type spirals.
A sketchy explanation of the trends (discussed so far) can be sought in a picture of galaxy formation where the halo material existed first and baryonic material formed galaxies by falling into pre-existing potential wells in the DM distribution. As is shown by the N-body simulations of Blumenthal *et al.* (1986), this process will severely influence the run of the density in the halo and therefore its rotation curve such that the present halo is much more concentrated than the initial one. For a given initial halo, the more massive or the more centrally concentrated is the disk, the more centrally condensed the final halo should be. The correlation between the central density of the halo and that of the disk reflects the fact that these two components are responding gravitationally to each other.

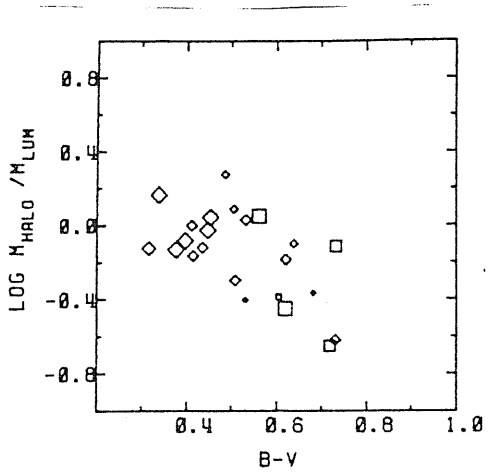

Figure 4.1: Ratio of halo-to-luminous mass (out to R_{25}) for the no m=1 solutions, as function of (B-V) colour. Galaxies of type Sa-Sb are shown as squares, galaxies of type Sbc and later as diamonds.

Chapter 5

The Shape of Dark Matter Halo

5.1 Are DM halos spherical or flattened?

As pointed out in the previous discussion, the existence and distribution of DM in the universe is one of the central problems of contemporary astronomy. On galactic scales the existence of significant amounts of DM is indicated by observations of the rotation curves in the disks of spiral galaxies. However, this technique does not distinguish between a disk-shaped and a spheroidal distribution of the Dark Matter. The discovery of S0 galaxies with polar rings provides a method of determining the shape of the gravitational potential.
These systems consist of a central galaxy encircled by a bright annulus whose apparent major axis nearly coincides with the apparent minor axis of the central galaxy. The ratio of the outer and inner radii of the annulus can be as great as 3. The annulus seems to be reasonably flat. In all cases spectroscopic and photometric observations have revealed that the central galaxy is a nearly edge-on S0 galaxy and that the bright annulus consists of gas and young stars.

Since the annuli or rings of these galaxies extend well beyond the visible parts of the underlying galaxies, they provided excellent probes of halos. As the ring consists of material in near-polar orbits around the disk, these orbits offer the rare opportunity to investigate the disk galaxy's gravitational field orthogonal to the symmetry plane and up to heights corresponding to three times the isophotal radius of the disk. The short term "spindle" is used as a conventional name for the main luminous body, without implying any specific spatial shape.

5.2 Observational Data

5.2.1 Collected Data for A0136-0801

This is a 16.5 spindle galaxy with a ring of gas, dust, and young stars; its redshift distance is 112 Mpc (recession velocity of 5576 km s^{-1}relative to the Local Group, $H_0 = 50$ km s^{-1} Mpc^{-1}. The spindle is a normal S0 disk seen nearly edge on as shown by its photometric profile and fast rotation (Schweizer, Whitmore, and Rubin, 1983).
Spindle–The spectrum of the spindle resembles that of an old stellar population. All the lines indicate a substantial velocity gradient of the stars along the major axis of the spindle, but not along the minor axis. The spindle seems to consist of a central bulge and a thin disk seen nearly edge on, embedded in a flattened spheroid. The apparent axial ratio of the main body of A0136-0801 is $b/a = 0.48 \pm 0.02$ for $5" < a < 7"$.
The surface photometry profile suggests the presence of two major components in the light distribution:

- a spheroid within 4" from the center which causes the central brightness peak, and
- a truncated exponential disk, which causes the nearly straight section of the light profile.

The integrated blue magnitude of the spheroid is $B = 18.3 \pm 0.4$ (assuming that the spheroid has spherical symmetry and integrating the light in the excess of the model disk). The integrated magnitude of the disk and spheroid combined (=spindle) is $B = 17.1 \pm 0.6$, the absolute blue magnitude is $M_B = -18.1 \pm 0.6$ (Schweizer, Whitmore, and Rubin, 1983).
In order to establish that the spindle is a rotating disk the stellar dispersion σ has to be measured because the ratio V_{rot}/σ must be significantly greater than 1.0 for the spindle to be a rotationally supported disk rather than a pressure supported spheroid. In the case of A0136-0801 the absorption lines are very narrow and only the central value of the velocity dispersion is measured: $\sigma = 67 \pm 7$ km s^{-1}. The critical ratio $V_{rot}/\sigma = 2.2 \pm 0.3$ exceeds significantly any ratio expected for a rotating oblate ($\cong 1.0$) or prolate ($\cong 0.6$) spheroid. The spindle is a rotationally supported spheroid.
Ring–This is a flat structure extending from $R \cong 10"$(5 kpc) out to at least $R = 32"$(17 kpc), the faint outer parts appear warped relative to the brighter inner parts. The ring contains gas, dust and young stars: gas emits the spectroscopically detected lines, the dust causes absorption across the spindle and the young stars give the ring its knotty appearance and blue colour. The ring passes in front of the spindle northwest of the nucleus and behind the spindle south-east, as judged

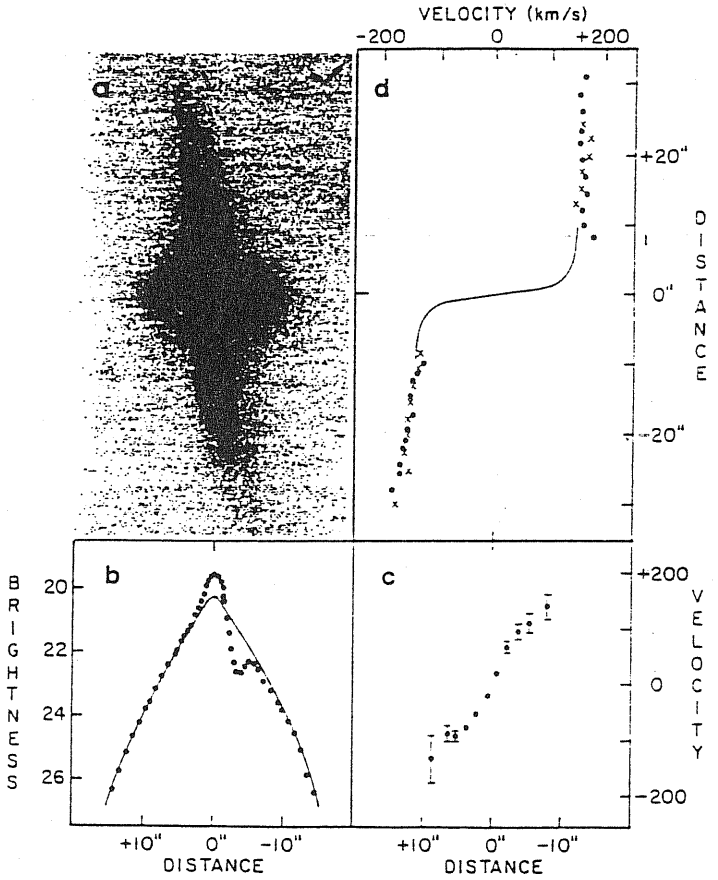

Figure 5.1: The four panels show, counterclockwise: (a) a blue photograph; (b) the profile of B surface brightness (in mag arcsec^{-2}) along the major axis of the spindle; (c) rotational velocities v_{rot} (in km s^{-1}) along the same axis; and (d) rotational velocities v_{rot} along the major axis of the polar ring. The scale of the photograph and the distance scales on the three graphs are identical. The long arrow in panel (a) points north and the short arrow east. The solid line in panel (d) represents schematically the corrected rotational velocities $V_{rot,c}$ in the main disk of the galaxy; the approximate match, at $R = 10$", of these velocities with those in the polar ring suggests that the dark halo of the galaxy is more spherical that flat.

by the presence and absence of absorption. The angle between the apparent major axis of the spindle and of the inner ring is $\gamma = 86.3^o \pm 0.8^o$.
Altough no proper photometry has been done, an estimate of the blue surface brightness in the ring is given:

$$\mu_B \cong 25.1 mag\ arcsec^{-2} \qquad R = 30" = 16.3\text{kpc}$$
$$\mu_B \cong 23.8 mag\ arc\ sec^{-2} \qquad R = 12" = 6.5\text{kpc}$$

The HI content of the ring: neutral hydrogen is evident in the radio maps, although it is not resolved (van Gorkom, Schechter, and Kristian, 1987). The HI is closely aligned with the major axis of the outer ring but is unresolved in the minor axis direction. The total hydrogen mass obtained by integrating the global profile over velocity is $8.3 \cdot 10^8 M_\odot$. The observed HI appears to coincide closely with the image of the ring: this implies that, however the system forms, the ring has time to settle into an equilibrium configuration and to form stars throughout its extent.

5.2.2 Collected Data for NGC 4650A

NGC 4650A (see Fig. 5.2) is at a distance of 53.3 Mpc (according to a recession velocity of 2667 km s^{-1} relative to the Local Group and $H_0 = 50$ km s^{-1} Mpc^{-1}).

Photometry-The luminosity profile along the major axis of NGC 4650A shows a well defined bulge component in the central part and an exponential profile in the intermediate region (Whitmore, McElroy, and Schweizer, 1987). A bulge decomposition indicates a moderately faint bulge ($M_B = -17.3 \pm 0.5$); the bulge-to-disk ratio is only 0.14, a figure typical of an Sc galaxy. The absolute magnitude of the ring is $M_B = -18.2 \pm 0.5$ and the relative fractions of light in the bulge, disk, and ring are 10%, 68%, and 22% respectively.
The ellipticity of the S0 component is 0.58 at $B = 21.5$ mag $arcsec^{-2}$. A fairly blue colour for the system has been measured, expecially for the ring. Whitmore, McElroy, and Schweizer find a total $(B - V) = 0.60$, a $(B - V) = 0.81$ for the inner component, and a $(B - V) = -0.09$ for the outer filament of the ring. Emissions characteristic of the HII regions are detected, indicating the presence of star formation in the ring.
Spectroscopy-The emission line rotation curve of the polar ring is similar to the rotation curve of any normal spiral galaxy, although it is measured vertically to the S0 disk. It extends out to 2.4 R_{25}(radius of the 25^{th} B isophote), much further than one can normally measure in a spiral galaxy using optical emission lines. The rotation curve shows no sign of a Keplerian fall off; it is slightly rising even at the most distant point.
The rotation curve of the S0 component extends to $\cong 0.9 R_{25}$ ($= 22' = 5.7$ kpc) and flattens in the outer regions. The central velocity dispersion is $\sigma_0 = 77 \pm 5$km s^{-1}

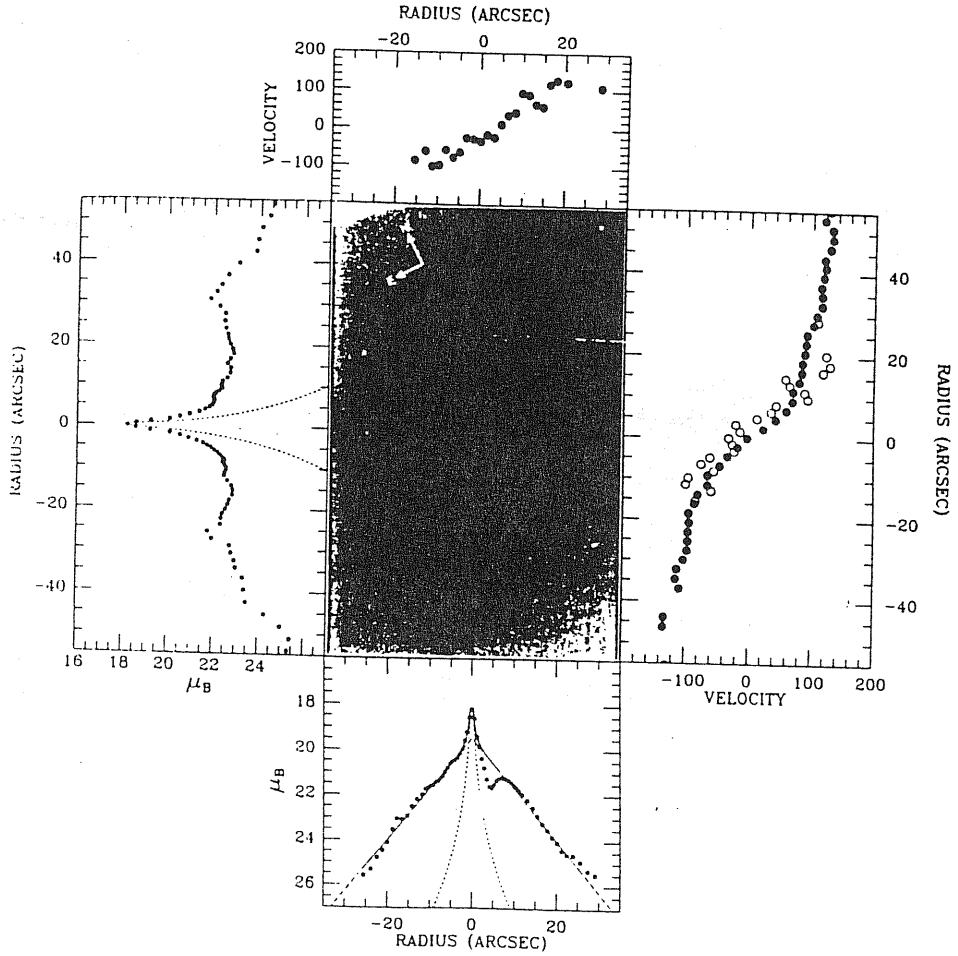

Figure 5.2: The spatial scale for the panels is approximately the same as the central photograph. The luminosity profiles of the polar ring and the S0 component are shown in the left and bottom panels respectively; their respective rotational velocities are shown in the right and upper panels. The right panel also has the rotational velocities for the S0 component superposed (*open circles*).

and the mean velocity dispersion is $\sigma_M = 70 \pm 4$km s^{-1}. The ratio V/σ for the S0 component of NGC 4650A is 0.96 ± 0.12.
The spectrum of the S0 component is a much more early-type one (with respect to the ring one), including a strong Balmer absorption and H_γ.
HI map–Neutral hydrogen is clearly evident in the radio maps (van Gorkom, Schechter and Kristian, 1987). There is a minimum in the HI distribution near the center of the system; this is taken as an indication that the HI truly forms a ring or an annulus and not just a disk. The HI in NGC 4650A twists on the plane of the sky following and then extending beyond the twist observed in the optical ring. The HI first twists toward the pole of the SO then twists away from it. The HI map is asymmetric, indicating that the hydrogen distribution is far from uniform.
The velocity field map is roughly symmetric about a velocity of 2895km s^{-1} with the line of symmetry significantly displaced to the north of the optical position. The mean of the extreme velocities in the position velocity diagram is 2910 km s^{-1} but its corresponding contour is displaced in the radio map yet further to the north. The HI extends 100" to the south and 144" to the north; since the optical ring extends roughly to 45", the star formation would seem to be confined to the inner parts of the HI distribution.

5.2.3 Collected Data for ESO 415-G26

ESO 415-G26 is at 89.5 Mpc (distance derived from its recession velocity of 4474 km s^{-1} relative to the Local Group and $H_0 = 50$ km s^{-1} Mpc^{-1}). Unlike A0136-0801 and NGC 4650A, the outer ring of ESO 415-G26 is very faint, see Fig. 5.3.

Photometry–The luminosity profile along the major axis of the S0 shows a central prominent bulge; a decomposition of both the major and the minor axis profiles yields a bulge absolute magnitude $M_B = -19.0 \pm 0.4$ and a bulge-to-disk ratio B/D=0.5 (Whitmore, McElroy, and Schweizer, 1987). In the region from 10" to 40" (4.3 to 17.2 Mpc) the luminosity follows an exponential profile. The relative fractions of light in the bulge, disk, and ring are 34%, 65%, and 1%. The apparent ellipticity of the S0 component is 0.66 at $B = 22.5$ mag arcsec^{-2}. The material in the S0 component is quite red: $(B - V) = 0.90 \pm 0.08$.
The bright part of the ring appears very narrow ($\cong 2.0" \pm 1.0"$) and is faint near the end point, unlike most other polar rings. A prominent loop is seen on the north side $\cong$ 43" from the nucleus and shells are seen in the northeast at $\cong$ 63" and $\cong$ 88" and possibly in the west-side at $\cong$ 52". The major axis of the faintest material is $53° \pm 10°$ which differs by 36° from the major axis of the S0 component. This makes ESO 415-G26 one of the few shell galaxies which have not an elliptical galaxy as central component.

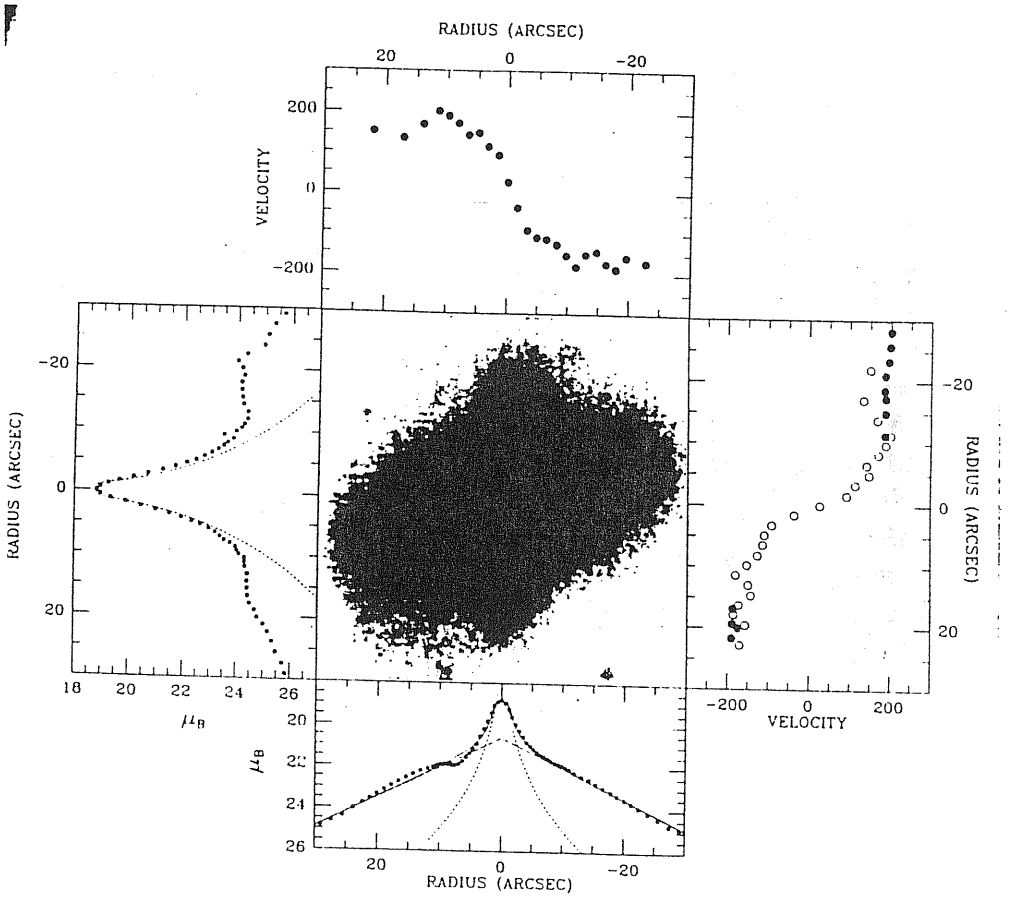

Figure 5.3: Photometric and kinematic data for ESO 451-G26. The luminosity profiles of the polar ring and the S0 component are shown in the left and bottom panels respectively; their respective rotational velocities are shown in the right and upper panels. The right panel also has the rotational velocities for the S0 component superposed (*open circles*).

The ring is considerably bluer $[(B-V) = 0.65 \pm 0.08]$ than the S0 disk $[(B-V) = 1.02 \pm 0.03$ in the cental 2".6].
Spectroscopy–The rotation curve of this object extends nearly as far as that of NGC 4650A. The maximum rotational velocity is 193 km s^{-1} within 32".6 (14.3 kpc). The rotation curve of the S0 component of ESO 415-G26 extends to $\cong 0.8R_{25}$. The central velocity dispersion is $\sigma_0 = 127 \pm 3$ km s^{-1}, considerably higher than for NGC 4650A or A0136-0801. This is consistent with a brighter bulge ($M_B = -19.0$): the relation for bulges of spiral galaxies would predict $\sigma_0 = 123$ km s^{-1}. The mean velocity dispersion is $\sigma_M = 102 \pm 5$km s^{-1}, and the ratio $V/\sigma = 1.14 \pm 0.08$ km s^{-1}.
HI map–ESO 415-G26 is different from the polar rings described above because it has a narrow ring which is smaller than its associated S0's and is very much less luminous (van Gorkom, Schechter and Kristian, 1987).
The HI distribution is rounder than the optical ring extending at least a factor of 2 beyond it and exhibiting a butterfly like shape. The velocity structure of the system is asymmetric: the mean of the extreme velocities gives $V_{sys} = 4585$ km s^{-1}, however the mean velocity of the gas at the center of the galaxy is 4620 km s^{-1}. The total Hydrogen mass is $1.8 \cdot 10^9 M_\odot$. The HI distribution is asymmetric with column densities roughly twice as high in the east as in the west and with the central peak offset to the east of the optical center. All the observational data are summarized in Fig. 5.2.3.

5.3 Rotation Velocities of Spindle and Ring and Error Analysis

Rotation velocities are calculated from the heliocentric velocities $V_{obs} = cz$ through the relation:

$$V_{rot} = \frac{cz - cz_{sys}}{\sin i\,(1 + z_\odot)}$$

where cz_{sys} is the conventional systemic velocity, i is the inclination of the plane of rotation to the plane of sky, and $(1+z)$ is the correction for the relativistic Doppler effect. Some corrections have to be applied to the measured velocities to convert them to circular velocities in the plane of sky: different authors have applied different corrections. Since their conclusions on the flatness of dark halos are different, we shall report the different procedures.
Two of the corrections to be applied to the measured velocities are straightforward:

1. the $1/(1+z)$ correction for the relativistic effect;
2. the $(1/\sin i)$ correction for the inclination of the S0 disk to the plane of the sky.

DATA FOR THE PROGRAM GALAXIES

Parameter	NGC 4650A	ESO 415-G26	A0136-0801
General properties:			
Heliocentric velocity (km s^{-1})	2904 ± 4	4560 ± 13	5528 ± 4
Velocity relative to Local Group[a] (km s^{-1})	2667	4474	5576
Distance (H_0 = 50) (Mpc)	53.3	89.5	111.5
Apparent B mag	14.27 ± 0.4	14.60 ± 0.2	16.6 ± 0.8
Absolute B mag[b]	−19.86 ± 0.4	−20.16 ± 0.2	−18.6 ± 0.8
Total $B-V$	0.60[c]	0.91	...
Scale (kpc arcsec^{-1})	0.259	0.434	0.541
Mass-to-light ratio in B for inner region	0.7 ± 0.2 within 14″	6.3 ± 1.3 within 18″	14 ± 8 within 15″3
Mass-to-light ratio in B within last observed point	4.5 ± 0.9 within 60″	9.3 ± 1.8 within 32″9	25 ± 14 within 31″3
Effective radius	19″	18″	6″5
Same (kpc)	4.9	7.8	3.5
Comparison radius	14″	18″	8″
Same (kpc)	3.6	7.8	4.3
V_{ring}/V_{disk}	0.89 ± 0.18	1.04 ± 0.14	0.98 ± 0.17
Flattening of gravitational potential c/a	0.86 ± 0.21	1.05 ± 0.17	0.98 ± 0.20
S0 Component:			
Radii at B = 25 mag arcsec^{-2} ($r_{25} \times R_{25}$)	10″3[d] × 24″5	19″5 × 30″4	6″8 × 12″2
Same (kpc)	2.7 × 6.3	8.5 × 13.2	3.7 × 6.6
Major axis position angle:			
Inner	61° ± 1°	17° ± 1°	138° ± 1°
Outer	60° ± 1°	17° ± 1°	...
Debris	...	53° ± 5°	...
Absolute B magnitude:			
Bulge	−17.3 ± 0.5	−19.0 ± 0.4	−16.9 ± 0.4
Disk	−19.4 ± 0.2	−19.7 ± 0.4	−17.6 ± 0.6
$B-V$	0.81[c]	1.02 ± 0.03 within 2″9	...
	...	0.90 ± 0.08 in halo	...
Bulge-to-disk ratio	0.14	0.52	≳0.5
Effective radius of bulge	1″1	2″5	0″7
Same (kpc)	0.3	1.1	0.4
Scale length for disk	4″79	7″61	2″30
Same (kpc)	1.24	3.30	1.24
$(\partial \ln \rho)/(\partial \ln R)$	2.92	2.37	3.48
Central velocity dispersion σ_0[e] (km s^{-1})	77 ± 5	127 ± 3	67 ± 7
V/σ_0	0.96 ± 0.12	1.14 ± 0.08	2.07 ± 0.34
Ellipticity	0.58 at B = 21.5	0.66 at B = 22.5	0.45 at B = 25
Inclination i	68° ± 4°	74° ± 4°	58° ± 5°
Velocity corrections:			
1/sin i	1.079 ± 0.03	1.040 ± 0.02	1.179 ± 0.06
$1/(1+z)$	0.991	0.985	0.982
Line of sight	1.10 ± 0.11	1.15 ± 0.11	1.05 ± 0.11
Asymmetrical drift	1.067 ± 0.05	1.067 ± 0.07	1.011 ± 0.01
Total correction	1.255 ± 0.12	1.257 ± 0.13	1.229 ± 0.13
Corrected rotational velocity at comparison radius V_{disk} (km s^{-1})	88 ± 9 at 14″	178 ± 11 at 18″	148 ± 19 at 8″
Polar ring component:			
Radius	54″8	19″5	...
Same (kpc)	14.2	8.5	...
Inner	...	...	10″
Same (kpc)	...	...	5.4
Outer	...	...	32
Same (kpc)	...	...	17.3
Major axis position angle:			
Inner	161° ± 1°	93° ± 1°	52° ± 1°
Outer	157° ± 1°	...	...
Inclination	85°[f] ± 5°	68° ± 2°	79° ± 2°
Absolute B magnitude	−18.2 ± 0.5	−15.5 ± 1.0	−17.6 ± 0.6
$B-V$	−0.09[c]	0.65 ± 0.08	...
Velocity corrections:			
1/sin i	1.004	1.079 ± 0.02	1.019
$1/(1+z)$	0.991	0.985	0.982
Warped disks	1.10 ± 0.10[g]	1.0 ± 0.0	1.0 ± 0.0
Total correction	1.094	1.063	1.001
Corrected rotational velocity at comparison radius V_{ring} (km s^{-1})	78 ± 3 at 14″	186 ± 2 at 18″	145 ± 9 at 8″
Maximum rotational velocity V_{max} (km s^{-1})	122 ± 6 at 60″	193 ± 4 at 32″9	168 ± 10 at 31″3

[a] Calculated using $V_{LG} = V + 300 \sin l \cos b$.
[b] A_B = 0.00 used for ESO 415-626 and A0136-0801, A_B = 0.49 used for NGC 4650A (Burstein and Heiles 1985).
[c] From Sérsic and Agüero 1972, using absorption and reddening corrections from Burstein and Heiles 1982.
[d] Minor axis based on major axis and ellipticity.
[e] Average of inner three measurements (4″8) in both major and minor axis when possible.
[f] From Laustsen and West 1980.
[g] Typical correction factor for various models of a warped ring.

Schweizer, Whitmore and Rubin (1983, hereafter SWR) have corrected the data of the equatorial rotation curve for the line-of-sight integration through the presumably transparent S0 disk. They calculate these corrections for the measured velocities of A0136-0801 by assuming that the disk is seen edge-on and by solving the integral equation for the true rotational circular velocity $V_{rot,c}$ numerically. The weighting factor for $V_{rot,c}$ in the integral along the line of sight was the intensity of the exponential light distribution determined by the photometry. Their computed correction factors are: $V_{rot,c}/V_{rot} = 1.75, 1.25$, and 1.10 at $r = 3", 6"$ and 9", to quote a few.
Whitmore, McElroy and Schweizer (1987, hereafter WMS) have measured the rotational velocities for NGC 4650A and ESO 415-G26, and have made corrections for (1) the line-of-sight integration and (2) for pressure support in the S0 disk.
(1)–In order to determine the shape of the halos they use only the velocity measurements in the outer regions of the S0: in those regions they calculate a maximum correction factor of 1.3. They recalculate this correction also for the A0136-0801 data of SWR obtaining the following correction factors at the comparison radius $0.61 \pm 0.04 R_{25}$: 1.10 for NGC 4650A, 1.15 for ESO 415 G26, and 1.05 for A0136-0801.
(2)-The rotational velocity of stars V_{disk} obtained after applying the previous three corrections is not the same as the circular velocity V_{circ} that a perfectly cold disk would have: yet it is the latter that one should use to determine the shapes of halos. The difference between these two velocities is given by the asymmetric drift:

$$V_c^2 - V_{disk}^2 = \sigma_\phi^2 - \sigma_R^2 \left(1 + \frac{\partial \log \sigma_R^2}{\partial \log R} + \frac{\partial \log \rho}{\partial \log R}\right) - R\frac{\partial V_R \bar{V}_z}{\partial z} \qquad (5.1)$$

where σ_ϕ and σ_R are the azimuthal and radial components of the velocity dispersion at radius R in the disk, and $\rho(R)$ is the spatial number density of stars. WMS have adopted the following approximate form for the asymmetric drift:

$$V_{circ}^2 = V_{disk}^2 - \sigma_R^2 \frac{\partial \log \rho}{\partial \log R}. \qquad (5.2)$$

This approximate equation is used to explain the asymmetrical drift of stars in the solar neighborhood. The term $\partial \log \rho / \partial \log R$ can be estimated by photometry. The values of σ_r at the comparison radii are unknown. They use

$$\sigma_z(R) = \sigma_z(0) \exp\left(-\frac{R}{2h}\right) \qquad (5.3)$$

where $\sigma_z(R)$ is the z component of the stellar velocity dispersion at radius R, $\sigma_z(0)$ is the central velocity dispersion of the disk and h is the exponential scale length of the disk. With the assumption $\sigma_R(R) = \sigma_z(R)$ it is possible to estimate the

asymmetric drift corrections V_{circ}/V_{disk}. At the comparison radius they are: 1.067 (NGC 4650A), 1.067 (ESO 415-G26), 1.011 (A0136-0801).
Sackett and Sparke (1989, hereafter SS) have made a mass model for the polar ring galaxy NGC 4650A using the data of WMS, the unpublished polar rotation curve of Nicholson (1989) and the neutral hydrogen contour map and ring velocity field of van Gorkom, Schechter and Kristian (1987). Their corrections for 1) the line-of-sight integration and 2) asymmetric drift are different from those of WMS. 1)-WMS assume a constant 10% correction for the line-of-sight integration effects independent of radius. The SS analysis indicates that these integration effects drop very rapidly as a function of radius so that at the comparison radius of 14" used by WMS they are less than 1%.
2)-SS have used the following equation to derive the asymmetrical drift:

$$V_c^2 - V_{disk}^2 = \sigma_R^2 \left[\frac{\sigma_\phi^2}{\sigma_R^2} - 1 + \frac{2R}{h} \right] \tag{5.4}$$

They obtained eq. 5.4 from eq. 5.1 by assuming that the last term is zero and that σ_z^2 (and thus σ_R^2 since their ratio is constant (van der Kruit and Freeman, 1986)) is proportional to ρ. The radial velocity dispersion of the disk then obeys:

$$\sigma_R^2(R) = \sigma_R^2(0) \exp\left(-\frac{R}{h}\right)$$

and they assume $\sigma_R^2/\sigma_\phi^2 = 1/2$. The asymmetric drift corrections derived by SS using these equations are much larger than those of WMS. At 14" WMS used a multiplicative factor of 1.067 to account for the asymmetric drift corrections, whereas SS estimate that it is about 1.5 at this radius and that it rises even more closer to the center of the disk.

5.4 Polar Ring Rotation Curves and DM Halos.

Rings appear to rotate in a way similar to disks of spiral galaxies, although rings are extended nearly perpendicular to S0 disks. This gives us the chance to probe the gravitational potential of disk galaxies out to large distances, and in directions nearly perpendicular to the plane. The rotation curves of polar rings have been measured out to 60" $= 2.4R_{25}$ for NGC 4650A, 32".9 $= 1.1R_{25}$ for ESO 415-G26, and 31".3 $= 2.6R_{25}$ for A0136-0801. The distances reached by these measurements are much greater relative to R_{25} than the distances out to which one can normally measure the rotation curves in spiral galaxies using optical emission lines, and are comparable to the most extended HI rotation curves. The rotation velocities do not show any sign of falling in a Keplerian fashion: there must be halos of DM in these systems which extend to the limiting radius or out to $\cong 2.5R_{25}$ for two of the three S0 disks.

5.4.1 Shape of the DM halo

SMR have pointed out that the ratio between the circular velocity in the ring and that in the disk could be related to the flatness of the equipotential surfaces of the galaxy's gravitational field. If they are nearly spherical, the circular velocity measured at a height z above the poles of the embedded S0 disk will be nearly equal to that measured at the corresponding radius $R = z$ within the plane of the S0 disk. If the halo is strongly flattened toward the same plane as the embedded S0 disk, then velocities measured above the poles will be lower than velocities at corresponding distances within the plane.
SMR estimated this effect analytically using a Kuzmin disk, for which the surface mass density falls off as $(R^2 + a^2)^{-3/2}$; a is the scale length. Closed polar orbits around a Kuzmin disk are ellipses with major axis coinciding with the disk axis and foci at $z = -a$ and $z = +a$. A test particle in such an orbit crosses the disk axis at right angles with a velocity:

$$V_{pol}(z) = \left[GM_{disk}\left(\frac{2}{z+a} - \frac{1}{z}\right)\right]^{\frac{1}{2}} \tag{5.5}$$

A test particle on a circular orbit within the disk has a velocity:

$$V_c(R) = \left[\frac{GM_{disk}R^2}{(R^2+a^2)^{\frac{3}{2}}}\right]^{\frac{1}{2}}. \tag{5.6}$$

For a given distance $x > a$, the ratio of polar to equatorial velocities is:

$$\frac{V_{pol}(x)}{V_c(x)} = \left[\frac{x-a}{x+a}\frac{(x^2+a^2)^{\frac{3}{2}}}{x^3}\right]^{\frac{1}{2}}. \tag{5.7}$$

At $x/a = 1.5, 2.5, 3.5, 4.5$, the velocity ratio is: $0.59, 0.73, 0.79, 0.83$. This suggests that over a wide range of distances from the center, polar velocities ought to be 20%-40% lower than the circular velocity in the disk. The SWR data for A0136-0801 show that the polar and disk velocities match well around $R = 10$" where the two sets of velocities overlap. SWR estimate that any possible mismatch is less than 10%-15% of the velocities themselves. A rough estimate of the halo shape may be obtained from polar orbits in the scale free potential given by Monet, Richstone, and Schechter for a non-flat mass distribution. Keeping the velocity mismatch smaller than 10%-15% ($V_{pol}(x)/V_c(x) \geq 0.85$-$0.90$), the halo must have equipotential surfaces with: $b/a \geq 0.88$-0.92.
From their analysis SWR concluded that the massive halo of A0136-0801 cannot be highly flattened and is more nearly spherical.

WMS computed velocities and axial ratios of closed polar orbits in the scale free gravitational potential of Monet, Richstone and Schechter of the form

$$\Phi(R,\theta) = V_{circ}^2 \log\left(\frac{R}{R_0}\frac{1+e|\cos\theta|}{1+e}\right). \tag{5.8}$$

where V_c is the circular velocity in the plane of the disk and following Monet *et al.*(1981)

$$e = \frac{M_D}{M_D + M_H}$$

is the fraction of the total mass which is in the disk. This analytic form represents the potential of a cold, flat disk embedded in a non-rotating isothermal halo with an isotropic velocity dispersion. The equipotentials are therefore ellipses with an eccentricity e and with axial ratio

$$\frac{b}{a} = \frac{1}{1+e} \tag{5.9}$$

WMS derived the value of b/a for different values of e, obtaining the following linear relation:

$$\frac{b}{a} = -0.215 + 1.212\frac{V_{pol}}{V_c}. \tag{5.10}$$

The flattening of the equipotential surfaces of the polar ring NGC 4650, ESO 415-G26, A0136-0801 can be estimated from the values of V_{ring}/V_{disk}.
After applying the corrections illustrated above to the measured data, WMS find the following ratios between the rotation velocities in the polar rings and the circular velocities in the S0 disk:

$$\begin{aligned}
\frac{V_{ring}}{V_{disk}} &= 0.89 \pm 0.18 \quad for\ NGC4650A \\
\frac{V_{ring}}{V_{disk}} &= 1.04 \pm 0.14 \quad for\ ESO415-G26 \\
\frac{V_{ring}}{V_{disk}} &= 0.98 \pm 0.17 \quad for\ A0136-0801
\end{aligned}$$

The derived flattenings of the equipotential surfaces are:

$$\begin{aligned}
\frac{b}{a} &= 0.86 \pm 0.21 \quad for\ NGC4650A \\
\frac{b}{a} &= 1.05 \pm 0.17 \quad for\ ESO415-G26 \\
\frac{b}{a} &= 0.98 \pm 0.21 \quad for\ A0136-0801
\end{aligned}$$

From their analysis, WMS concluded that, at radii of $\cong 0.6R_{25}$, the equipotentials of all three systems are nearly spherical. Since the distribution of luminous matter is highly flattened, a nearly spherical dark halo must be the dominant massive component within this radius. We dare to say that these conclusions about the shape of the potential are valid only for $\cong 0.6R_{25}$, where polar-ring and disk velocities can be compared. It might be that at smaller radii the equipotentials tend to be flatter because of the increased influence of the flat and truncated mass distributions of the S0 disk.

Sackett and Sparke (1989) re-analysed the dynamics of NGC 4650A using a physically realistic potential that includes the effects of the bulge, disk, halo and of the ring itself and compared their model to the entire extent of both rotation curves. Their model consists of:
1) a spherically symmetric Plummer bulge with luminosity and scale radius dictated by photometry. Its density is given by:

$$\rho_B = \frac{3M_B}{4\pi R_B^3}\left(1+\frac{R^2}{R_B^2}\right) \tag{5.11}$$

corresponding to a bulge potential:

$$\Phi_B = -\frac{GM_B}{\sqrt{R^2+R_B^2}} \tag{5.12}$$

where M_B is the total mass and R_B is its core radius.
2)A thick exponential disk with luminosity and scale length also given by photometry. Its density distribution is given by:

$$\rho_D = \rho_0 \exp\left(-\frac{R}{h}\right)\exp\left(-\frac{|z|}{z_0}\right) \tag{5.13}$$

where h is the exponential scale length and z_0 is the exponential scale height; it is assumed $z_0 \cong h/4$. The gravitational potential that satisfies Poisson's equation for this density is:

$$\Phi_D(R,z) = -GM_D\int_0^\infty dk \frac{J_0(kR)[kz_0 e^{-\frac{|z|}{z_0}} - e^{-|z|}]}{[1+h^2k^2]^{3/2}[k^2z_0^2-1]}. \tag{5.14}$$

This reduces to that for a thin exponential disk in the limit $z_0 \to 0$.
3) An axially symmetric flattened DH constrained to give an asymptotically flat rotation curve. SS parametrize the shape of the dark halo in terms of the halo isodensity surfaces rather than the gravitational equipotential surfaces: the latter are more spherical at a given radius than the former. This procedure allows one

to separate the non-sphericity of the gravitational potential due to the halo from that supplied by the disk. The isodensity surfaces are assumed to be flattened axially-symmetric spheroidal shells of constant axial ratio q, with a radial density distribution that yields asymptotically flat rotation curves for orbits in the symmetry plane of the halo and in the polar plane. Its density is given by:

$$\rho_H(R,z) = \frac{\rho_0}{1+\left(R_H^2\left(R^2+\frac{z^2}{q^2}\right)\right)^{-1}} \tag{5.15}$$

where ρ_0 is the central density and r_H the core radius. When $q \to 1$ this density tends to that of a pseudo-isothermal sphere. The gravitational potential generated by this density distribution is:

$$\Phi_H(R,z) = 2\pi G\rho_0 q R_h^2 \int_0^{1/q} dx \log\left[\frac{1+\frac{x^2}{R_H^2}\left(\frac{R^2}{e^2x^2+1}+z^2\right)}{e^2x^2+1}\right] \tag{5.16}$$

where e is the eccentricity of the halo, $e = \sqrt{1-q^2}$. The asymptotic velocity in the symmetry plane of the halo is:

$$V_H^2 = 4\pi G\rho_0 R_H^2\sqrt{1-e^2}\left(\frac{\arcsin e}{e}\right). \tag{5.17}$$

4) A thin two component annulus with a surface density chosen to reflect the approximate stellar and HI mass distributions of the polar ring. Each annulus is centered on and precisely polar to the central galaxy and is modelled with the difference of two Toomre disks (precisely, of two n=2 Toomre disks). The surface density is:

$$\Sigma(R) = \left(\frac{3a^3M}{2\pi}\right)(a^2+R^2)^{-5/2} \tag{5.18}$$

where M is the mass of the Toomre disk and a is the characteristic scale length. The derived potential is:

$$\Phi(R,z) = -GM\frac{[a(a+|z|)+R^2+(a+|z|)^2]}{[R^2+(a+|z|)^2]^{3/2}} \tag{5.19}$$

in the natural cylindrical coordinate system of the ring plane.
Each annulus is described by 4 parameters; choosing the total mass of the annulus and requiring that its density vanishes at the center reduces the number of the free parameters to 2. These parameters have been chosen to provide reasonable estimates of the stellar and HI mass distribution in the polar ring.

The mass-to-light ratios of bulge and disk are assumed to remain constant with radius (that is equivalent to assuming that the light distribution of these two components is a reasonable reflection of the corresponding mass distribution). The free parameters of the model are: M/L ratio of the disk, M/L ratio of the bulge, core radius, asymptotic circular rotation velocity and flattening of the dark halo, and mass of the polar ring.

The four components described above are added to give the total gravitational potential of the model. The orbits that do not lie in the equatorial symmetry plane of the total potential must be determined iteratively, and when a massive ring is added to the total potential, the closed orbits in the plane of the galactic disk are not circular.

5.4.2 Constraints Given by the Observational Data.

The best fit to the luminosity profile of NGC 4650A for a thin exponential disk plus Plummer bulge indicates a scale length of 1".08 for the bulge and 4".89 for the disk, with corresponding luminosities of $0.43 \cdot 10^9 L_\odot$ and $2.78 \cdot 10^9 L_\odot$ respectively (SS assumed $H_0 = 75$ km s^{-1} Mpc^{-1}).

Three model parameters are associated with both the stellar and the HI annuli that form the two component polar ring model: 1) the total mass of the annulus and 2) the characteristic scale lengths of the two Toomre n=2 disks. These parameters are relatively easy to define for the neutral hydrogen component of the polar ring model. The integrated HI mass measured by GSK is $4.6 \cdot 10^9 M_\odot$. Correction for the cosmic abundance of helium (M(He)=0.4M(H), Spitzer 1978) brings the total mass in the ring to at least $6.4 \cdot 10^9 M_\odot$. The narrowness of the HI contours together with the nearly edge on aspect of the optical ring suggest that the HI may be becoming optically thick in the 21cm line resulting in an underestimate of the total HI. The total mass of $6.4 \cdot 10^9 M_\odot$ should be considered a strict lower limit on the HI.
The scale length parameters of 20" and 90" for the HI annulus were chosen by comparing neutral hydrogen observations to the predicted HI profile of a model annulus which had been warped, inclined to the sky, and smoothed with a 20" beam.

For the stellar annulus the proper choice of model parameters is not so obvious since the M/L of the stellar component is unknown for the polar ring. Its light distribution is dominated by the very bright blue HII regions. SS chose a stellar annulus with a surface density profile which is much sharper than that of the HI but which peaks at the same position and integrates to the same total mass.

5.5 Results and Discussion

The derived halo flattening may be shown to be only weakly dependent on assumptions about the disk mass by considering two extreme cases: a minimal halo model (corresponding to the maximum disk hypothesis of van Albada *et al.* 1985.) and a maximum halo model where the rotation curves are assumed to reflect closed orbits in a gravitational potential provided only by the halo itself. In the minimal halo model much of the potential flattening is provided by the stellar disk: the halo will be rounder than in the minimal halo models. The DH flattening intermediate between those given by these two model choices. A massive ring partially counters the flattening of the gravitational potential and allows halos that are even flatter than those of the max. halo models.
SS begin by considering models with no DH and increase the mass-to-light ratios of the luminous components (bulge and disk only) to the maximum values consistent with the observed rotation: the upper limit for the M/L is imposed both by the polar and the equatorial rotation curves.
No combination of mass-to-light ratio was found that could simultaneously fit the inner and the outer regions of both rotation curves. SS conclude that another mass component is necessary to provide the rotation speeds observed in the outer regions of the rotation curves.
Models that give the same M/L to bulge and disk do not produce good fits to the inner regions of the rotation curves. A reasonable fit was obtained using a model with a disk M/L=2.5 and a bulge M/L=0.5. In the minimal halo models these values set the maximum mass of the central spindle at about $7 \cdot 10^9 M_\odot$. The SS estimate of M/L=2.5 for the disk is to be compared with the value $M/L \cong 1.0$ derived by WMS for the whole galaxy inside 14". The discrepancy is due to the difference in the methods employed to estimate the mass of the disk: SS's method relies on fitting the inner regions of both the polar and equatorial rotation curve. WMS estimate the mass of the galaxies from velocities at radius $R = 14$", the furthest point at which rotational velocities are available from both sides of the disk.
Since the velocity enters as the square, the reliability of the rotation velocity at the chosen R is critical; at $R = 14$" the rotation speeds are anomalously low.

5.5.1 Limits on Halo Flattening

As we have already noticed, luminous matter in the disk and bulge cannot account for the high rotation speeds observed at large radii in the polar ring of NGC 4650A. Assuming that the required gravitational force is supplied by a DM halo of the form described previously, SS's procedure can place constraints on the free parameters of the halo: the core radius R_H of the halo, the asymptotic speed V_H

of the flat equatorial curve produced by the halo at large radii, and the axial ratio q of the halo density profile. Since the polar curve is the better of the two, the halo parameters were varied by SS until the best polar fit was obtained.
Maximum Halo Models-Among them, halo flattenings in the range E4 to E5 provide the best fit to the data: a spherical halo gives an extremely poor fit.
Minimal Halo Models-A disk and a bulge component were added. Since the disk is supplying some of the flattening of the gravitational potential, the best fit now corresponds to an E3 or E4 halo, although the entire range E0 to E6 is allowed by the data. Even for the E0 minimal halo model the gravitational potential is flattened along the plane of the central spindle. Even if the halo mass distribution is spherical inward of 5", the equipotential surfaces remain noticeably flattened at a few scale lengths.

5.5.2 Effects of the Massive Polar Ring

The average slope of the polar emission-line rotation-curve between 20" and 45" is steeper than that in either the minimal or the maximum halo model. The "wiggle" of the polar emission line data, together with the apparent slight drop in the HI rotation speed reported by GSK at large radii ($\cong$ 90") suggests that the ring mass is influencing the shape of the polar rotation curve. The upper limit of M/L =2.5 for the central disk of NGC 4650A yields an upper limit on the total spindle mass of $\cong 7 \cdot 10^9 M_\odot$, scarcely more than the lower limit on the ring mass of $6.4 \cdot 10^9 M_\odot$ measured by neutral hydrogen.
To test the hypothesis that the ring mass plays an important role, SS add the ring contribution to the total potential. The ring is assumed to have a total mass equal to twice that inferred from the neutral hydrogen measurements, shared equally between the stellar and HI annuli.
It turns out that the massive ring is an important dynamical element: it ensures a superior fit to the polar rotation curve while acting to decrease the equatorial rotation speeds in the regions for which data are available.
The class of models which determines the extreme upper limit of the allowed halo flattening is the maximum halo model (i.e. no disk or bulge) with a massive ring. In this class of models the best fit is provided by an E6 to E7 flattened halo, and a spherical halo is strictly ruled out. The addition of disk and bulge improves the overall fits over a wide range of halo flattenings with the best results given by flattenings in the range E6-E7. A spherical halo gives a poor fit in these minimal halo models with massive disk and ring. The effect of the ring is not only to give a better fit to the polar rotation curve, but also to allow somewhat larger values of the halo flattening.
Could the ring be supplying all of the rotational support at large radii? Is it possible that no DM is required at all? In this case the derived equatorial rotation

curve is marginally acceptable and the wiggle in the polar rotation curve is reproduced. The most notable departure from the DM models is the drop in rotation speed at large distance but this does not occur until about 75". At 120" the polar rotation speed is still consistent with that indicated by the observation of GSK. The solution derived in this way is not unique.

5.6 Conclusions

The peculiar orientation of rings with respect to their central disk allows us to determine the three–dimensional distribution of matter. Moreover an evolutionary picture of the polar ring should explain why it appears non–randomly inclined: too many polar rings are too nearly polar. This peculiarity seems to be related to their formation history: probably it includes a "second event", an accretion of gas and other material from a former companion. The accreted material should be settled in to a disk and form stars (as is observed). Possible explanations for the peculiar orientation of the rings could be: 1) secondary disks of accreted material may form at all radii, but may last longer near the poles where differential precession is weaker; [1] or 2) some alignment mechanism may exist that makes secondary disks migrate towards the poles; this could occur if S0 disks or their associated halos were triaxial.

If massive halos dominate the potential and are nearly spherical, then secondary gas disks ought to occur at random tilts: this is clearly not the case, hence massive halos are either not dominant, or not spherical; or both. If the gravitational potential of a polar ring galaxy were exactly spherical at every radius, it would be difficult to understand why polar rings are found to be nearly orthogonal to the inner S0 disk since any angle would be stable.

The principal result of the work of SS is that the DH of the polar ring NGC 4650A is probably not spherical. Models with massless rings admit the range E0 to E6 for the flattening of the halo isodensity contours with an E3 or E4 halo providing the best fit. The introduction of a massive ring improves the overall fit to the polar rotation curve: a spherical halo then gives a very bad fit to the disk rotation curve. The preferred range of halo flattening includes E8, with the best result given by a halo flattening of E6-E7.

The mass of the polar ring of NGC 4650A has many dynamical consequences: it produces the characteristic wiggle in the polar rotation curve and depresses the equatorial rotation curve within the optical radius. Sparke (1986) has shown that a massive polar ring can remain stable to differential precession if it warps towards the pole on the outside. The polar ring of NGC 4650A does precisely that, and dynamical modeling shows that warping may be due to self gravity. If flattened

[1] a near polar disk would be favoured by statistical selection

halos are common, they could be responsible for maintaining the warp commonly seen in the outer HI disks of spirals.

According to the model proposed by Sackett and Sparke, if the measured polar and equatorial rotation curves of NGC 4560A are dominated by the dark matter halo, then it is indeed not spherical. If polar ring galaxies generally have flattened halos, this would explain why the rings are so often nearly polar.

Appendix A

Logarithmic Derivative

The circular velocity of the exponential thin-disk model (see Chapter 1, Sec 1.3) is:

$$V^2_{Disk}(R) = G\frac{M_D}{R_D}\frac{1}{2}\left(\frac{R}{R_D}\right)^2 (I_0K_0 - I_1K_1) \tag{A.1}$$

where I_n, K_n are modified Bessel functions evaluated at $1/2(R/R_D)$. Using the new variable:

$$x = \frac{1}{2}\frac{R}{R_D}, \tag{A.2}$$

it is straightforward to see that

$$\frac{\mathrm{d}\log V(R)}{\mathrm{d}\log R} = \frac{R}{V}\frac{\mathrm{d}V}{\mathrm{d}R} = \frac{x}{V}\frac{\mathrm{d}V}{\mathrm{d}x} = \frac{\mathrm{d}\log V(x)}{\mathrm{d}\log x} \tag{A.3}$$

and the velocity becomes

$$V(x) = \left(G\frac{M_D}{R_D}\right)^{1/2} \sqrt{2}x(I_0K_0 - I_1K_1)^{1/2}. \tag{A.4}$$

Using these properties of Bessel functions

$$\begin{array}{rl} xI'_n(x) = & xI_{n+1}(x) + nI_n(x) \\ xI'_n(x) = & xI_{n-1}(x) - nI_n(x) \\ xK'_n(x) = & -xK_{n-1}(x) - nK_n(x) \\ xK'_n(x) = & nK_n(x) - xK_{n+1}(x) \end{array} \tag{A.5}$$

where (') means $\mathrm{d}/\mathrm{d}x$, it follows

$$\begin{aligned} \tfrac{\mathrm{d}V}{\mathrm{d}x} = & \sqrt{2}\left(G\tfrac{M_D}{R_D}\right)^{1/2}(I_0K_0 - I_1K_1)^{1/2}. \\ & [1 + \tfrac{1}{2}(I_0K_0 - I_1K_1)^{-1/2}(xI'_0K_0 + xI_0K'_0 - xI'_1K_1 - xI_1K'_1)] = \\ = & \sqrt{2}\left(G\tfrac{M_D}{R_D}\right)^{1/2}(I_0K_0 - I_1K_1)^{1/2}\left[\frac{I_0K_0 - x(I_1K_0 - I_0K_1)}{(I_0K_0 - I_1K_1)}\right] \end{aligned} \tag{A.6}$$

and

$$\frac{\mathrm{d}\log V(R)}{\mathrm{d}\log R} = \frac{I_0K_0 - x(I_1K_0 - I_0K_1)}{(I_0K_0 - I_1K_1)} = \frac{I_0K_0 - 0.5\dfrac{R}{R_D}(I_1K_0 - I_0K_1)}{(I_0K_0 - I_1K_1)} \qquad \text{(A.7)}$$

Appendix B

Determination of the Halo-to-Disk Mass Ratio Using the Logarithmic Derivative of the Velocity

As we have seen in Chapter 3, Sec 3.1.4, from centrifugal equilibrium

$$V^2(R) = V_D^2(R) + V_H^2(r), \tag{B.1}$$

where $V_D^2(R)$, and $V_D^2(R)$ are the contributions to the total velocity at R from the mass in the disk and halo respectively. Taking the first derivative of eq. B.1 we have

$$V(R)\frac{\mathrm{d}\,V(R)}{\mathrm{d}\,R} = V_D(R)\frac{\mathrm{d}\,V(R)}{\mathrm{d}\,R} + V_H(R)\frac{\mathrm{d}\,V(R)}{\mathrm{d}\,R}. \tag{B.2}$$

Dividing eq. B.1 by eq. B.2 and multiplying by R, it follows

$$\frac{R}{V}\frac{\mathrm{d}\,V}{\mathrm{d}\,R} = \frac{R}{V_D^2 + V_H^2}\left[V_D\frac{\mathrm{d}\,V}{\mathrm{d}\,R} + V_H\frac{\mathrm{d}\,V}{\mathrm{d}\,R}\right], \tag{B.3}$$

$$V_D^2\left[\frac{\mathrm{d}\,\log V}{\mathrm{d}\,\log R} - \frac{\mathrm{d}\,\log V_D}{\mathrm{d}\,\log R}\right] = V_H^2\left[\frac{\mathrm{d}\,\log V_H}{\mathrm{d}\,\log R} - \frac{\mathrm{d}\,\log V}{\mathrm{d}\,\log R}\right]. \tag{B.4}$$

It is easy to derive eq. 4.6 from the last equality. Using eq. 4.7 and eq. 4.8 the disk-to-halo mass ratio is immediately derived

$$M_D(R) = G^{-1}\left[\frac{1}{2}\left(\frac{R}{R_D}\right)^3 (I_0K_0 - I_1K_1)\right]^{-1} V_D^2 R \tag{B.5}$$

$$= G^{-1}\left[\frac{1}{2}\left(\frac{R}{R_D}\right)^3 (I_0K_0 - I_1K_1)\right]^{-1} RV_H^2 \frac{\left[\dfrac{\mathrm{d}\log V_H}{\mathrm{d}\log R} - \dfrac{\mathrm{d}\log V}{\mathrm{d}\log R}\right]}{\left[\dfrac{\mathrm{d}\log V}{\mathrm{d}\log R} - \dfrac{\mathrm{d}\log V_D}{\mathrm{d}\log R}\right]}.$$

Therefore,

$$\frac{M_D(R)}{M_{tot}(R)} = \frac{M_D(R)}{M_H(R) + M_D(R)} = \frac{\dfrac{\mathrm{d}\log V_H}{\mathrm{d}\log R} - \dfrac{\mathrm{d}\log V}{\mathrm{d}\log R}}{f\left(\dfrac{R}{R_D}\right)\left(\dfrac{\mathrm{d}\log V}{\mathrm{d}\log R} - \dfrac{\mathrm{d}\log V_D}{\mathrm{d}\log R}\right) + \dfrac{\mathrm{d}\log V_H}{\mathrm{d}\log R} - \dfrac{\mathrm{d}\log V}{\mathrm{d}\log R}} \tag{B.6}$$

Bibliography

[1] Aaronson, M., Huchra, J., Mould, J.,Schechter, P.L., and Tully, R.B. 1982 Astrophys. J., **258**, 64.

[2] Van Albada, T.S., Bahcall, J.N., Begeman, K., and Sancisi, R. 1985. *Astrphys. J.*, **295**, 305.

[3] Van Albada, T.S., and Sancisi, R. 1986. *Phil. Trans. R. Soc. London.* A, **320**, 465.

[4] Allen, C.W. 1973. *Astrophysical quantities*, 3rd ed. London: Athlone Press .

[5] Arnaboldi, M. 1990, *Mon. Not. Roy. Astr. Soc.*, , ., submitted.

[6] Athanassoula, E., and Bosma, A. 1985. *Ann. Rev. Astron. Astrophys.*, **23**, 147.

[7] Athanassoula, E., Bosma, A. and Papaioannau, S. 1987. *Astron. Astrophys.*, **179**, 23..

[8] Bahcall, J.N., and Soineira, R.M. 1980. *Astrophys. J. Suppl.*, 44, 73.

[9] Bahcall, J.N., Schmidt, M., and Soneira, R.M. 1983, *Astrophys. J.*, **265**, 730..

[10] Bachall, J.N. 1983. *Astrophys. J.*, **267**, 52..

[11] Bahcall, J.N. 1984a. *Astrophys. J.*, **276**, 169.

[12] Bahcall, J.N. 1984b. *Astrophys. J.*, **287**, 926.

[13] Bahcall, J.N., and Casertano, S. 1985. *Astrophys. J.*, **293**, L10.

[14] Barnes, J., and White, S.D.M. 1984. *Mon. Not. Roy. Astr. Soc.*, **211**, 753.

[15] Begeman, K., 1986 *Ph.D. thesis*, University of Groningen, the Netherlands.

[16] Binney, J.J., and Tremaine, S. 1987. Galactic Dynamics, ed. Princeton University Press.

[17] Binney, J.J. 1986. *Phil. Trans. R. Soc. Lond.* **A**, **320**, 465.

[18] Blumenthal, G.R. 1987. *Dark matter and Galaxy Formation*, preprint

[19] Blumenthal, G.R., Faber, S.M., Flores, R., Primack, J.R. 1986. *Astrophys. J.*, **301**, 27..

[20] Boroson, T. 1981. *Astrophys. J. Suppl.*, **46**, 177.

[21] Bosma, A. 1981.*Astrophys. J.*, **86**, 1825..

[22] Burstein, D., and Rubin, V.C., Thonnard, N., Ford, W.K. 1982. *Astrophys. J.*, **253**, 70..

[23] Burstein, D., and Rubin, V.C. 1985. *Astrophys. J.*, **297**, 423.

[24] Carignan, C., and Freemann, K.C. 1985. *Astrophys. J.*, **294**, 494..

[25] Carignan, C., Sancisi, R., and van Albada, T.S. 1988. *Astrophys. J.*, **95**, 37.

[26] Carney, B., and Latham, D.W. 1987. In *Dark Matter in the Universe*, IAU Symposium No. 117, ed. J. Kormendy and G.R. Knapp, p. 39. Dordrecht: Reidel.

[27] Carr, B.J., Bond, J.R., and Arnett, W.D. 1984. *Astrophys. J.*, **277**, 445.

[28] Casertano, S. 1983, *Mon. Not. Roy. Astr. Soc.*, **203**, 735..

[29] Corradi, R. 1989. Dissertation, University of Padova.

[30] Davis, M., and Huchra, J. 1982. *Astrophys. J.*, **254**, 437.

[31] Davis, M., and Peebles, P.J.E. 1983. *Ann. Rev. Astron. Astrophys.*, **21**, 109.

[32] De Vaucouleurs, G. 1959. *Handbuch der Physic*, **53**, p. 275, ed. Springer Verlag.

[33] De Vaucouleurs, G. 1962. *Problems in External Research*, IAU Symposium No. 15, ed. Mc Vittie, p. 3. Mcmillan: New York.

[34] De Vaucouleurs, G., and Pence, W.D. 1978. *Astron. J.*, **83**, 1163.

[35] Dubal, M.R., Salucci, P. and Persic, M. 1990. *Astron. Astrophys.*, **227**, 33..

[36] Efstathiou, G., Lake, G., and Negroponte, J. 1982. *Mon. Not. Roy. Astr. Soc.*, **199**, 1069..

[37] Faber, S.M., and Gallagher, J.S. 1979. *Ann. Rev. Astron. Astrophys.*, **17**, 135.

[38] Faber, S.M. 1982. In *Astrophysical Cosmology*, ed. H.A. Bruck, G.V. Cayne, and M.S. Longair, (Vatican City: Pontificia Academia Scientiarum), p. 191.

[39] Fabricant, D., and Gorestein, P. 1983. *Astrophys. J.*, **267**, 535.

[40] Felten, J.E. 1985, *Comments Astrophys.*, **11**, 53.

[41] Forman, W., Jones, C., and Tucker, W. 1985. *Astrophys. J.*, 293, 535.

[42] Freeman, K.C., 1970. *Astrophys. J.*, **160**, 811.

[43] Griersmith, D. 1980. *Astrophys. J.*, **85**,1135..

[44] Van Gorkom, J.H., Schecter, P.L. and Kristian, J. 1987. *Astrophys. J.*, **314**,457..

[45] Gunn, J.E., and Peterson, B.A. 1965 *Astrophys. J.*, **142**,1633..

[46] Hainebach, K.T., and Schramm, D.N. 1977. *Astrophys. J.*, **212**, 347.

[47] Harris , W.E., Hesser, J.E., and Atwood, B. 1983. *Astrophys. J. Lett.*, **268**, L11.

[48] Hegyi, D.J., and Olive, K.A. 1983. *Phys. Lett.*, **126 B**, 28.

[49] Hohl, F. 1971. *Astrophys. J.*, **168**,343..

[50] Huchra, J.P., and Geller, M.J. 1982. *Astrophys. J.*, **257**, 423.

[51] Kahn, F.D., and Waltjer, L. 1959. *Astrophys. J.*, **130**, 705.

[52] Kalnajs, A.J. 1982a. *Astrophys. Lett.*, **11**, 41.

[53] Kalnajs, A.J. 1972b. *Astrophys. J.*, **175**,63..

[54] Kalnajs, A.J. 1983. In *Internal Kinematics and Dynamics of Galaxies*, IAU Symposium No. 100, ed. Athanassoula, pp. 87, 109. Dordrect: Reidel.

[55] Kalnajs, A.J. 1987. In *dark matter in the Universe*,IAU Symposium No. 117, ed. J. Kormendy and G.R. Knapp, p. 67, 109. Dordrect: Reidel.

[56] Kent, S.M., 1986. *Astron. J.*, **91**, 1301.

[57] Kent, S.M., 1987. *Astron. J.*, **93**, 816.

[58] Kent, S.M., 1988. *Astron. J.*, **96**, 514.

[59] Kerr, F.J., and Lynden-Bell, D. 1986. *Mon. Not. Roy. Astr. Soc.*, **221**, 1023.

[60] Van der Kruit, P.C. and Freeman, K.C., 1986. *Astrophys. J.*, **303**, 556..

[61] Van der Kruit, K.C. 1987. *Astron. Astrophys.*, **107**, 66..

[62] Lin, D.N.C., and Lynden-Bell, D. 1982. *Mon. Not. Roy. Astr. Soc.*, 198, 707.

[63] Lynden-Bell, D., Cannon, R.D., and Godwin, P.J. 1983. *Mon. Not. Roy. Astr. Soc.*, **204**, 87P.

[64] Milgrom, M. 1983a. *Astrophys. J.*, **270**, 365..

[65] Milgrom, M. 1983b. *Astrophys. J.*, **270**, 371..

[66] Milgrom, M. 1983c. *Astrophys. J.*, **270**, 384..

[67] Milgrom, M. 1984. *Astrophys. J.*, **287**, 571..

[68] Milgrom, M. 1986. *Astrophys. J.*, **302**, 617..

[69] Monet, D., Richstone, D.O., and Schechter, P.L. 1981. *Astrophys. J.*, **245**, 454..

[70] Murai, T., and Fujimoto, M. 1980. *Publ. Astron. Soc. Japan.*, **32**, 581.

[71] Oort, J.H. 1932. *Bull. Astron. Inst. Netherlands*, **6**, 349.

[72] Oort, J.H. 1965. In *Galactic Structure*, ed. A. Blaauw and M. Schmidt, p. 455. Chicago: University of Chicago Press.

[73] Ostriker, J.P., and Peebles, P.J.E. 1973 *Astrophys. J.*, **186**, 467..

[74] Peebles, P.J.E. 1971. *Physical Cosmology.* Princeton, N.J.: Princeton University Press.

[75] Persic, M., and Salucci, P. 1988. *Mon. Not. Roy. Astr. Soc.*, **234**, 131..

[76] Persic, M., and Salucci, P. 1990a. *Astrophys. J.*, **355**, 44..

[77] Persic, M., and Salucci, P. 1990b. *Mon. Not. Roy. Astr. Soc.*, in press.

[78] Persic, M., and Salucci, P. 1990c. *Astrophys. J.*, submetted.

[79] Rubin, V.C., Ford, W.K., and Thonnard, N. 1980.*Astrophys. J.*, *238*, 439.

[80] Rubin, V.C., Ford, W.K., Thonnard, N. and Burstein, D. 1982. *Astrophys. J.*, *261*, 439.

[81] Rubin, V.C., Burstein, D., Ford, W.K., and Thonnard, N. 1985 *Astrophys. J.*, **289**, 81.

[82] Sackett, P.D., and Sparke, L.S. 1989. Preprint.

[83] Salucci, P. 1986. Ph.D. Dissertation, SISSA, Trieste.

[84] Salucci, P. and Frenk, C.S. 1989. *Mon. Not. Roy. Astr. Soc.*, **237**,247..

[85] Sancisi, R., and van Albada, T.S. 1987. In *Dark Matter in the Universe*, IAU Symposium No 117, ed J.Kormendy and G.R. Knapp, p. 67. Dordrecht: Reidel.

[86] Sanders, R.H. 1984, *Astron. Astrophys.*, **136**,L21..

[87] Sanders, R.H. 1986a, *Astron. Astrophys.*, **154**,135..

[88] Sanders, R.H. 1986b, *Mon. Not. Roy. Astr. Soc.*, **223**,539..

[89] Sanders, R.H. 1990, *Astron. Astrophys. Rev.*, **2**, 1.

[90] Sciama, D.W. 1982a, *Phys. Letter. B*, **112**, 211.

[91] Sciama, D.W. 1982b, *Phys. Letter. B*, **114**, 19.

[92] Sciama, D.W. 1982c, *Mon. Not. Roy. Astr. Soc.*, **198**,1P..

[93] Sciama, D.W. 1982d, *Astrophysical Cosmology*, ed H.A. Bruck, G.V. Coyne and M.S. Lonfair, Pontificial Academy of Sciences.

[94] Sciama, D.W. 1984, Big Bang: G. Lemaitre in a Modern World, ed A. Berger. Dordrecht: Reidel

[95] Sciama, D.W. 1988, *Mon. Not. Roy. Astr. Soc.*, **230**,13P..

[96] Schweizer, F., Whitmore, B.C., and Rubin, V.C. 1983, *Astron. J.*, **88**, 909.

[97] Sellwood, J.A. 1981. *Astron. Astrophys.*, **99**,362..

[98] Siemen, F., and de Vaucouleurs, G. 1986. *Astrophys. J.*, **302**,564..

[99] Sparke, L.S. 1986. *Mon. Not. Roy. Astr. Soc.*, **219**,657..

[100] Spitzer, Lyman Jr. 1978. *Physical Processes in the Interstellar Medium*, ed. Jon Wiley and Sons.

[101] Stewart, G.C., Canizares, C.R., Fabian, A.C., and Nulsen, P.E.J. 1984. *Astrophys. J.*, **278**, 536.

[102] Tinsley, B.M., 1981. *Mon. Not. Roy. Astr. Soc.*, **194**, 63..

[103] Toomre, A., 1962. *Astrophys. J.*, **138**, 385..

[104] Toomre, A., 1964. *Astrophys. J.*, **139**, 1217..

[105] Toomre, A., 1974. In *Highlights of Astronomy*, ed G. Contopoulos, p. 457. Dordrecht: Reidel.

[106] Trimble, V. 1987. *Ann. Rev. Astron. Astrophys.*, **25**, 425.

[107] Turner, E.L. 1987. In *Dark Matter in the Universe*, IAU Symposium No. 117, ed. J. Kormendy and G.R. Knapp, p. 227. Dordrecht: Reidel.

[108] Vader, J.P. 1985. In *Formation and Evolution of Galaxies and Large Structures in the Universe*, ed. J. Audouze and J. Tran Thanh Van, p. 227, Dordrecht: Reidel.

[109] VandenBerg, D.A. 1983. *Astrphys. J. Suppl.*, **51**, 29.

[110] Wevers, B.M.H.R. 1984. *A study of spiral galaxies.* Ph.D. Thesis, University of Groningen.

[111] White, S.D.M., Huchra, J., Latham, D., and Davis, M. 1983. *Mon. Not. Roy. Astr. Soc.*, **203**, 701.

[112] Whitmore, B.C., McElroy, D.B., and Schweizer, F. 1987. *Astrophys. J.*, **314**, 439..

[113] Yahil, A., Sandage, A. and Tammann, G.A. 1980. *Astrophys. J.*, **242**, 448.

[114] Yang, J., Turner, M.S., Steigman, G., Schramm, D.N., and Olive, K.A. 1984. *Astrophys. J.*, 241, 507.

[115] Zang, T.A. 1976. Unpublised Ph.D. Thesis, Massachussetts Institute of Technology.

[116] Zang, T.A., and Hohl, F. 1978. *Astrophys. J.*, **226**, 521..

[117] Zwicky, F. 1933.*Helvetica Physica Acta*, **6**, 110.